2017•2018
Faculteit Industriële ingenieurswetenschappen
master in de industriële wetenschappen: bouwkunde

Masterthesis

Load bearing capacity of compound box or I-girders with corrugated steel web

PROMOTOR :
Prof. dr. ir. Herve DEGEE
PROMOTOR :
Prof. dr. Géze Balázs KOVESDI

Rob Vandeweyer
Scriptie ingediend tot het behalen van de graad van master in de industriële wetenschappen: bouwkunde

Universiteit Hasselt | Campus Diepenbeek | Agoralaan Gebouw D | BE-3590 Diepenbeek
Universiteit Hasselt | Campus Hasselt | Martelarenlaan 42 | BE-3500 Hasselt

2017 • 2018

Faculteit Industriële ingenieurswetenschappen

master in de industriële wetenschappen: bouwkunde

Masterthesis

Load bearing capacity of compound box or I-girders with corrugated steel web

PROMOTOR :

Prof. dr. ir. Herve DEGEE

PROMOTOR :

Prof. dr. Géze Balázs KOVESDI

Rob Vandeweyer

Scriptie ingediend tot het behalen van de graad van master in de industriële wetenschappen: bouwkunde

UHASSELT KU LEUVEN

Preface

This master's thesis was carried out as part of a semester abroad at the faculty of Civil Engineering, department Structural Engineering at Budapest University of Technology and Economics (BME) in Hungary from February 2018 to June 2018. The subject was suggested by professor Géza Balázs Kövesdi who also took on the function of internal supervisor for this project. My personal interest for the subject comes from the fact that innovative developments, like replacing a standard flat web of an I-girder with a corrugated web to improve certain features, intrigue me. Further, a part of this research was supposed to be the experimental phase. Combining theory with reality by performing experiments makes a project more interesting in my opinion, since it can provide stronger visual insight in the examined subject. Unfortunately, due to certain circumstances the experimental phase was delayed and the results will therefore not be a part of this thesis.

I could not have achieved the objectives that were obtained in this thesis without a strong support group. First of all, my parents who supported me throughout this semester abroad and gave me the opportunity to choose my preferred education. Secondly, Phd student Németh Gábor who helped me with the numerical modelling software GiD and the calculation software ATENA. Further, I would like to thank professor Géza Balázs Kövesdi as my internal supervisor and Bence Jager who provided me with the data I needed during the elaboration of this project. Additionally, I would like to show my gratitude to Lara Wyremblewski for drawing up a guide to scientific writing and to Hervé Degée as my contact person from my home university (UHasselt) in Hasselt, Belgium.

Table of contents

List of tables

List of figures

Glossary

Roman upper-case letters

N	Axial force
N_c	Axial force in concrete
N_r	Axial force in prestressing reinforcement
M	Bending moment
$M_{R,EC}$	Bending moment resistance provided by the flanges based on EC2
CS	‘Composite’ girders with steel lower flange
A	Cross-section area
A_r	Cross-section area of prestressing reinforcement
L_i	Distance between applied load and support i
$M_{R,FEM}$	FEM based bending moment resistance
$V_{R,FEM}$	FEM based shear force resistance
$F_{R,FEM}$	FEM based total load
$H6$	‘Hybrid’ girder with 6 prestressing tendons in the lower concrete flange
$H4$	‘Hybrid’ girder with 4 prestressing tendons in the lower concrete flange
M_c	Moment capacity as a result of concrete
M_s	Moment capacity as a result of steel
M_{sc}	Moment capacity as a result of the steel lower flange in a ‘composite’ girder
M_{sh}	Moment capacity as a result of steel prestressing reinforcement in a ‘hybrid’ girder
I_i	Moment of inertia in the i direction
$M_{f,Rd}$	Moment resistance based on the flanges
R_i	Reaction force in support i
$V_{R,EC}$	Shear buckling resistance of the web based on EC3
$V_{w,Rd}$	Shear resistance based on the web
E	Young's modulus / Elastic modulus

Roman lower-case letters

n	Amount of tendons
a_4	Axial length of the not axially oriented part of the corrugation, see Appendix A
a_1	Axially oriented part of the corrugation, see Appendix A

f_{ck}	Characteristic value of concrete cube compressive strength
f_{yk}	Characteristic yield strength
d	Effective depth of a cross-section
s	Half the actual length of the periodic part of a corrugation or $a_1 + a_2$, see Appendix A
w	Half the axial length of the periodic part of a corrugation or $a_1 + a_4$, see Appendix A
h_w	Height of the web of a girder
h_f	Height or thickness of the flange of a girder
h_{fl}	Height or thickness of the lower flange of a girder
f_{pr}	Initial pre-tension in the tendons
x_c	Neutral axis depth
a_2	Part of the corrugation that is not axially oriented, see Appendix A
t_f	Thickness of the flange of a girder
t_{fu}	Thickness of the upper flange
t_{fl}	Thickness of the lower flange
t_w	Thickness of the web of a girder
a_3	Total corrugation dept (see Appendix A)
b_f	Width of the flange of a girder
b_{fl}	Width of the lower flange of a girder
b_{fu}	Width of the upper flange of a girder
b_w	Width of the web of a girder
f_{yf}	Yield strength of the flange
f_{yw}	Yield strength of the web
f_{ys}	Yield strength of steel

Greek lower-case letters

α	Angle of corrugation fold, see Appendix A
χ_c	Lowest value of the reduction factors for local and global buckling
γ_M	Partial factor for a material property, taking account of uncertainties in the material property itself, in geometric deviation and in the design model used
$\chi_{c,g}$	Reduction factor for global buckling
$\chi_{c,l}$	Reduction factor for local buckling
χ	Reduction factor for out of plane buckling according to 6.3 of ENI993-J-J

λ	Slenderness
ε	Strain
σ	Stress
τ	Torsional shear stress

Abstract

Since the 1960s, there has been ongoing research of using box or I-girders with corrugated webs. Because of its advantages, the steel corrugated webs are widely used in bridge constructions. Developments concerning the girder compositions are continually implemented to improve certain attributes of the structure. This thesis is a part of an overarching research project with as aim, determining the load bearing capacities of composite and hybrid box and I-girders with a trapezoidal corrugated steel web.

The conducted literature review forms a basis for the study. With this acquired information, the load bearing capacities, namely the shear and bending capacities, are hand calculated. The results from these hand calculations are used in the FE-modelling[1] of the specimens. The found results from the hand calculations and the FE-modelling are verified and used to determine the correct experimental setup. The experimental phase itself, to verify the computational results, is not part of this project.

The aim of the diploma thesis is to check the conceptional design of the laboratory tests and to predict the bending and shear buckling resistance and the M-V interaction behaviour of the composite or hybrid girders with trapezoidal corrugated web. Further aim is to verify that the capacity of the Structural Laboratory of the Department of Structural Engineering at BME is sufficient for the planned research program.

[1] FE-modelling: creating a model for Finite Element Analysis

Abstract in het Nederlands

Sinds de jaren zestig is er onderzoek gaande naar het gebruik van koker- of I-liggers met trapeziumvormig geplooide lichamen. Vanwege de voordelen, worden de geplooide lichamen in veel brugconstructies toegepast. Ontwikkelingen omtrent de samenstelling van de balk worden continu geïmplementeerd. Deze scriptie is een deel van een onderzoeksproject met als doel, het draagvermogen van samengestelde koker- en I-liggers te bepalen.

Het uitgevoerde literatuuronderzoek vormt een basis voor het onderzoek. Met behulp van deze verkregen informatie worden de draagvermogens, namelijk de dwarskracht- en momentcapaciteiten, met de hand berekend. De resultaten van deze handberekeningen worden gebruikt in de EEM[2] berekening. De gevonden resultaten van de hand berekeningen en EEM-analysen worden geverifieerd en gebruikt ter bepaling van de juiste experimentele testopstelling. De experimentele fase zelf maakt geen onderdeel uit van deze scriptie.

Het doel van de diplomascriptie is om het conceptontwerp van de laboratorium testen te controleren en de buig- en afschuifsterkte en M-V interactiegedrag van de composiet of hybride liggers met trapeziumvormig geplooide lichamen te voorspellen. Verder is het doel om na te gaan of het structureel laboratorium van het departement Structural Engineering van op BME voldoende capaciteit bezit voor het uitvoeren van het geplande onderzoeksprogramma.

[2] EEM: Eindige Elementen Methode

Introduction

Background

The first real appearance of an I-beam or -girder was around 1849. The advantages of the cross-sectional composition were recognised and patented by Alphonse Halbou of the company Forges de la Providence. The company produced I-beams by rolling it from a single piece of steel. Not long after, the first compound I-girders were fabricated [1]. Compound girders are often a collaboration between concrete and steel. Concrete for its high compression capacity and steel for its high tensile capacity.

The main advantages of the composition, that helped the I-girder to become widely used in the engineering world, are a result of the high load bearing capacity combined with a relatively low self-weight. The high load bearing capacity is a result of the cooperation between the flanges and the web. The web takes on most of the shear forces, while the flanges resist most of the bending moment experienced by the girder. On the other hand, the development should only be applied where its benefits can be exploited. The cross-section has a reduced capacity in the transverse direction, and is also inefficient in carrying torsion because of its cross-sectional composition.

The I-girder with a corrugated steel web, is a variation on the standard I-girder. The main difference finds itself of course in the fact that the web is corrugated instead of a flat plate. The corrugation of the web results in a higher resistance against web buckling. Therefore, the thickness of the web can significantly be reduced without the need for extra stiffeners. Reducing the thickness of the web contributes to a decrease in dead weight of the structural elements and therefore the entire structure. Decreasing the weight facilitates the transport and the installation of the structural elements, and lowers the need for extensive supporting structures. Because of these, but also other advantages of the I-girder with corrugated web, this development keeps gaining popularity since its creation by Swedish engineers in 1966.

Objectives

The purpose of this master's thesis is to investigate the load bearing capacity of compound girders with corrugated steel web. Further, the aim is to – through FE-analyses – study how the flexural and shear capacity of a girder with corrugated steel web is affected by changes in the load setup and the composition of the girder. Also, the composition of the experimental setup is discussed and the capacity of the laboratory at BME, which is needed for the tests to confirm the obtained results, is verified.

Method

In order to reach the aforementioned aim, the project is divided into six stages: Initially, a literature review is conducted to achieve deeper knowledge of the subject and to locate the best composition of the cross-section of compound girders with corrugated webs. Included in this stage is a study in which the objective is to investigate the best way to hand calculate the load bearing capacity for the compound I-girders. Secondly, the research specimens and their accompanying load situations are presented. After this, hand calculations, to find the ultimate loads based on the flexural and shear capacities of the concerned girders, are performed. In the fourth step, based on the girders that will be used in the contemplated experimental tests, FE-models are created and analysed with software tools ATENA and ANSYS, to determine the behaviour of the girders exposed to the discussed load situations. For ATENA, the modelling is executed with pre and post processing software GiD. In the fifth stage the contemplated experimental test setup is discussed. As a final step, the obtained results are validated, compared and discussed on the basis of a parametric study, and the capacity of the laboratory of BME is checked.

Limitations

The scope of this project is limited as follows:

- girders with webs of constant depth will be analysed;
- loads are placed on the top flange and at positions within positive moment;
- the corrugation profiles regarded in this thesis will be of trapezoidal shape and will only differ in plate thickness and height;
- the main focus will be on the results concerning the ultimate loads;
- all examined girders have the same length;
- the composition of the upper flange is the same for every examined girder.

Outline and content

In chapter 1, a literature review to form a basis for this research is presented involving a historical general background research of the compound girder with corrugated web. More specific, also the bridge erection methods, shear behaviour, bending behaviour, M-V interaction and the possible joint compositions are discussed.

In chapter 2, the setup of the load situations and the compositions of the girders that is used for the FE-modelling and hand calculations are presented. The features presented in this chapter will of course also be implemented for the experimental tests.

In chapter 3, the hand calculations for the shear and moment capacity of the concerning girders are given. With these obtained capacities, the ultimate loads of the accompanying load situations are calculated.

Chapter 4 presents the finite element modelling and analyses of the examined compound girders. The aim is to provide a preliminary estimate for the ultimate load bearing capacity and to investigate the structural behaviour of the girders.

Chapter 5 presents the experimental phase. The results of the experimental phase are not part of this research due to delay during the manufacturing of the specimens by construction company Rutin.

Chapter 6 presents the results from the FE-modelling. The results are divided into two main sections according to the numerical analysis software used to simulate the behaviour of the discussed specimens under the influence of their accompanying load situations.

Chapter 7 composes a discussion of the found results. The influence of the parameters web thickness, girder type (hybrid or composite) and load situation are discussed. A separate section is also dedicated to the verification of the experimental setup and capacity of the BME laboratory.

Chapter 8 includes the conclusions and suggestions for further research.

1 Literature Review

This chapter is divided into six sections: Background; Bridge erection; Shear Behaviour; Bending Behaviour; M-V interaction; Connections. The first section provides a base for this project by going over the background of the discussed subject. This involves a summary of the advantages, the historical background, some example applications and a composition explanation. In the second section, the contemporary bridge erection methods are discussed. After this, the third section presents information concerning the shear behaviour of compound girders with corrugated webs. The fourth section focusses on the information about the bending behaviour, and the fifth section discusses the shear and bending resistance interaction in the girders. The last section concerns the connection between the different materials (concrete and steel) of the compound girders.

1.1 Background

Compound girders with corrugated steel webs and concrete slabs, as shown in Figure 1, are one of the promising concrete-steel hybrid developments used in bridges.

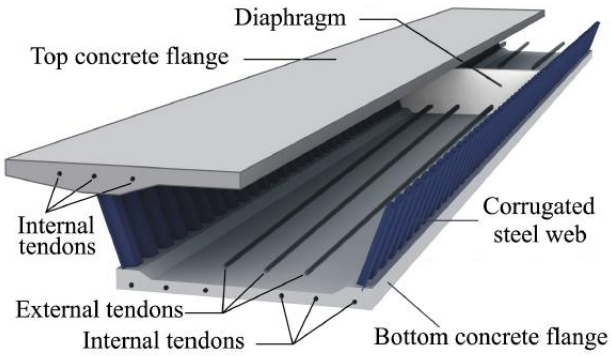

Figure 1: Typical box girder with corrugated steel webs [2] p.2

The general idea of using compound products is to achieve better performance and utilize the best of each material. Concrete is good in compression but weak in tension, while steel is good in tension but tends to buckle under compression. The combination of prestressed concrete and steel, both used under the influence of forces against which they can offer the highest resistance, makes the development ideal for load bearing situations, while keeping a relatively low self-weight. Lower self-weight can result in a larger possible span and less extensive supporting structures. With a correct design, the strength, stability of the structure and the material efficiency can be improved. The features of corrugated steel webs, see Figure 2, lead to advantages for composite constructions.

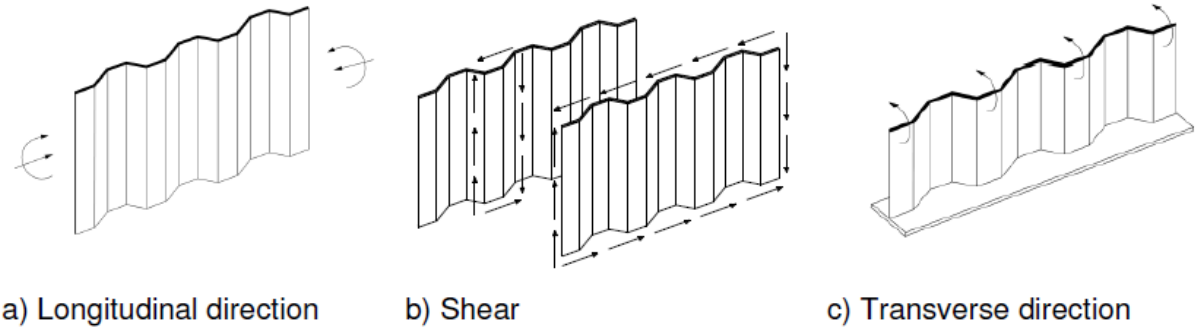

Figure 2: Stiffness depending on the direction of stress [17] p.12

Due to the use of corrugated webs, no restraint will exist between the concrete slabs and the web because of the small stiffness in the longitudinal direction (situation a in Figure 2). Because of this, structural tensions that are a result of creep of concrete, drying shrinkage, and temperature differences between slabs and webs, can be alleviated. This effect that comes with the use of corrugated steel webs, named 'accordion effect' also substantially improves the effectiveness of prestressing when applying prestressing reinforcement in the concrete flanges of the beam [2], [3].

Listed below are functional benefits of replacing the conventional webs of box or I-girders with corrugated steel webs.

- The reduction in dead weight compared to concrete webs, leads to less sizable substructures, less labour-intensive placement, and less necessary precautions in the seismic design of the structure, which will result in lower construction cost and a greater possible span of the girder.
- Higher resistance to in-plane shear forces due to narrow folds (see situation b of Figure 2), combined with higher transverse stiffness due to the corrugation depth, results in higher resistance to local and global buckling of the web.
- The corrugated steel webs have higher shear buckling resistance and out-of-plane flexural stiffness, see Figure 2 situation b respectively c, compared to flat steel webs with the same thickness. This means that the number of intermediate diaphragms or stiffeners can be significantly reduced in girders with corrugated webs.
- The fabrication process of girders with corrugated steel webs is less complicated in comparison with the fabrication process of girders with concrete webs. Elimination of the need for concrete placement for the webs ensures a reduce in field work and labour.
- Prestressing can be efficiently performed in the top and bottom concrete flanges, due to the so-called 'accordion effect' of corrugated steel webs. Because of this effect no residual stress will remain in the web after prestressing of the flanges. Also, shrinkage, creep or temperature effects will not induce residual stress in the corrugated steel web. The residual stress that arises in non-corrugated webs due to for example the prestressing of the flanges, decreases the load bearing capacity of the beam.
- The possibility to use external tendons to improve cross-sectional efficiency. Usage of external tendons instead of internal tendons can result in easier maintenance and replacement of the prestressing elements.
- In a correct setup, where the two parts are used efficiently (reinforced or prestressed concrete flanges to sustain flexure and steel webs to carry shear forces.), the collaboration of the two materials can lead to a product with large load bearing capacities and a smaller dead load. This because of the fact that the shear forces can be optimally distributed into the corrugated steel webs, while the bending forces can be distributed in the concrete slabs.
- The stiffness of compound girders compared to solely steel compositions, with the same load bearing capacity, is much higher. Therefore, the structural height can be decreased. A higher stiffness is also favourable because it can provide a stiffer superstructure, which is opportune for the isolation, the covering and the lifespan of the structure.

These are some of the more important advantages of compound girders with corrugated webs [2], [3], [4], [5], [6].

In bridge constructions two different structural compositions can be subdivided for the compound girders with corrugated steel webs: the 'composite' and the 'hybrid' composition. 'Composite' girders are box or I-girders with a reinforced concrete upper flange, a steel web and a steel lower flange. In case of 'hybrid' structures, both flanges are made of reinforced concrete, and only the web is made of steel. Usually the web has a corrugated profile, but other shaped or fabricated webs are also possible.

The most important building materials of this time are steel and concrete. The large geographical spread and usage range of these materials is a result of the many advantageous properties. Every material has also its own disadvantages. As a result, the materials are preferably used in applications where their benefits come out as much as possible. The 'composite' and 'hybrid' girders combine the beneficial properties of steel and concrete, while the disadvantages are avoided as much as possible. These developments have multiple advantages, and depending on the situation, they also have certain disadvantages. One of the disadvantages of this compound product is that its composition might complex the calculations of the structure. Hand calculations but also computer aided calculations (during processing or calculation phase) will become more time consuming and there will be more possibilities for errors. As a second disadvantage, the arrangement for constructing the composition may be more difficult to fabricate. The shape of the corrugated web can easily deform during the concreting as a result of the small web stiffness in the longitudinal direction and the time-changing properties of the concrete. By use of proper calculations and implementations this problem can be avoided. The span range of these girders used in bridge constructions is from 15 m up to 120 m. Both lower and upper limit have economic reasons [6].

The idea of using corrugated steel plates to manufacture the web of beams, finds its origin in the design of buildings. The advantages of box or I-girder compound elements with corrugated steel webs for bridge constructions, were first recognized in 1982 by the French company Campenon Bernard BTP. Alongside of considerable theoretical analyses, as an experimental bridge the first highway bridge using corrugated steel webs in combination with external prestressing, named the Cognac Bridge, was built in France in 1986. The Cognac bridge (that crosses the Charente river) has a continuous prestressed box girder with a trapezoidal corrugated steel web (see Figure 3).

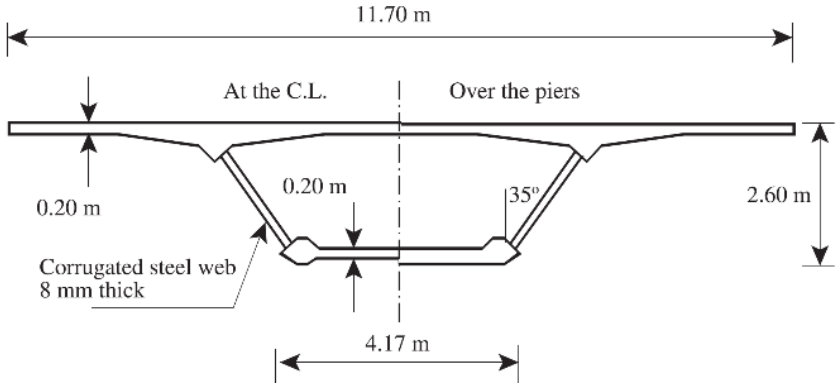

Figure 3: Cross-section of the Cognac Bridge box girder [5] p.658

The total length of the three-span bridge is 107.82 m, which includes an intermediate span of 42.91 m and two side spans of 32.455 m each. The top and bottom concrete flanges in the cross-section of the box girder (see Figure 3) are respectively 11.70 and 4.17 m wide. The trapezoidal corrugated web has a thickness of 8 mm with a corrugation panel (or fold) width of 420 mm, a panel height of 1.771 m, a corrugation depth of 240 mm, and is placed at a 35 degrees angle. The total depth of the box girder is 2.60 m. The bridge is longitudinally prestressed with four Freyssinet tendons, each made of nineteen 5/8-inch strands. These prestressing tendons are fitted inside the box girder and are anchored into solid reinforced concrete blocks at the ends of the deck [5].

Subsequent to the success of the Cognac Bridge, three more bridges with trapezoidal corrugated steel webs were built in France during the period from 1987 to 1995. In 1987 the Val de Maupre Viaduct, that crosses the river Charente, was built (see Figure 4).

Figure 4: Val de Maupre Viaduct [24] p.1

It is a 7 span 324 m long bridge with spans between 41.00 and 53.55 m. The cross-section has a triangular shape with a concrete top slab (see Figure 5).

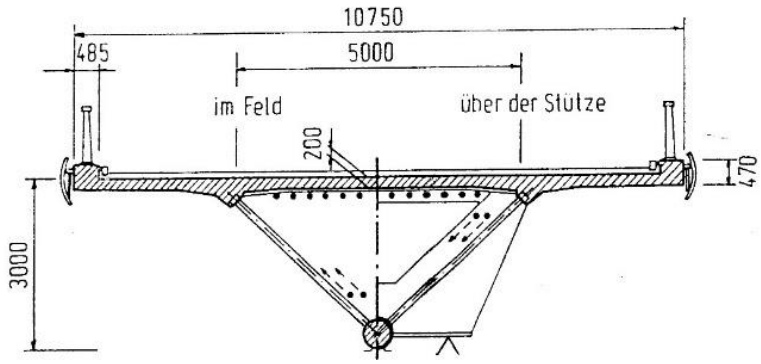

Figure 5: Cross-section of the Val de Maupre Viaduct, dimensions in mm [6] p.13

The inclined webs are made of corrugated steel and are connected at the bottom of the section with a steel tube. The steel tube is filled with concrete [5], [6].

The total width of the cross-section is 10.75 m, and the height 3.00 m. The upper part of the triangular construction is closed with a 1.2 mm thin steel plate that was used as formwork during construction of the concrete slab. The corrugation depth of the steel plates is 180 mm, the length of one fold is 300 mm and the thickness of the plate is 8 mm (Figure 6) [6].

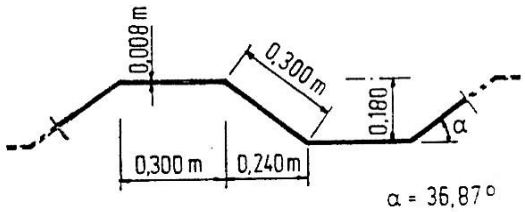

Figure 6: Corrugation of inclined steel plates in Val de Maupre Viaduct [6] p.13

The Val de Maupre Viaduct was followed by the Parc Asterix Bridge, that was completed in 1989, and the Dole bridge that was finished in 1995. Many girder bridges with corrugated steel webs have subsequently been constructed in other countries around the world, such as the Tronko Bridge in Norway, the Alterwepfergrund Bridge in Germany, the Caracas Bridge in Venezuela, the Ilsun Bridge in Korea, and the Shinkai Bridge in Japan. The Shinkai Bridge, built in 1993, gave the start of the proliferation of these structures in Japan, which is often hit by strong earthquakes. The cross-section of this bridge exists out of twin box girders and has a skew angle of 70°. The width of the deck is 14.80 m and it spans 30 m. The dept of each box girder is 1.90 m, the lower concrete flange is 2.10 m wide and the height of the corrugated steel plate is 1.183 m. The bridge is longitudinally prestressed with internal and external cables. Secondly in Japan, the Matsunoki bridge (also known as the Ginzan-Miyuki Bridge) was completed in 1995, followed by the Hondani Bridge in 1997. The Matsunoki bridge is a 5 span bridge and has a total length of 210 m and a deck width of 9.30 m. The cross-section is presented in Figure 7:

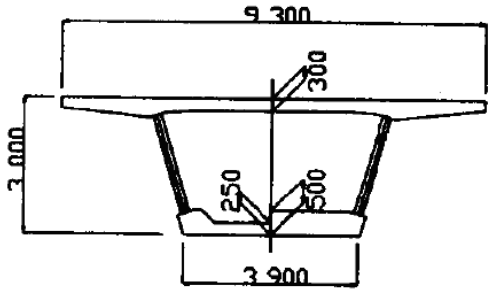

Figure 7: Cross-section of the Matsunoki bridge, dimensions in mm [6] p.15

The approach span is 27.40 m long and the other four spans are each 45.50 m long. The dept of the box girder is 3 m and the corrugated steel web has a thickness of 8 or 12 mm and a panel height of 2.21 m. The bridge with corrugated steel webs did not make its appearance in China until 2005, when the Huaian Changzheng Footbridge was constructed. The number increased considerably since then and present there are more than 30 of this type of bridges build in China. In addition to its use in box and I-girder bridges, corrugated steel webs have also successfully been adopted in cable-stayed PC[3] girder and extradosed[4] bridges [2], [3], [5], [6].

A considerable amount of theoretical and experimental studies on girders with corrugated steel webs have been carried out since the 1970s. In steel beams with corrugated webs, the flexural strength is provided by the flanges, with almost no contribution from the web. Furthermore, there is no intercommunication between the bending and shear behaviour. Thus, the moment and shear resistances of steel beams with corrugated web can be examined dissociated from each other. This attribute was also investigated for compound girders with corrugated steel webs and concrete prestressed flanges. For the investigated compound girders, the same conclusion was found. A lot of compound girder compositions are possible, for example: compound box girders, T-girders, I-girders, etc. In this project, the focus is mainly on the compound I-girders. Certain conclusions can nevertheless be extended to the other compositions. An example of a compound I-girder with corrugated steel web is given in Figure 8.

[3] PC: Prestressed Concrete

[4] Extradosed: an extradosed bridge is a structure which combines the main elements of both a prestressed box girder bridge and a cable-stayed bridge

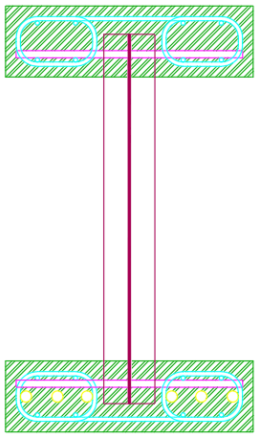

Figure 8: Cross-section example 'composite' I-girder with a corrugated steel web

The shear capacity of a steel or compound I-girder with corrugated steel web, depends on the properties of the steel web. The flexural strength of an I-girder can be based on the tensile yield strength of the flange under tension and the compression strength of the flange under compression. For the 'composite' I-girder given in Figure 8 this means that the flexural capacity (if subjected to downwards pointing loads while simply supported at both ends) is based on the yield strength of the tendons in the lower flange and the compression strength of the upper flange [2].

1.2 Bridge erection

Many bridge construction techniques were developed in the past. The choice of construction technique is depending on environmental conditions, economic factors, aesthetics, available time, etc. In this section some important contemporary techniques that can be used for composite girder bridges are cited.

1.2.1 Incremental launching method (ILM)

The name of this bridge construction technique reveals the working process: incremental launching method. Incremental stands for the fact that the spans are accomplished in steps (or increments). Launching refers to the movement manner that happens by longitudinally pushing (or launching) the structure to the next pillar. Figure 9 presents an execution example of the incremental launching method in use.

Figure 9: Execution example incremental launcing method [25]

The principle of the incrementally launched bridge consists of building the superstructure segments in a casting yard placed behind the bridge abutment. Each segment is constructed against the already existing superstructure. The entire superstructure is then jacked forward as far as the length of this newly made segment (see Figure 10).

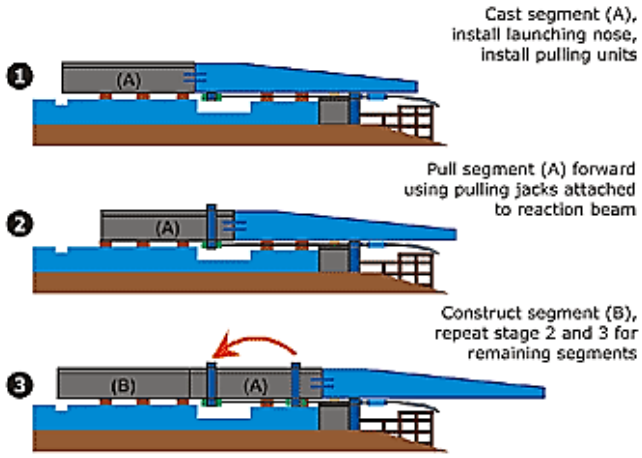

Figure 10: Construction cycle incremental launching method [8]

This process is repeated until the bridge is in its final position. The construction technique can be used for bridges with a constant cross-section throughout their length. The bridge should be straight or have a constant horizontal and vertical curvature [8].

Some advantages of the incremental launching method are:

- minimal disturbance to surroundings;
- little space necessary for superstructure assembly;
- high work safety since all erection work is performed near the abutment (on low elevation);
- can be used for composite and prestressed girders;
- can be used to construct over a wide range of challenging sites which feature limited or restricted access, like deep valleys, steep slopes or poor soil conditions making equipment access difficult, environmental protected area, etc [9].

1.2.2 Cantilever construction technique

The cantilever construction technique uses the upper part of the pillars of the structure as yards to build the spans while keeping the pillars in balance. Figure 11 provides an execution example of the cantilever construction technique.

Figure 11: Execution example cantilever construction technique [27]

The cantilever construction technique can be executed as cast in place segmental (Figure 11) or precast segmental method. When scaffolding and other temporary supports are difficult to install (like previous example given in Figure 11), this method saves all temporary work and allows bridges to be built at great heights. Once the pillars are built, they are used as an erection platform from where the spans are built. This technique is not serviceable for bridges made with prestressed girders because the rather small parts must be added one by one and should immediately be ready to work load-bearing [10].

Some advantages of the cantilever construction technique are:

- the system is easily adaptable to irregular and long span lengths;
- it is the preferred method for construction of cable-stayed bridges (once segments are positioned, they are supported by new cable-stays in each erection stage);
- it can be used to construct over a wide range of challenging sites which feature limited or restricted access, like deep valleys, steep slopes or poor soil conditions making equipment access difficult, environmental protected area, etc [10].

1.2.3 Span by Span technique

Span by span technique is a relatively new construction technique, historically associated with the cantilever construction. The advancement in external prestressing has helped to ensure the potential of this precast segment technique. Today it is considered to be one of the most economic and rapid methods available for long bridges and viaducts with individual spans up to 60 m. Figure 12 presents two execution examples of the discussed technique.

(a) (b)

Figure 12: Execution example span by span construction technique: (a) with assembly structure, (b) with temporary falsework [11]

As can be seen from Figure 12, there are different execution possibilities to position and keep the segments in place. The spans are made one by one, by positioning the needed segments and then running longitudinal prestressing tendons through the segments ducts to prestress the total span. Deck joints are then casted and closed and ducts grouted. When the span is complete, the assembly structure or temporary falsework is moved and the cycle starts over for the next span [12].

Some advantages of the span by span technique are:

- often the economic and less time-consuming choice;
- when chosen for the assembly structure not much space is needed;
- can be used for composite and prestressed girders;
- segments are precast in factory casting environment and therefor have very high concrete material quality;

- can be used to construct over a wide range of challenging sites which feature limited or restricted access, like deep valleys, steep slopes or poor soil conditions making equipment access difficult, environmental protected area, etc [12], [11].

1.2.4 Full span technique

As the name would suggest, the full span technique positions a hole span in one time. The technique is a precast segmental technique and can be performed by use of for example a launching gantry or heavy lift. Both these options are presented in Figure 13.

(a) (b)

Figure 13: Execution examples full span construction technique: (a) with launchin cantry, (b) with heavy lift [11]

The construction cycle is straightforward: the precast spans are one by one positioned in full [11].

Some advantages of the full span construction technique are:

- minimal follow up work;
- quick construction on site;
- can be used for composite and prestressed girders;
- segments are precast in factory casting environment and therefor have very high concrete material quality;
- if adjusted to the situation, it can be used to construct over a wide range of challenging sites which feature limited or restricted access, like deep valleys, steep slopes or poor soil conditions making equipment access difficult, environmental protected area, etc [11].

Bridges constructed with corrugated compound box or I-girders (as discussed in this thesis) can best be made with a precast construction method. Casting in situ would complicate the process enormously because of the corrugated steel web. Working based on the span by span technique is possible but after prestressing, the webs between all segments should be welded together and this again complicates the construction process. The full span technique is a good technique for this kind of structures because large prefabricated parts are positioned at once.

The following part of the literature review is subdivided according to the major characteristics of structural behaviour of the compound I-girders. As main subdivisions of the structural behaviour for the girders with corrugated steel webs, shear behaviour, bending behaviour and the connection between the web and flanges will be investigated in following sections [7].

1.3 Shear Behaviour

Corrugating of steel plates can ensure higher resistance against shear buckling, which reduces the need for stiffeners. The shear behaviour of corrugated steel plates has been extensively studied, starting with the research of Shimada in 1965. Easley and McFarland came in 1969 with their proposal for a global shear buckling equation of corrugated webs by treating it as a flat orthotropic web. The corrugated steel web is assumed to resist the occurring shear forces on the girder and thus provide the girder with its shear capacity. The shear strength of the girder is controlled by buckling and/or shear yielding of the steel web. Linder and Aschinger presented in 1988 test results for the shear strength of trapezoidal corrugated webs and suggested to use 70% of the shear buckling stress as nominal shear strength for the design calculations [3], [13].

Another important issue concerning the shear behaviour of PC girder bridges with corrugated steel webs, is the distribution of shear between the corrugated web and concrete slabs. In generally it is assumed that the shear forces are resisted by the steel webs. By conducting experiments on scaled models and simulation of finite element analyses, Shiratani et al. (2002) found that the measured shear stress carried by the corrugated steel web, especially in the region around the middle support, was smaller than the calculated value. This would be a result of the restraint by concrete slabs against shear deformation of the web. Even after the formation of cracks, this behaviour remained significant. Shiratani el al. could conclude that if appropriately reinforced, a concrete flange can carry significant shear and improve the global shear resistance of a composite girder with corrugated steel web. By conducting experiments on full- and half-size models, Shitou et al. (2008) found that by propagation of cracks in the concrete slabs, the contribution of the corrugated steel webs to shear increased, but gradually decreased after reaching the yield strength of the slab. From experiments on a simply supported PC girder with a corrugated steel web, Kadotani et al. (2002) determined that 65% of the acting shear on the girder was resisted by the web. This value will decrease after reaching the yield strength in the corrugated steel web. In 2004 Kano et al. developed an economical and practical method to design the corrugated steel webs by starting from the investigation of the distribution of shear forces between the corrugated steel web and the concrete flanges while considering the shear lag effect[5] [2].

Fujioka and Kauta performed in 2005 full-scale one-point loading tests on a model of the main girder of the Sougawa River Bridge from Ishikawa, Prefecture. Investigation of the results showed that the measured shear stress in the corrugated steel web of the test was found to be rather small compared to the conservative design value (see Figure 14).

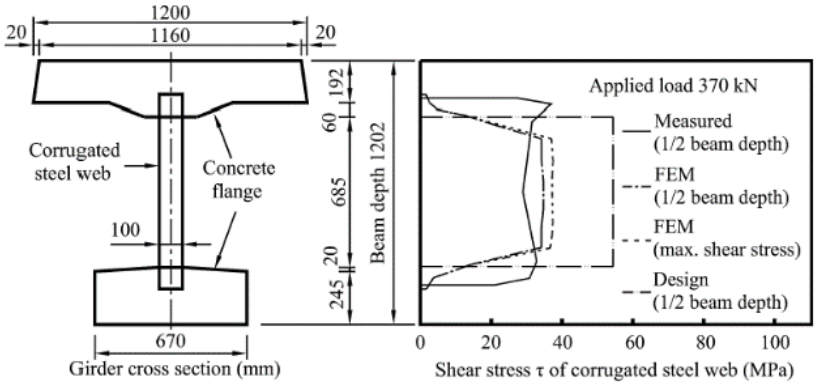

Figure 14: Shear stress distribution of corrugated steel web (data from Fujioka and Kakuta 2005) [2] p.3

[5] Shear lag effect: Uneven shear stress distribution across length or cross-section area of a member or connection.

This is a result of the fact that in the design calculation the shear is assumed to be resisted exclusively by the corrugated steel webs, hereby excluding the parts of corrugated steel embedded in the concrete flanges. In practice, the embedded corrugated steel and the concrete flanges will also absorb a part of the shear stresses that gets distributed in the girder. The difference in shear stress between the test results and the finite element analysis may be caused by the simplifications of the connections between the concrete flanges and the steel webs in the modelling. Fujioka and Kauta have successfully proved the fact that the shear stress in the girder is not only resisted by the web, but also by the embedded corrugated steel in the flanges and the concrete flanges. Therefore, it can be concluded that the characteristics of the shear connector between the corrugated steel web and the concrete flanges may affect the overall shear strength of the PC girder with corrugated steel webs [2].

Shear behaviour of prestressed compound sections with corrugated steel webs is mainly depending on the characteristics of the steel web. The stresses in the steel web are almost pure shear stresses, what means that the instability problem, almost always shear buckling is. In 1981, the Division of Steel and Timber Structures at Chalmers University of Technology, began research on the shear behaviour of girders with

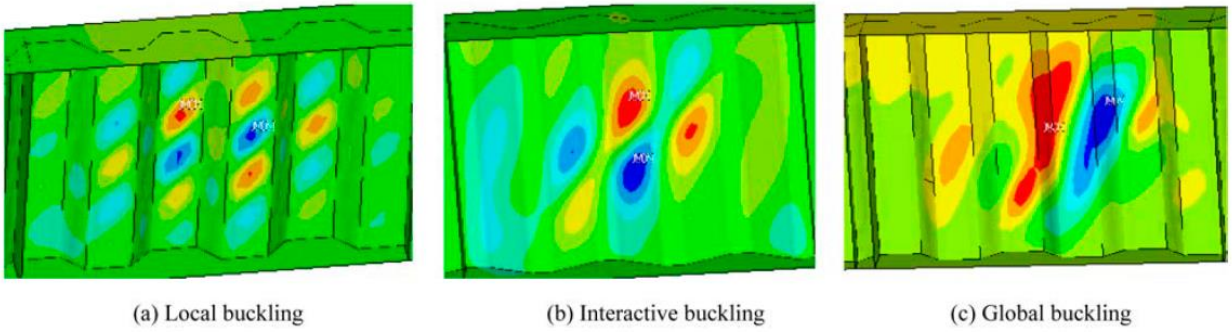

Figure 15: Shear buckling modes [3] p.324

trapezoidal corrugated webs. Experimental tests were performed on 15 girders with varying depth (low, medium and deep) in order to study the buckling behaviour. From the test results, it was observed that the failure mode was dependent on the depth of the girder. Based on experimental and numerical studies of shear behaviour for corrugated web girders, it can be noted that shear buckling of corrugated webs is often classified as either local buckling (Figure 15a) or global buckling (Figure 15c). The interactive shear buckling mode (Figure 15b) is attributed to the reciprocity between local and global buckling modes. Local shear buckling corresponds to the deformation within a single flat steel panel or fold of the web. This instability problem is critical for corrugated webs with deeper folds. Global shear buckling of a corrugated steel web on the other hand is similar to the buckling mode observed in a flat orthotropic plate. Logically, the global shear buckling mode is critical in webs with shallow folds. Corrugated steel plates produce a higher resistance against shear buckling compared to flat steel plates, leading to elimination of stiffeners. Generally, local buckling is controlled by the slenderness of the individual folds of the web. The global buckling is then controlled by the slenderness of the entire web [2], [3], [14].

Figure 16 shows a comparison of experimental results and predicted shear strength based on the relation

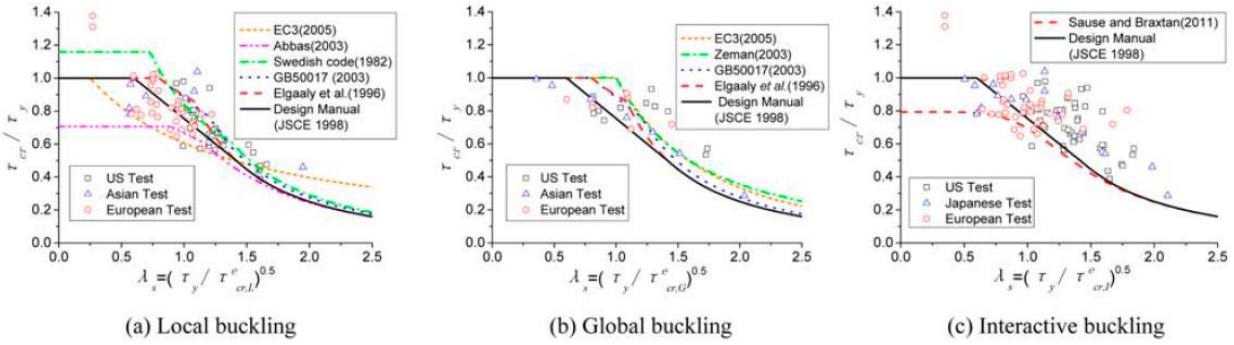

(a) Local buckling (b) Global buckling (c) Interactive buckling

Figure 16: Comparison of experimental and predicted shear strength [3] p.324

between nominal shear stress (critical buckling stress τ_{cr}/yield shear stress τ_y) and slenderness λ_s, made by He (2011) for steel girders with a corrugated web. For the specimens failed by local buckling (Figure 16a), Abbas (2003) underestimates the test results, while the Swedish code (1982) overestimates the results. The values predicted by the Design Manual (JSCE 1998) provide practically an average of the test results, while the values calculated with EN 1993-1-5 (2005) approximately provide a lower limit of the test results. Using the EN 1993-1-5 during the design stage is therefore a safe consideration. For global buckling (Figure 16b), EN 1993-1-5 (2005) and Zeman (2003) practically provide the same results, and here the Design Manual (JSCE 1998) delivers a lower limit that for safety considerations can be used during the design stage. The most disparate values can be found in the non-elastic region ($0.7 < \lambda s < 1.0$), and may be caused by residual stress and initial geometric imperfection of the corrugated web. The interactive buckling mode results from the interaction between the local and global buckling modes. To verify the applicability of the interactive buckling concept, the test results of the local and global buckling were compared with the Design Manual (JSCE 1998) and the formula provided by Sause and Braxtan (2011) (Figure 16c). The calculated values of Sause and Braxtan (2011) provide the lower limit of the test results. All the critical buckling stress in the test was calculated as interactive buckling ($\tau_{cr,I}$) [2], [3].

When discussing the stability of the web, it is stated that two buckling modes are associated with corrugated webs: local and global buckling. According to Sayed-Ahmed (2005), the local buckling mode is corresponding to the instability of a flat panel simply supported by two adjacent folds. The support is generated by the corrugation alignment of the web which acts as a series of flat panels mutually supporting each other. Similar as for flat webs, the critical shear stress $\tau_{cr,l}$ for the local buckling mode can be derived from the theory of stationary potential energy. Undermentioned, the equation given in Eurocode 3 for the local critical shear stress of a trapezoidal corrugated web:

$$\tau_{cr,l} = 4.83 \cdot E \cdot \left[\frac{t_w}{a_{max}}\right]^2$$

Here, a_{max} should be taken as the greater of a_1 and a_2 (see Appendix A) [15], [14].

The buckling mode for global failure is characterized by diagonal buckling over multiple folds or panels. In 1969, Easley and McFarland presented an equation to calculate the critical shear stress for global buckling:

$$\tau_{cr,g} = k_g \frac{\sqrt[4]{D_y \cdot {D_x}^3}}{{h_w}^2 \cdot t_w}$$

The global buckling coefficient k_g is stated as 32.4 in Eurocode 3 [15], [14].

Based on these equations, Eurocode 3 prescribes to determine the slenderness of respectively the local and the global buckling mode. With these, the reduction factors per mode can be calculated and at last the shear capacity of the corrugated web [15].

1.4 Bending Behaviour

Due to the 'accordion effect' of corrugated steel plates, the flexural strength of steel girders with corrugated steel webs is provided by the flanges with almost no contribution form the webs. In other words, only the upper and lower concrete flanges of the girders are considered to resist the bending moments and axial forces acting on the bridge deck. Furthermore, there is no interaction between the bending and shear behaviour of these girders. Therefore, the maximum flexural capacity of steel girders with a corrugated steel web can be based on the yield strength of the flanges. For design purposes, the normal ultimate moment of a steel I-beam with corrugated steel web may be defined by Equation (1):

$$M_{ult} = \left(b_f \cdot t_f \cdot f_{ys}\right) \cdot \left(h_w + t_f\right) \tag{1}$$

In which b_f and t_f are respectively the width and the thickness of the flanges, h_w is the height of the web and f_{ys} is the yield stress of the steel used for the flanges. Based on various experiments and analyses, the hypothesis that plane sections remain plane for compound girders as for steel girders has been verified, meaning that previous aspects defined for steel girders are also applicable to compound girders with flanges made of reinforced concrete and the web of corrugated steel. For these compound members, the ultimate moment capacity M_{ult} may be calculated considering that the top flange carries the compressive stresses and the prestressing tendons in the bottom flange carry the tensile stresses. Metwally and Loo confirmed this theory in 2003 with their investigation on the flexural capacity of compound girders with corrugated steel webs [2], [3], [5].

Many investigations on the flexural behaviour of corrugated web girder bridges have been executed focussing on steel I-beams with corrugated webs. In 1997 Elgaaly et al. concluded that the contribution of the corrugated web to the flexural rigidity of an I-beam to be negligible. Similar work was done by El-Metwally in 1999. El-Metwelly completed an experimental investigation on the behaviour of composite prestressed beams with corrugated steel webs. The dimensions of the experimental beams (in particular the relative dimensions and the span to depth ratio) were chosen to be comparable to those of practical bridge girders. Since I-shaped girders are easier to construct and the obtained results are also applicable to box girders, only I-girders were tested. Also, for the same reasons a zigzag profile instead of a trapezoidal folding was chosen for the corrugated webs of all the tested girders. Five different fold widths were chosen for the corrugation: 80, 110, 175, 215 and 285 mm. The plate thickness was 0.91 mm and the corrugation angle 20° for all test girders. The top and bottom concrete flanges were respectively 100 and 130 mm thick. For each beam the bottom flange was prestressed using three concentric straight 7-wire strands. All the beams were tested in the four-point loading test. A typical load-deflection curve for one of the tested beams is plotted in Figure 17.

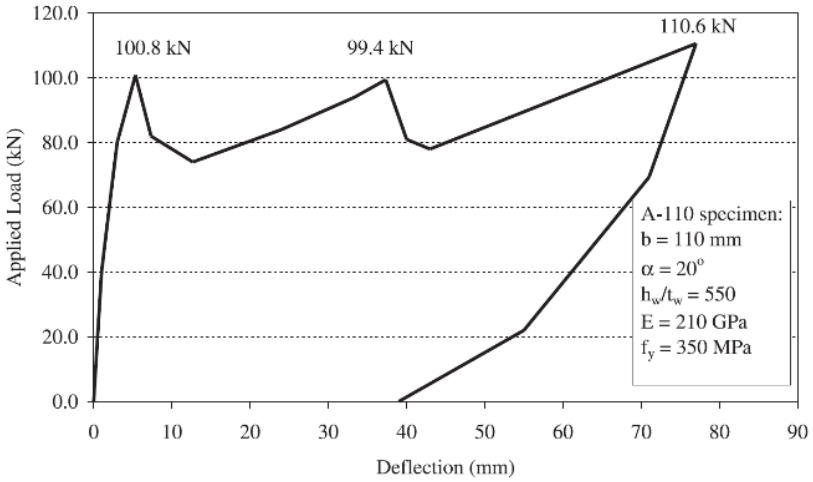

Figure 17: Load–deflection curve of specimen A-110 tested in four-point loading test [5] p.664

The flexural behaviour for the five girders is similar in the sense that there is an initial load peak and that the failure load exceeds the value of this initial load peak by 5 to 15%. For a conservative approach in the design, the initial peak may be considered as the ultimate load for the beam. This value can be calculated with a formula based on the same idea as Equation (1). With their test results, El-Metwally and Loov could find two basic conclusions that earlier were also demonstrated for steel beams with a corrugated web: the contribution of the corrugated steel web to the flexural strength of a compound beam is negligible and there is no intercommunication between the flexure and shear behaviour of the beam. This means that the ultimate moment capacity (M_{ult}) of a composite prestressed beam with steel corrugated web may be calculated considering that the top flange carries the compressive stresses and the prestressing reinforcement in the bottom flange carries the tensile stresses. In 1988 Combault found a similar conclusion while studying the PC box girder bridge with corrugated steel webs [2], [5].

Investigation of the effect of web corrugation on the strength of steel beams was conducted by Chan et al. in 2002 and by Khalid et al. in 2004. By making use of finite element method, it could be concluded that corrugated steel web beams with larger corrugations are able to resist to higher bending moments. Watanabe and Kubo (2006) performed pure bending tests and numerical analyses of corrugated web girders on four different trapezoidal corrugation configurations. Also, based on the parametric analysis of corrugated web girders, a predicting method of the maximum strength considering local flange buckling was proposed. As for the steel I-girder with corrugated web, local buckling of the flange under compression affects the bending strength of the girder. To prevent local buckling of the flange before yielding, the limitation on the flange outstand-to-thickness ratio should be satisfied. Based on the investigation of Johnson and Cafolla in 1997, it was recommended that the average flange outstand b_{av} may only be used if a ratio R is less than 0.14, with R the ratio of area EFGH to area ABCD (see Figure 18).

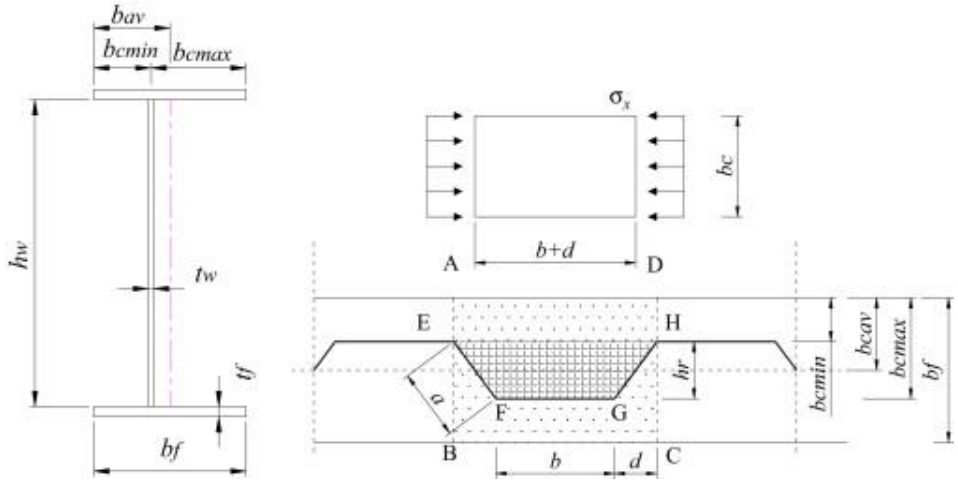

Figure 18: Outstands of compressive flange for a corrugated web [3] p.325

When R is greater than 0.14, it is suggested to be conservative by using the large flange outstand b_{cmax}. Nonetheless, a considerable uncertainty still exists regarding the right appropriate value for the flange outstand of corrugated web girders [2], [3], [5].

In 2003 Mo et al. presented experimental and analytical results of four scaled prestressed concrete box girders with corrugated steel webs. With these it was found that both thickness of end diaphragms and the location of prestressing strands at both ends of the specimens are inconsequential when the specimen fails in mid-span due to concrete crushing. He et al. (2008) evaluated the mechanical behaviour of corrugated steel web box girders with internal and external tendons under flexural load, by varying the characteristics of the internal and external tendons. Varied properties were arrangement and prestressing force of the internal and external tendons, positioning of the anchorage points, and distance of the diversion devices. Based on the quasi-plane assumption of flexural strain distribution and the axial force-bending moment-curvature relationship at cross-section, Song (2003) and Li et al. (2009) developed a nonlinear program to examine the maximum flexural capacity of the external prestressed composite box girder with corrugated steel webs [3]. Based on the experimental and analytical results mentioned above, the maximum flexural capacity of composite girders with corrugated steel webs can be determined on the basis of the strength of the concrete flanges and the prestressing forces of the internal and external tendons without taking into account the contribution from the corrugated web. This will generate a rather conservative predication.

1.5 M-V interaction

In the international literature there are many research papers dealing with the bending resistance and shear buckling resistance of corrugated web girders separately but only a few number of investigations deal with the combined loading situation. It is commonly accepted by researchers and designers, that the bending moment in a corrugated web girder, is absorbed by the flanges and the shear force by the web. It is also known from previous investigations that the shear stress in the corrugated web results in a transverse bending moment in the flanges. Different proposals are developed to determine the maximum value of this additional bending moment, but there is a very small number of investigations focusing on the effect of the modified normal stress field, on the bending resistance of the girder.

In current state of art, contradictory ideas can be found considering the influence of the additional normal stresses on the bending resistance. In the design method of EN1993-1-5 Annex D [15] a reduction factor can be found for the bending resistance of the corrugated web girders of girders which are also subjected

to shear force. The bending resistance of the corrugated web girders according to the Eurocode can be determined based on Equation (2).

$$M_{Rd} = \min\left(\frac{b_{fu}\cdot t_{fu}\cdot f_{yf}}{\gamma_{M0}}\cdot\left(h_w+\frac{t_{fu}+t_{fl}}{2}\right);\frac{b_{fl}\cdot t_{fl}\cdot f_{yf}}{\gamma_{M0}}\cdot\left(h_w+\frac{t_{fu}+t_{fl}}{2}\right);\frac{b_{fu}\cdot t_{fu}\cdot \chi\cdot f_{yf}}{\gamma_{M0}}\cdot\left(h_w+\frac{t_{fu}+t_{fl}}{2}\right)\right) \quad (2)$$

If the girder is also subjected to shear force, the bending resistance may be reduced by a reduction factor (f_T) which depends on the flange yield strength and on the maximum normal stress resulting from the transverse bending moment. The reduced bending resistance can be determined by Equation (3) and (4), provided that the value of the reduction factor χ equals to 1,0.

$$M_{V,Rd} = f_T \cdot M_{Rd} \quad (3)$$

with reduction factor (f_T) given in Equation (3):

$$f_T = 1 - 0.4\cdot\sqrt{\frac{\sigma_x(M_z)}{\frac{f_{yf}}{\gamma_{M0}}}} \quad (4)$$

In which f_{yf} stands for the yield strength of the flange, γ_{M0} for the partial factor for stress check and $\sigma_{x(Mz)}$ for the maximum value of the additional normal stresses coming from transverse bending moment.

The reduction factor given in Equation (4) was developed by Lindner [16] and was also implemented in the DASt-Richtlinie 015 standard [17]. This reduction factor however is not considered in the Austrian and Swedish design rules. The effect of the additional normal stresses on the bending resistance is not significant. The commentary document of the EN1993-1-5 [18] also emphasizes that from a theoretical point of view these bending moments are required for reasons of equilibrium. However, it is questionable how important they actually are in real life. They have been included in the code just as a precaution, for sinusoidal corrugated webs the factor is always put to 1. Elgaaly et al. (1997-1998) investigated the bending and shear resistance of the trapezoidal corrugated web girders. The found conclusion was that there is no interaction between the bending and shear resistance of the trapezoidal corrugated web girders. This is proved by Pasternak and Hannebauer (2003). They found that in case of sinusoidal corrugation profiles the effect of the additional bending moment can be neglected, and the reduction factor can be set to 1. In 2006 Kuchta proposed an M-V interaction equation for girders with sinusoidal corrugated webs. However, it has to be noted that only a small interaction behaviour is observed during the investigations [17].

Kövesdi et al. (2015) investigated the bending resistance reduction of the girders with trapezoidal corrugated webs due to the transverse bending moment originated from a shear stress in the webs [17]. In the research project numerical simulations are carried out to analyse the effect of the transverse bending moment on the bending resistance and the M-V interaction behaviour. Results of the GMNIA[6] analyses showed, there is no significant resistance reduction due to the combined loading situations. The evaluation of the numerical calculations showed, that the current proposal of EN1993-1-5 results in a conservative design. From the 20 analysed girders, the maximum reduction on the bending resistance due to the combined M-V loading situation is 7.2%. The calculations proved the experimental results of Kuchta (2006) who also observed small resistance reductions due to combined loading situations. It also demonstrated the conclusion of Elgally (1997), that the M-V interaction for girders with trapezoidal corrugated webs could be neglected. The observed resistance reductions are not greater than the web contribution in the bending resistance or the flange contribution in the shear buckling resistance. These resistances are usually neglected

[6] GMNIA: Geometrically and Materially Nonlinear Analysis with Imperfections

in the design of the corrugated web girders. Based on the numerical calculations it is also observed that the M-V interaction behaviour of the corrugated web girders does not depend on the corrugation profile, the maximum value of the transverse bending moment however does depend on it. No relationship is observed between the magnitude of the transverse bending moment and the bending resistance reduction, if plastic design is applied [17]. For the further development of this theses, the M-V interaction is considered neglectable. This means that the moment and shear resistance of the girders can be assessed separated from each other.

1.6 Connections

In previously discussed criteria it was assumed that the failure of the compound girders with corrugated webs happens in the flanges or respectively the web of the girder. This means that the connection between the two different components is assumed to be strong enough not to fail before one of the other parts do. For the compound joints of the girder with corrugated steel webs, different compositions are possible. In general, a distinction can be made between an arrangement with a steel flange, and an embedded steel web in the concrete slab. In Figure 19, two different possibilities, one for each connection group, is shown. The right composition (Figure 19a) gives an example for the connections constructed with a steel flange, here in combination with vertical steel studs. The left composition (Figure 19b) gives an example for the connections where the embedded steel web provides the attachment, here in combination with horizontal steel studs. The function of the studs is to pass on the longitudinal forces between web and concrete slab.

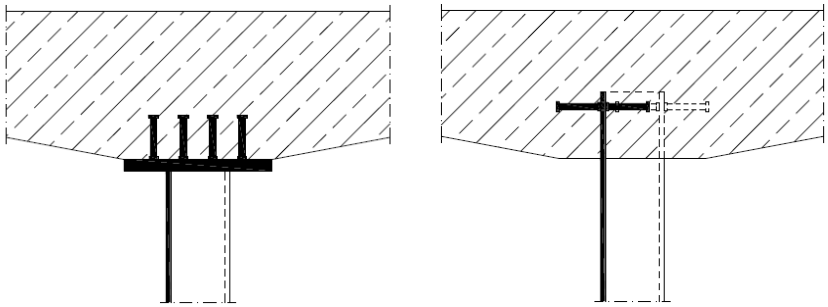

a) Arrangement with steel flange and vertical studs

b) Arrangement with an embedded web and horizontal studs

Figure 19: Basic arrangement options of compound joints between steel corrugated web and concrete flange [16] p.140

In addition, the realized designs also differ in the type and number of connecting elements. Shown in Figure 20, are some connection using a steel flange, used in bridges constructed in Japan. The choice between the various possible connections is determined, among other things, based on the forces acting on the bridge [16], [17].

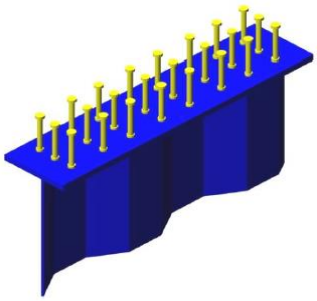

a) Steel flange with vertical studs

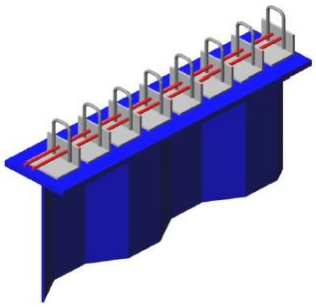

b) Steel flange with steel angles and loops

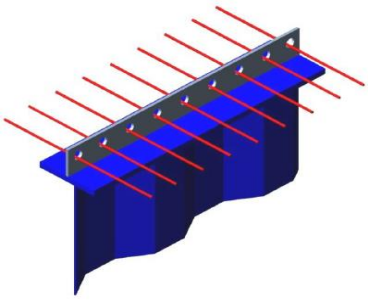

c) Single steel strap with steel rebars

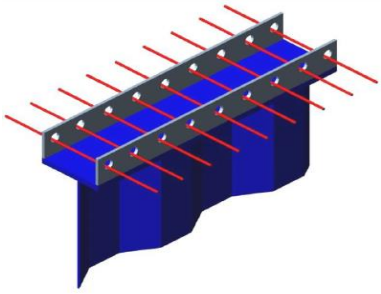

d) Double steel strap with steel rebars

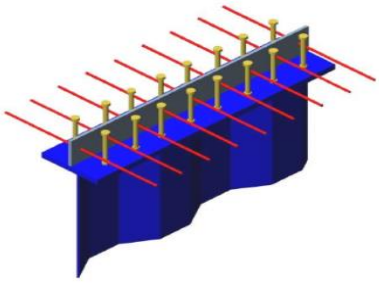

e) Single steel strap with steel tendons and studs

Figure 20: Compound joint with steel flanges [16] p. 142

Going over to the second group presented in Figure 19: connections using an embedded part of the corrugated web. In the embodiments in which the corrugated steel incorporates into the concrete slab, there usually are two reinforcing rods welded longitudinally (see Figure 21a). The rebars, which act as concrete dowels, are inserted in the transverse direction through the holes in the web. This arrangement was for the first time realised in the Hondani Bridge in Japan. At the Kurobegawa Bridge, the longitudinal reinforcing rods were replaced by sheets, which were fixed by screwing them on the side of the bridge (Figure 21b). The sheets were provided of additional holes for concrete anchors [16].

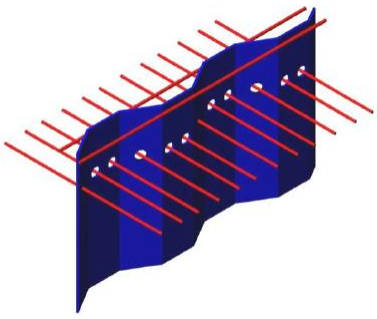

a) Two reinforcing rods and transverse crossing rebars

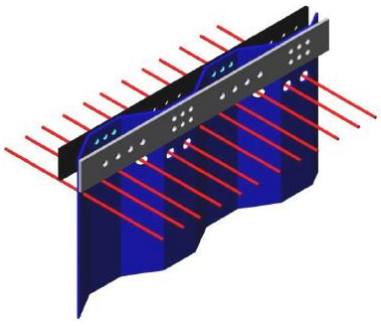

b) Two reinforcing sheets and transverse crossing rebars

Figure 21: Compound joints with embedded corrugated steel web in concrete [16] p.143

2 Research setups

In this chapter the examined specimens and the applied load situations are explained. First in section 2.1, the compositions of the research models or specimens of this project are presented. After the compositions, the different load situations, accompanying the specimens, are given in section 2.2. The compositions of the girders, and the applied load situations are chosen to be able to clearly determine the influence of certain parameters.

2.1 Research models

The research samples that will be discussed and analysed in this project are I-girders with a steel corrugated web like the example given in Figure 22. The modelling of the girder displayed in Figure 22 is conducted with the pre and post processor for numerical simulations in science and engineering, named GiD.

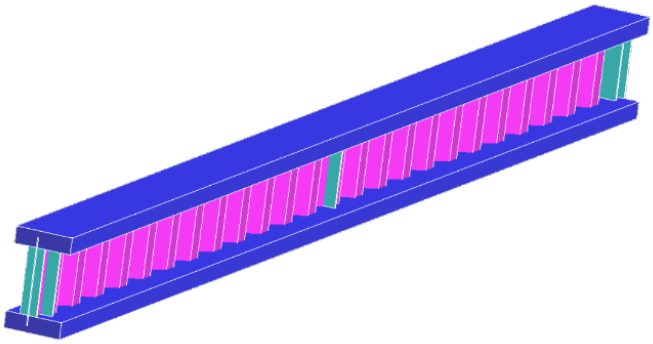

Figure 22: Example test specimen

Fifteen different specimens will be examined, the parameters that provide the difference between these specimens are the composition of the flanges, the web thickness and the locations of the stiffeners. All specimens have a span of 8.00 m. For this span to be applied during the experimental phase, the real length of the girders is 8.20 m.

The specimens can be divided into three main I-girders types, all with a corrugated steel web. The difference between these three main subdivisions finds itself in the flanges. The upper flanges of all types are constructed out of concrete with a material quality of C40/50. As can be seen in Figure 23, the lower flanges make the difference.

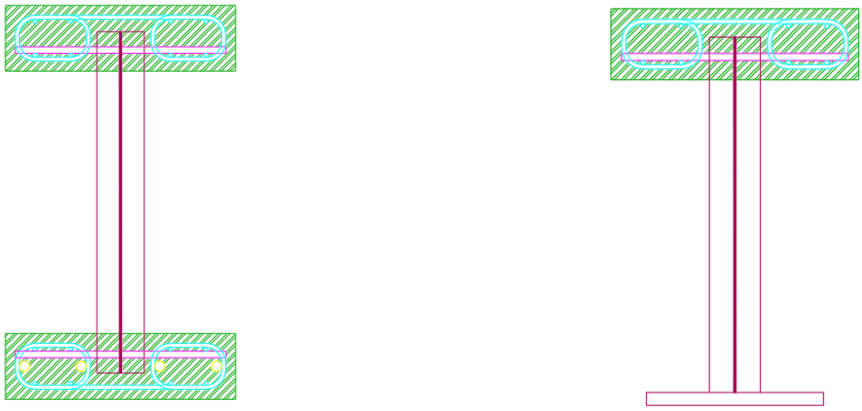

(a) (b)

Figure 23: General cross-section of examined specimen: (a) 'hybrid' girder type, (b) 'composite' girder type

Further in the text, the left composition in Figure 23 will be referred to as the ‘hybrid’ girder, and the right composition as the ‘composite’ girder. For the ‘hybrid’ girder the lower flange is composed out of prestressed concrete material quality C40/50, while the ‘composite’ girder has a S235 steel lower flange. The third subdivision is also a ‘hybrid’ girder but with six tendons (see Figure 24) instead of four (Figure 23a).

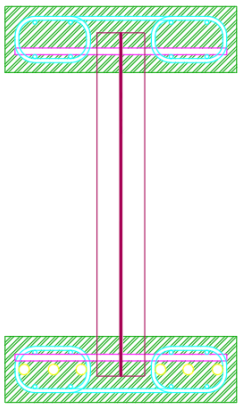

Figure 24: ‘Hybrid’ girder with 6 tendons

The tendons of the ‘hybrid’ girders are of the sort Fp 150/1860. These are each made of 7 steel strands and have a real diameter of 15.7 mm and a nominal diameter of 12.9 mm, which equals to an effective cross-section area of 150 mm². They are imposed to a prestressing stress of 1475 MPa or in other words a prestressing force of 221.4 kN is imposed in each tendon. For all the specimens, the corrugated web is made of S235 steel. Because the ultimate strength of the girders is under examination and not the design strength, the mean yield strength of the steel web is used in all calculations instead of the design yield strength. The mean value for material S235 equals 280 MPa. During compression tests, on the concrete that will be used in the experimental setups, a mean cylinder compressive strength of 50 MPa was obtained. In all calculations and numerical analyses, this value will be used. The transverse rebars that keep the concrete from expanding in axial direction, are of sort B500B and have a diameter of 6 mm. For each of, the ‘hybrid’ girder with four tendons, the ‘hybrid’ girder with six tendons and the composite girder, five different specimens are analysed. The difference of the five specimens for each type is the same and finds itself in the thickness of the corrugated web and the location of the stiffeners. The thickness of the web varies between 3 and 6 mm. The locations of the stiffeners depend on the locations of the applied loads during the execution of the experiments (see further).

The connection between the concrete slab and the corrugated steel web, is a result of two composition/connectivity systems. As can be seen in Figure 23 and Figure 24, these connections are executed by embedding the corrugated steel web in the concrete slab, while additionally using transverse steel bars which go through the steel web and are clamped in the concrete slab. Figure 21 depicts two possible arrangements of the joint type used in the specimens of this thesis. In the connection arrangement used for this research, there are no axial reinforcement rods or sheets. The transverse connectivity bars are 6 mm thick and in each longitudinally orientated fold, two transverse crossing bars are placed. The geometrical properties of the web are presented in Figure 25.

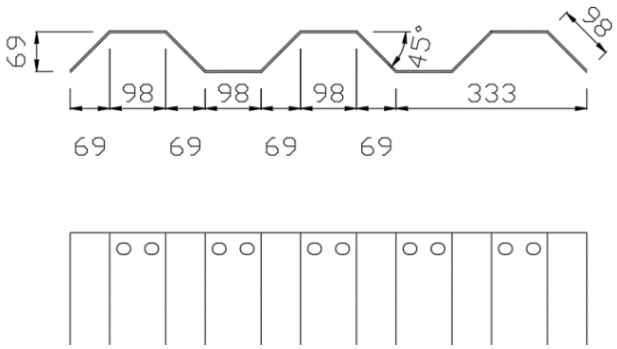

Figure 25: corrugation used for the discussed specimens, dimensions in mm

The bars will cross the corrugated web through the holes in the longitudinal folds of the web, as shown in Figure 25. These holes have an oval shape with a minimum diameter of 20 mm. The holes are significantly larger than the cross-section of the transverse bars to ensure that the concrete secures the steel connection. The non-variable dimensions of the corrugated web for each discussed specimen, are also given in Figure 25. Each fold is 98 mm long and the angles are always 45 degrees. For the web, the only differences between the specimens can be the plate thickness and the web height. The plate thickness, of the corrugated steel web, varies from 4 to 6 mm. The connection of the steel flange to the corrugated web in the composite girder is accomplished by a double-sided fillet weld with throat thickness of 4 mm.

What the dimensions of the cross-sections concern, in Figure 26 the values for the 'hybrid' girder with 6 tendons are displayed:

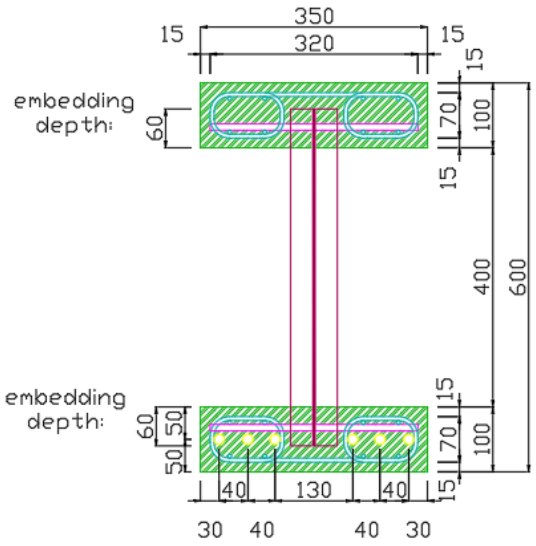

Figure 26: Cross-sectional properties of the 'hybrid' girder with 6 tendons, dimensions in mm

These values are the same for all 'hybrid' girders with 6 tendons in the lower flange. As already explained, the differences between the specimens of one girder type lays in the plate thickness of the web and the position of the stiffeners.

Figure 27 gives a representation of the cross-section of the 'hybrid' girder with 4 tendons in the lower flange. Except for the difference in the number of tendons, the cross-sectional dimensions of the 'hybrid' girder with 4 tendons are exactly the same as for the 'hybrid' girder with 6 tendons.

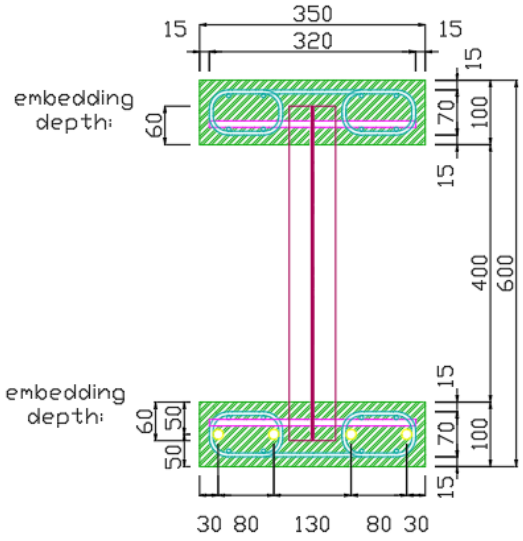

Figure 27: Cross-sectional properties of the 'hybrid' girder with 4 tendons, dimensions in cm

For the third and final girder type, Figure 28 provides a representation of the cross-sectional dimensions.

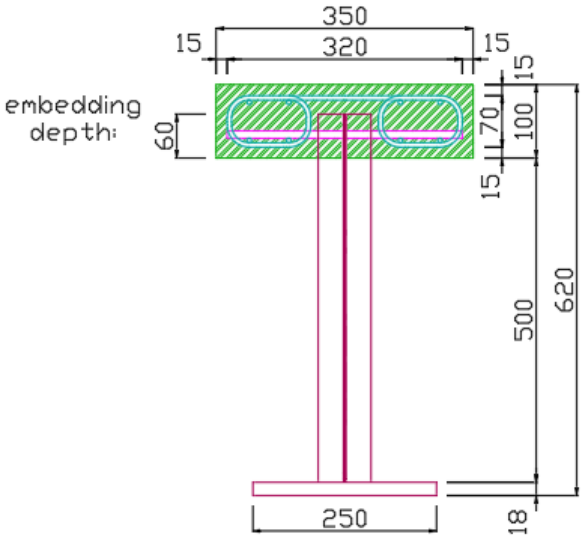

Figure 28: Cross-sectional properties of the 'composite' girder, dimensions in cm

2.2 Applied loads

For each of the main girder types, five different specimens will be examined. As mentioned before, the difference between these specimens depends on the web thickness and the locations of the stiffeners. For each of the specimens of one main girder type, a different load situation is used. In Figure 29 the different load situations are illustrated (dimensions are given in meters). The to be tested beam span is always 8 m, therefor the specimens are 8.20 m long. This extra length is necessary for a proper test setup.

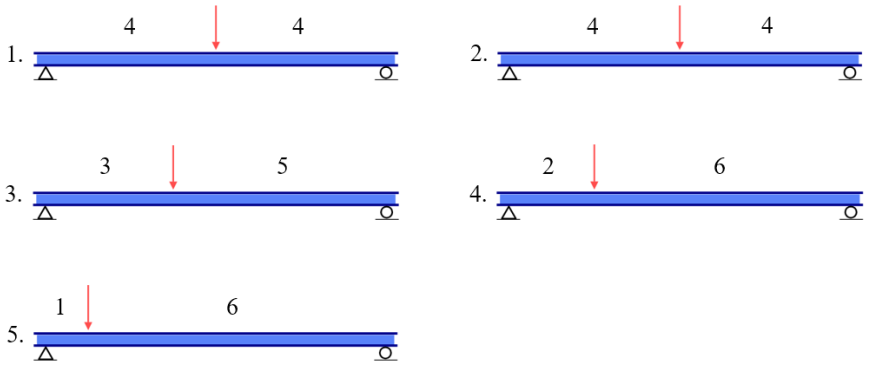

Figure 29: Load situations used for one main girder type, dimensions in meters

All specimens count five stiffeners, two are placed at each side of the beam: one at the height of the supports and one at the real ending of the beam. The fifth stiffener is located at the position where the load in the particular load situation will be placed. Load situation 1 and 2 are the same, for these specimens in each girder type, the difference is provided by the web thickness. Table 1 provides an overview of the changing parameters for the fifteen different specimens. Appendix B is a representation of the 'hybrid' specimen with six tendons that during the test subjected is to situation 1. In Table 1 this girder is referred to as specimen number 1. Appendix C and Appendix D give the setup of specimens 6, respectively 11 (each the first specimen of their girder type). From here further, the specimens will be referred to by the numbers presented in Table 1.

Table 1: Parameters of different specimens

Specimen	Girder type	Middle stiffener position starting from left support [m]	Thickness of the web [mm]
1.	*H6*	4	6
2.	*H6*	4	4
3.	*H6*	3	4
4.	*H6*	2	4
5.	*H6*	1	4
6.	*H4*	4	5
7.	*H4*	4	3
8.	*H4*	3	3
9.	*H4*	2	3
10.	*H4*	1	3
11.	*CS*	4	6
12.	*CS*	4	4
13.	*CS*	3	4
14.	*CS*	2	4
15.	*CS*	1	4

In Table 1: *H6* stand for ‘hybrid’ composition with 6 tendons, *H4* for ‘hybrid’ with 4 tendons and *CS* for composite composition with steel lower flange. The dimensions accompanying these compositions are explained in previous section. As stated, for all specimens the axial position of the load is the same as the axial position of the accompanying middle stiffener. Therefore, the third column in Table 1 which refers to the position of the middle stiffener, could just as easily be the column for the load position. As can be noticed from the specimens and the load situations, the test arrangements are ideal for an investigation of shear and moment capacity. No torsion will be introduced in the girders, and the axial forces are taken into account by the moment examination.

3 Hand calculations

In this section, a hand calculation of the models presented in chapter 2 is conducted. The goal is to determine the magnitude of the implied loads required to get the girders into their yield points. From this point further, this load will be referred to as the ultimate load. The yield point of a girder corresponds to the crushing of the concrete upper flange and the yielding of the steel in the bottom flange in the case that the maximum bending moment is reached, and yielding of the steel corrugated web in the case that the maximum shear force is reached. The influence for each selected parameter on the ultimate loads is examined. The 3 parameters considered are: web thickness, load situations and cross-sectional composition. Section 3.1 presents the ultimate shear capacity calculations. Sections 3.2 covers the moment capacity calculations. In section 3.3 the results from section 3.1 and 3.2 are used to determine the maximum loads to be applied for every specimen in their related load situations. Further, the results will be plotted and compared in graphs for each studied parameter.

3.1 Shear capacity

The hand calculations for the 'hybrid' and the 'composite' girders are based on the grounded assumption that the shear capacity of the girder is solely provided by the web. Determining the shear capacity solitary based on the web gives conservative results. This also means that the calculation process for both types, 'hybrid' and 'composite', are identical and only differ because of the varying web thickness and the height of the non-embedded web part. The calculations are performed with use of Eurocode 3. The calculation process used is explained next.

According to Eurocode 3 the shear resistance $V_{w,Rd}$ should be calculated with Equation (5) [15]:

$$V_{w,Rd} = \chi_c \cdot \frac{f_{yw}}{\gamma_{M1} \cdot \sqrt{3}} \cdot h_w \cdot t_w \tag{5}$$

where χ_c is the lesser of the values of the reduction factors for local buckling $\chi_{c,l}$ and global buckling $\chi_{c,g}$ obtained from Equation (6) and (7). The reduction factor $\chi_{c,l}$ for local buckling should be calculated from:

$$\chi_{c,l} = \frac{1.15}{0.9 + \bar{\lambda}_{c,l}} \leq 1.0 \tag{6}$$

Where:

$$\bar{\lambda}_{c,l} = \sqrt{\frac{f_{yw}}{\tau_{cr,l} \cdot \sqrt{3}}} \quad \text{and} \quad \tau_{cr,l} = 4.83 \cdot E \cdot \left[\frac{t_w}{a_{max}}\right]^2$$

a_{max} should be taken as the greater of a_1 and a_2.

The reduction factor $\chi_{c,g}$ for global buckling should be taken as:

$$\chi_{c,g} = \frac{1.5}{0.5 + \bar{\lambda}_{c,g}^{\ 2}} \leq 1.0 \tag{7}$$

where:

$$\bar{\lambda}_{c,g} = \sqrt{\frac{f_{yw}}{\tau_{cr,g} \cdot \sqrt{3}}} \quad \text{and} \quad \tau_{cr,g} = \frac{32.4}{t_w \cdot {h_w}^2} \cdot \sqrt{D_x \cdot {D_z}^3}$$

$$D_x = \frac{E \cdot {t_w}^3}{12 \cdot (1 - \nu^2)} \cdot \frac{w}{s} \quad \text{and} \quad D_z = \frac{E \cdot I_z}{w}$$

I_z [18]:

$$I_z = \frac{t_w \cdot {a_3}^2 \cdot (3a_1 + a_2)}{12}$$

As an explanatory example, the first specimen of Table 2 has been worked out.

Data of specimen 1 is presented in Table 2 and Figure 30:

Table 2: Material and dimensional properties of specimen 1

t_f [mm]	b_f [mm]	t_w [mm]	h_w [mm]	α [°]	$a_1 = a_2$ [mm]	$a_3 = a_4$ [mm]	f_{yw} [MPa]
100	350	6	400	45	97.63	69.03	280

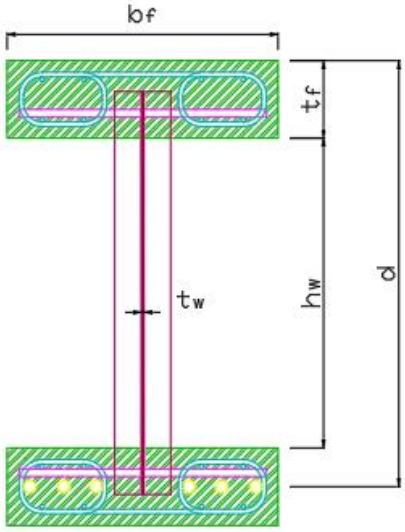

(a)

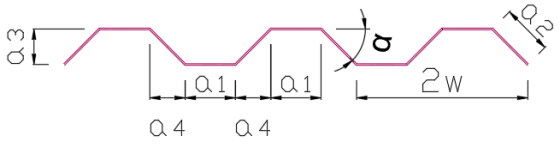

(b)

Figure 30: Propertie symbols of the 'hybrid' composition: (a) cross-section girder, (b) cross-section web

First the needed factors for the calculation of the local buckling reduction factor are determined:

$$\bar{\lambda}_{c,l} = \sqrt{\frac{f_{yw}}{\tau_{cr,l} \cdot \sqrt{3}}} = \sqrt{\frac{280 \text{ MPa}}{3830.83 \text{ MPa} \cdot \sqrt{3}}} = 0.21$$

With

$$\tau_{cr,l} = 4.83 \cdot E \cdot \left[\frac{t_w}{a_{max}}\right]^2 = 4.83 \cdot 210000 \frac{\mathrm{N}}{\mathrm{mm}^2} \cdot \left[\frac{6\ \mathrm{mm}}{97.63\ \mathrm{mm}}\right]^2 = 3830.83\ \mathrm{MPa}$$

a_1 and a_2 are both 97.63 mm, this means that a_{max} is equal to 97.63 mm. The yield strength of steel class S235 in design would be 235 MPa, in this case the real ultimate strength is examined, which means that the mean values have to be used. The mean yield strength of S235 steel is 280 MPa.

With these, the local buckling reduction factor $\chi_{c,l}$ can be calculated according to Equation (6):

$$\chi_{c,l} = \frac{1.15}{0.9 + 0.21} = 1.04$$

The reduction factor may not be greater than 1, so:

$$\chi_{c,l} = 1$$

The same process applies for the global buckling reduction factor. First the needed factors for Equation (7) are determined:

$$\bar{\lambda}_{c,g} = \sqrt{\frac{f_{yw}}{\tau_{cr,g} \cdot \sqrt{3}}} = \sqrt{\frac{280\ \mathrm{MPa}}{9279.94\ \mathrm{MPa} \cdot \sqrt{3}}} = 0.13$$

$$\tau_{cr,g} = \frac{32.4}{t_w \cdot {h_w}^2} \cdot \sqrt{D_x \cdot {D_z}^3} = \frac{32.4}{6\ \mathrm{mm} \cdot 400^2 \mathrm{mm}^2} \cdot \sqrt{3545529.50 \cdot 1172558936.06^3} = 9279.94\ \mathrm{MPa}$$

$$D_x = \frac{E \cdot {t_w}^3}{12 \cdot (1 - \nu^2)} \cdot \frac{w}{s} = \frac{210000 \frac{\mathrm{N}}{\mathrm{mm}^2} \cdot 6^3 \mathrm{mm}^3}{12 \cdot (1 - 0.3^2)} \cdot \frac{166.67\ \mathrm{mm}}{195.26\ \mathrm{mm}} = 3545529.5030$$

Given that the Poisson-factor of steel is equal to 0.3.

$$D_z = \frac{E \cdot I_z}{w} = \frac{210000 \frac{N}{mm^2} \cdot 930602.87\ mm^4}{166.67\ mm} = 1172558936.06$$

With

$$\mathrm{I_z} = \frac{\mathrm{t_w} \cdot {\mathrm{a_3}}^2 \cdot (3\mathrm{a_1} + \mathrm{a_2})}{12} = \frac{6\ \mathrm{mm} \cdot 69.03^2 \mathrm{mm}^2 \cdot (3 \cdot 97.63\ \mathrm{mm} + 97.63\ \mathrm{mm})}{12}$$

$$= 930602.87\ \mathrm{mm}^4$$

With these, the global buckling reduction factor $\chi_{c,g}$ can be calculated according to Equation (7):

$$\chi_{c,g} = \frac{1.5}{0.5 + {\bar{\lambda}_{c,g}}^2} = \frac{1.5}{0.5 + 0.1320^2} = 2.90$$

Also here, the reduction factor may not be greater than 1, so:

$$\chi_{c,g} = 1$$

The local and global reduction factors, for this specimen, both are equal to 1, therefore χ_c is also 1. For the calculation of the shear resistance (Equation (5)) this means:

$$V_{w,Rd} = \chi_c \cdot \frac{f_{yw}}{\gamma_{M1} \cdot \sqrt{3}} \cdot h_w \cdot t_w = 1 \cdot \frac{280 \frac{\text{N}}{\text{mm}^2}}{1 \cdot \sqrt{3}} \cdot 400 \text{ mm} \cdot 6 \text{ mm} = 387.98 \text{ kN}$$

The hand calculated shear capacities $V_{w,Rd}$ of the specimens are presented in Table 3:

Table 3: Shear capacities Vw,Rd [kN] by hand calculation

Nr.	Shear capacity [kN]	Nr.	Shear capacity [kN]
1.	387.98	**9.**	170.19
2.	246.21	**10.**	170.19
3.	246.21	**11.**	484.98
4.	246.21	**12.**	307.76
5.	246.21	**13.**	307.76
6.	323.32	**14.**	307.76
7.	170.19	**15.**	307.76
8.	170.19		

Appendix E gives an overview of the properties and the results for all specimens. For each girder type, the second until fifth number have the same web thickness. Therefore, the shear capacity for these specimens must be the same.

3.2 Moment capacity

For the moment capacity calculations, a distinction must be made between the 'hybrid' and 'composite' girders.

First, the calculations of the 'hybrid' girders are presented. By help of Eurocode 2 following Equations (8) and (9a) were constructed for the determination of the ultimate moment capacity $M_{f,Rd}$ of the 'hybrid' girders. These two equations must result in the same value. Both are calculated to double check the results. The equations are both based on the moment equilibrium of the girder. One based on the compression strength of the concrete in the upper flange, and one based on the tensile strength of the tendons in the lower flange. The tensile strength of the bars, that keep the rebars to avoid transverse expansion of the concrete in place, is neglectable. The resistance against the imposing moments is provided by the collaboration of the reaction forces that result from the prestressed reinforcement in the lower flange, and the compression strength of the upper flange [19].

Moment equilibrium:

$$\sum M = 0 \quad \rightarrow \quad M_c + M_s = 0$$

$$M_c = x_c \cdot f_{cm} \cdot b_f \cdot \left(d - \frac{x_c}{2}\right) \tag{8}$$

$$M_{sh} = n \cdot A_r \cdot \sigma_r \cdot \left(d - \frac{x_c}{2}\right) \tag{9a}$$

Equation (8) is the moment capacity of the beam calculated according to the compression resistance of the upper concrete flange, assuming that x_c is smaller than the thickness of the upper flange. Equation (9a) is the capacity based on the tensile strength of the tendons in the lower flange. The results obtained with Equation (8) and (9a) have to be equal to each other because of the total moment equilibrium of the beam. This found value (from both equations) is the ultimate moment capacity of the 'hybrid' girder. The formula for M_{sh} has equation number (9a) to point out that this equation is different for the 'hybrid' and the 'composite' girders (see further).

For the 'hybrid' girders, the effective depth (d) used in previous moment capacity equations equals to the sum of the non-embedded web part (h_w), half of the lower flange thickness (t_{fl}) and the full upper flange thickness (t_{fu}). Only half of the lower flange thickness because the tendons are positioned at half height of the flange:

$$d = h_w + \frac{t_{fl}}{2} + t_{fu}$$

The volume of the transverse connectivity bars, the rebars to keep the concrete from expanding in the directions perpendicular to the direction of compression (see Figure 23a and b) and the bars that keep the rebars in place, are relatively low compared to the total volume of the upper flange. Therefore, the influence of the transverse bars, the place-keeping bars of the rebars and the rebars in the equilibrium, are neglected.

In Equations (8) and (9a) all parameters for the calculation of the flexural capacity (M_c *or* M_{sh}), except for x_c, are properties that can be derived from the composition of the cross-section of the beam, see Figure 30. The value of x_c can be obtained from the axial forces equilibrium. The axial forces equilibrium for the 'hybrid' girder is:

$$\sum N = 0 \quad \rightarrow \quad 0 = N_c - N_r$$

$$0 = x_c \cdot f_{cm} \cdot b_f - n \cdot A_r \cdot \sigma_r$$

This is only valid if x_c is smaller than b_f. Otherwise, in the balance of forces, x_c must be replaced by h_f.

The value of stress in the tendons σ_r that must be entered in the axial forces equilibrium has a bilineair stress-strain diagram (see Figure 31). Therefore, the stress must be calculated as follows:

$$\sigma_r = f_{2.0} + \sigma_{r2} = f_{2.0} + E_{r2} \cdot \varepsilon_{r2}$$

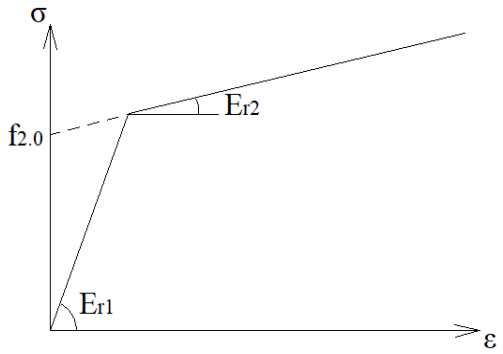

Figure 31: Bilinear stress-strain curve of the prestressed reinforcement used in the 'hybrid' girders

The value of the $f_{2.0}$ tension is determined by extending the second Young's modulus towards the stress axis of the curve in Figure 31. The value of the strain ε_{r2} of the reinforcement tendons can be calculated by composion of the strain equilibrium of the cross-section:

$$\varepsilon_{r2} = \frac{\varepsilon_{cu} \cdot (d - 1.25 \cdot x_c)}{1.25 \cdot x_c}$$

ε_{cu} is equal to the maximum compressive strain of concrete: 0.0035.

Combined with previous equation for σ_r, this forms:

$$\sigma_r = f_{2.0} + E_{r2} \cdot \frac{\varepsilon_{cu} \cdot (d - 1.25 \cdot x_c)}{1.25 \cdot x_c}$$

At last, the final axial force equilibrium (Equation (10a)) has as only unknown parameter x_c:

$$0 = x_c \cdot f_{cm} \cdot b_f - n \cdot A_r \cdot \left(f_{2.0} + E_{r2} \cdot \frac{\varepsilon_{cu} \cdot (d - 1.25 \cdot x_c)}{1.25 \cdot x_c} \right) \quad (10a)$$

This equilibrium is indicated with number (10a) to point out that the composition for the composite girders is different from this one for the 'hybrid' girders (see further). From this equation, x_c can be calculated. With the value of x_c and Equations (8) and (9a), the flexural capacity of the 'hybrid' girders can be calculated.

Also here, as an explanatory example of the 'hybrid' girders, the first specimen of Table 4 has been worked out.

Data of specimen 1 is presented in Table 4 and Figure 32:

Table 4: Material and dimensional properties of specimen 1

t_f [mm]	b_f [mm]	t_w [mm]	h_w [mm]	f_{cm} [MPa]	f_{yw} [MPa]
100	350	6	400	50	280

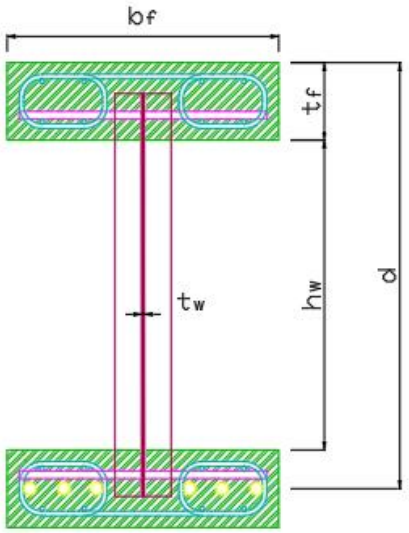

Figure 32: Cross-sectional propertie symbols of the 'hybrid' composition

Determination of x_c is obtained by use of Equation (10a). Filled in for the explanatory example, this becomes:

$$0 = x_c \cdot 50\ \text{MPa} \cdot 350\ \text{mm} - 6 \cdot 150\ \text{mm}^2 \cdot \left(1570.415\ \text{MPa} + 8274\ \text{MPa} \cdot \frac{0.0035 \cdot (550\ \text{mm} - 1.25 \cdot x_c)}{1.25 \cdot x_c}\right)$$

With the effective height (*d*) for the 'hybrid' girders:

$$d = h_w + \frac{t_{fl}}{2} + t_{fu} = 400\ \text{mm} + \frac{100\ \text{mm}}{2} + 100\ \text{mm} = 550\ \text{mm}$$

As mentioned in chapter 2 (Research setups), for the target mean cylinder strength (f_{cm}) of concrete class C40/50, 50 MPa is used to accurately predict the capacity and behaviour of the specimens. E_{r2} for the bilinear stress-strain curve is equal to 83 MPa for all prestressed tendons in the specimens. Equation (10a) filled in for specimen 1 gives a value of 86.82 mm for x_c. This is smaller than the thickness of the upper flange which is 100 mm, what means that previous made assumptions for the composition of the moment and axial forces equilibria are well-founded.

Once x_c is found, Equations (8) and (9a) can be calculated. For the maximum moment capacity based on the compression capacity of the upper flange or in other words Equation (8) this means:

$$M_c = x_c \cdot f_{cm} \cdot b_f \cdot \left(d - \frac{x_c}{2}\right) = 86.8225\ \text{mm} \cdot 50\ \text{MPa} \cdot 350\ \text{mm} \cdot \left(550\ \text{mm} - \frac{86.8225\ \text{mm}}{2}\right) = 769.71\ \text{kNm}$$

For the flexural capacity based on the tensile strength of the tendons in the lower flange or in other words Equation (9a), the stress in the tendons must be determined the same way as for the axials forces equilibrium:

$$M_{sh} = n \cdot A_r \cdot \sigma_r \cdot \left(d - \frac{x_c}{2}\right) = n \cdot A_r \cdot \left(f_{2.0} + E_{r2} \cdot \frac{\varepsilon_{cu} \cdot (d - 1.25 \cdot x_c)}{1.25 \cdot x_c}\right) \cdot \left(d - \frac{x_c}{2}\right)$$

Filled in for the explanatory example, this becomes:

$$M_{sh} = 6 \cdot 150 \text{ mm}^2 \cdot \left(1570.415 \text{ MPa} + 8274 \text{ MPa} \cdot \frac{0.0035 \cdot (550 \text{ mm} - 1.25 \cdot 86.8225)}{1.25 \cdot 86.8225}\right) \cdot \left(550 \text{ mm} - \frac{86.8225}{2}\right) = 769.71 \text{ kNm}$$

The values obtained with Equation (8) and (9a) are equal to each other. For this specimen this means, that the beam has a maximum flexural capacity of 769.71 kNm. The moment capacity of a beam is dependent on the flanges. This means that the capacity of the first 5 specimens (that only differ in web-thickness, load setup and the place of the stiffeners) should all be the same and equal to 769.71 kNm. For specimens 6 to 10 the calculation process is exactly the same as for specimens 1 to 5, only here the cross-section setup is made with 4 instead of 6 tendons. The depth of the neutral axis x_c for these specimens, becomes 60.12 mm. For the moment capacity of the beams this means 547.00 kNm. Logically this value is lower than the flexural capacity of specimens 1 to 5.

The calculations of the flexural capacity of the composite girders are similar to the calculations of the flexural capacity of the 'hybrid' girders. First x_c has to be determined. This is obtained in a similar way as for the 'hybrid' girders. Once x_c is calculated, the ultimate moment capacity can again be calculated with use of the moment equilibrium. The main difference here is the calculation of the moment capacity based on the lower flange. Instead of tendons, embedded in a concrete flange, here there is a steel plate as a lower flange to withstand the tensile forces (see Figure 33).

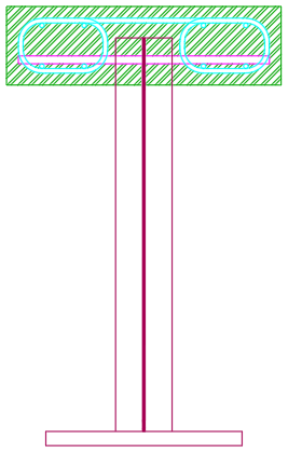

Figure 33: Cross-section composite girder

The moment calculations based on the lower flange of the composite girders are based on following equation (9b):

$$M_{sc} = b_{fl} \cdot h_{fl} \cdot f_{yf} \cdot \left(d - \frac{x_c}{2}\right) \quad (9b)$$

As an explanatory example, the first composite girder listed in with specimen number 11 is worked out. The cross-sectional dimensions are depicted in Table 5 and Figure 34:

Table 5: Material and dimensional properties of specimen 11

t_{fu} [mm]	b_{fu} [mm]	t_w [mm]	h_w [mm]	b_{fl} [mm]	t_{fl} [mm]	f_{cm} [MPa]	f_{yw} [MPa]	f_{yf} [MPa]
100	350	6	500	250	18	50	280	280

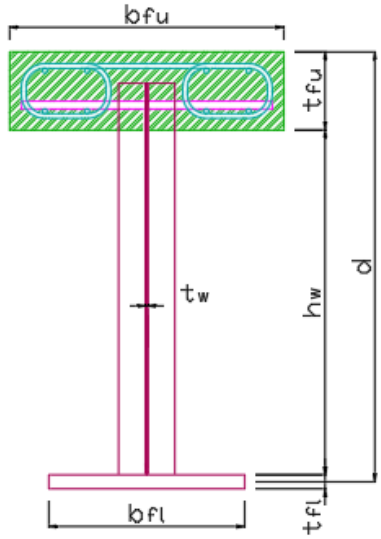

Figure 34: Cross-sectional properties of specimen 11, dimensions in cm

First step, as always: determination of x_c based on the axial forces equilibrium.

$$0 = x_c \cdot f_{cm} \cdot b_{fu} - b_{fl} \cdot h_{fl} \cdot f_{yf} \tag{10b}$$

Equation (10b) filled in for specimen 11:

$$0 = x_c \cdot 50\ \text{MPa} \cdot 350\ \text{mm} - 250\ \text{mm} \cdot 18\ \text{mm} \cdot 280\ \text{MPa}$$

This forms a value of 72 mm for x_c. This value is smaller than the thickness or height of the upper flange, what verifies previously made assumptions for the composition of the moment and axial forces equilibria.

Once x_c is found, Equations (8) and (9b) can be calculated. The effective height (d) for specimen 1, to be filled in for the moment capacity calculations, is:

$$d = h_w + \frac{t_{fl}}{2} + t_{fu} = 400\ \text{mm} + \frac{100\ \text{mm}}{2} + 100\ \text{mm} = 550\ \text{mm}$$

The calculation of flexural capacity for the composite girders is executed with the same equation as for the 'hybrid' girders. Equation (8) solved for specimen 11 gives:

$$M_c = x_c \cdot f_{cm} \cdot b_{fu} \cdot \left(h_w + \frac{h_{fl}}{2} + t_f - \frac{x_c}{2}\right)$$

$$= 72\ \text{mm} \cdot 50\ \text{MPa} \cdot 350\ \text{mm} \cdot \left(500\ \text{mm} + \frac{18\ \text{mm}}{2} + 100\ \text{mm} - \frac{72\ \text{mm}}{2}\right)$$

$$= 721.98\ \text{kNm}$$

The flexural capacity based on the tensile strength of lower steel flange of composite specimen 11 is found with Equation (9b):

$$M_{sc} = b_{fl} \cdot h_{fl} \cdot f_{yf} \cdot \left(h_w + \frac{h_{fl}}{2} + t_f - \frac{x_c}{2}\right) \tag{9b}$$

$$= 250\ \text{mm} \cdot 18\ \text{mm} \cdot 280\frac{\text{N}}{\text{mm}^2} \cdot \left(500\ \text{mm} + \frac{18\ \text{mm}}{2} + 100\ \text{mm} - \frac{72\ \text{mm}}{2}\right) = 721.98\ \text{kNm}$$

The values acquired by Equations (8) and (9b) for composite specimen 11 are the same. The maximum flexural capacity is equal to 721.98 kNm. This means that for all composite specimens (11 to 15) the moment capacity of the girder equal is to 721.98 kNm.

The moment capacity $M_{f,Rd}$ of each discussed specimen are given in Table 6:

Table 6: Moment capacity results of all specimens

Nr.	Neutral axis depth [mm]	Moment capacity [kNm]
1-5	90.15	769.71
6-10	62.35	547.00
11-15	72.00	721.98

3.3 Ultimate loads

With the results from section 3.1 and 3.2, for the shear and moment capacity of the girders, the ultimate loads accompanying the applied load situations can be determined. ´

3.3.1 Ultimate loads (shear)

This section presents the calculations of the ultimate loads of the specimens, exposed to their accompanying load situations, based on the shear capacity of each girder. The final results from the shear capacity calculations (section 3.1) are as presented in Table 7:

Table 7: Shear capacities Vw,Rd [kN] by hand calculation (copie of Table 3)

Nr.	Shear capacity [kN]	Nr.	Shear capacity [kN]
1.	387.98	**9.**	170.19
2.	246.21	**10.**	170.19
3.	246.21	**11.**	484.97
4.	246.21	**12.**	307.76
5.	246.21	**13.**	307.76
6.	323.32	**14.**	307.76
7.	170.19	**15.**	307.76
8.	170.19		

All load situations are again presented in Figure 35. Specimen 1 is imposed to load situation 1, specimen 2 to load situation 2, etc. Specimen number 6 (first specimen of second girder type) is again imposed to load situation 1, number 7 to load situation 7 and so on. The same goes for the third girder type.

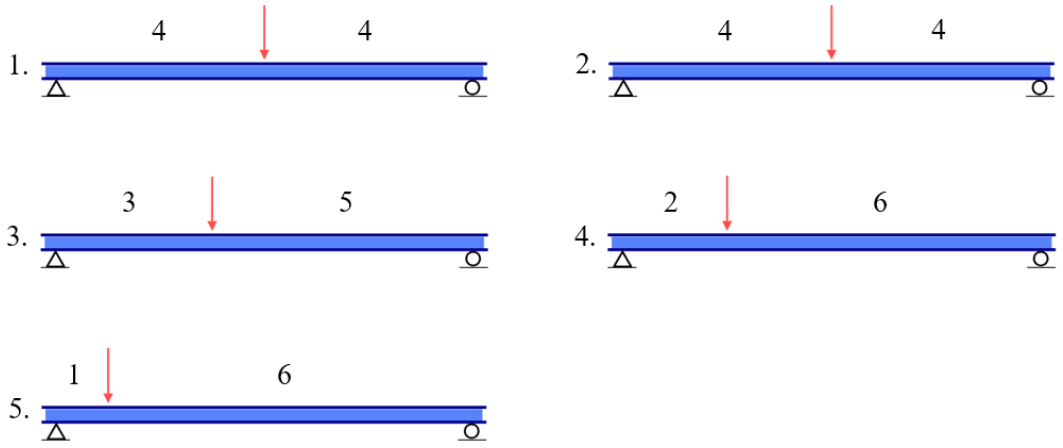

Figure 35: All used load situations, dimensions in meter (copie of Figure 29)

The ultimate load for specimen 1 is double the shear capacity of the girder (387.98 kN · 2 = 775.96 kN) since the load is applied in the middle of the girder. Appendix F presents the shear force diagram of specimen 1. For specimen 3, 4 and 5 the load is not positioned in the middle of the girder, therefor the shear capacity is not multiplied by 2 but by a smaller value. This value decreases with the movement of the load

position towards one of the supports. Starting the load in the middle of the girder with a multiplication factor 2, and ending almost above one of the supports with a multiplication of approximately 1. The multiplication factor can be calculated by dividing the total span (8.00 m) by the distance between the load and the furthest support. This applies for all load situations. For specimen 3 this means a multiplication factor of 8 over 5, what makes that the ultimate load here (246.21 kN · 8/5) 393.93 kN is. Appendix G presents the shear force diagram of specimen 3.

Table 8 provides an overview of the ultimate loads based on the shear capacities of the girders. In other words, these values are the approximate maximum loads to be applied during the experimental phase and the FE-modelling, assuming that the shear capacity of the girder is dominant over the moment capacity.

Table 8: Ultimate loads based on the shear capacities

Nr.	Ultimate load (shear) [kN]	Nr.	Ultimate load (shear) [kN]
1.	775.96	**9.**	226.91
2.	492.41	**10.**	194.50
3.	393.93	**11.**	969.95
4.	328.28	**12.**	615.51
5.	281.38	**13.**	492.41
6.	646.63	**14.**	410.34
7.	340.37	**15.**	351.72
8.	272.30		

To ensure a clear comparison of the results from Table 8, the results are depicted in a line chart. All results from one girder type are grouped via the same colour. This is presented in Figure 36.

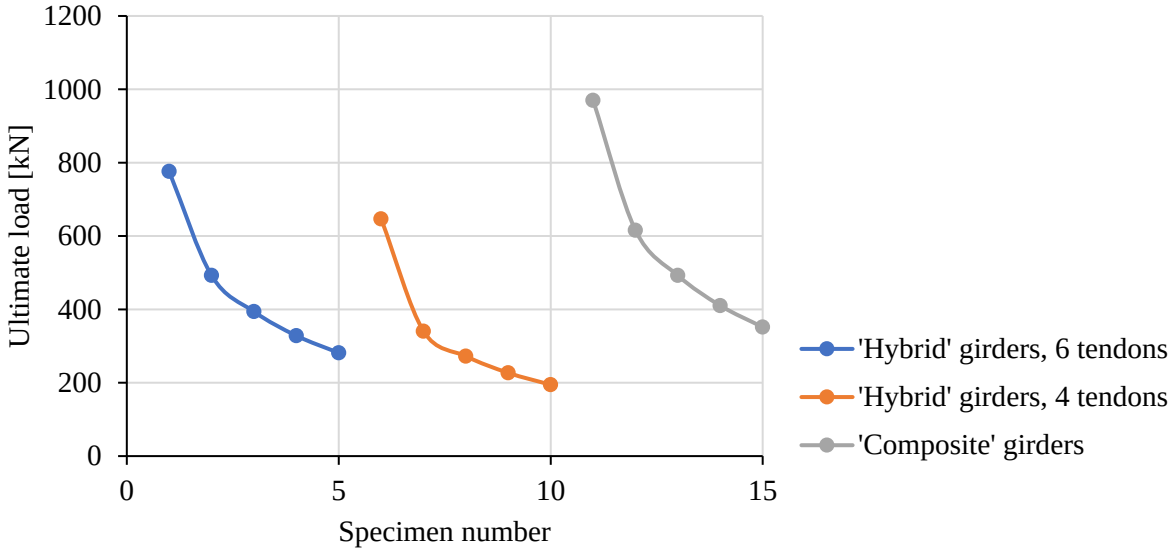

Figure 36: Ultimate loads of discussed specimens based on the shear capacities

The results for all girder types have the same relationship towards each other. The downwards shift of the *H4* ('hybrid' girders with 4 tendons) results, compared to the *H6* ('hybrid' girders with 6 tendons) results is entirely due to the smaller thickness of the webs. The *CS* (Composite girders with steel lower flange) results are higher than the *H6* results; the two girder types have the same web thicknesses but different web heights. Conclusion: smaller web thickness means easier buckling and a lower shear resistance of the web, while a higher web provides more slender folds and therefore a higher shear strength.

The shape of the lines that connect the results for one girder type can be explained based on two varying parameters: the web thickness and the place of the load in the different load situations. The web thicknesses of all specimens for one girder type are the same, except for the first specimen which has a more sizable web thickness. The more sizable the web thickness, the higher the shear capacity of the girder and therefore also the higher the ultimate load based on the shear capacity. What the load positions concerns: a more centrally located load, means a higher ultimate force based on the shear capacity. When the load is placed in the middle, the load will in fact be distributed equally over the two supports, while when the load is close to one of the supports, this support will absorb most of the load.

3.3.2 Ultimate loads (moment)

In this section the ultimate loads, when only considering the moment capacity of the specimens, are calculated. As a starting point, the final results from section 3.2 Moment capacity are used. These results are shown again in Table 9.

Table 9: Moment capacity results of all specimens (copie of Table 6

Nr.	Neutral axis depth [mm]	Moment capacity [kNm]
1-5	90.15	769.71
6-10	62.35	547.00
11-15	72.00	721.98

The ultimate loads, are in this case to be calculated starting from the moment capacity of the girders. The loads in load situation 1 and 2 are because of their symmetry calculated by dividing the ultimate moments by a fourth of the total span, which is 2 m. For specimen 1, imposed to load situation 1, this means ultimate loads of 384.85 kN. This 384.85 kN centrally located load forms a moment in the girder equal to the moment capacity of the girder: 769.71 kNm. The ultimate bending moment diagram for specimen 1 is added in Appendix H. Because load situation 1 and 2 are the same and only the web differs for the first two specimen of each girders type, the ultimate loads based on the moment capacities for the first two specimens are always the same.

The ultimate loads for all other load situations are calculated using the moment equilibria of the girders. Equations for the reaction forces in the supports are created as follows:

$$M_{f,Rd} = R_1 \cdot L_1 \quad \rightarrow \quad R_1 = \frac{M_{f,Rd}}{L_1}$$

and

$$M_{f,Rd} = R_2 \cdot L_2 \quad \rightarrow \quad R_2 = \frac{M_{f,Rd}}{L_2}$$

In these equations, R_1 and R_2 are the reaction forces in the supports and L_1 and L_2 are the distance between the load and the accompanying support. Figure 37 provides an explanatory illustration:

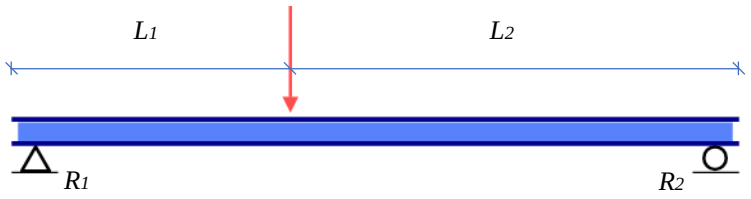

Figure 37: General setup for load situation 2 to 5

With the moment capacities of the girders (found in section 3.2), L_1 and L_2 of the load situations, and previous equations for R_1 and R_2, the reaction forces are calculated. Using these calculated reaction forces in the vertical force equilibrium of the girder, the ultimate load based on the moment capacity is obtained:

$$\text{Ultimate load (moment)} = R_1 + R_2$$

For specimen 3 (with load situation 3) the reaction forces are:

$$R_1 = \frac{M_{f,Rd}}{L_1} = \frac{769.71\ \text{kNm}}{3\ \text{m}} = 256.57\ \text{kNm}$$

and

$$R_2 = \frac{M_{f,Rd}}{L_2} = \frac{769.71\ \text{kNm}}{5\ \text{m}} = 153.94\ \text{kNm}$$

As the ultimate load is a summation of these two reaction forces, the ultimate load equals to:

$$\text{Ultimate load (moment)} =$$

$$R_1 + R_2 = 256.57\ \text{kNm} + 153.94\ \text{kNm} = 410.51\ \text{kNm}$$

Appendix I presents the bending moment diagram of specimen 3.

The ultimate loads, based on the moment capacities of the girders, for all specimens are given in Table 10.

Table 10: Ultimate loads based on the moment capacity of the specimens

Nr.	Ultimate load (moment) [kN]	Nr.	Ultimate load (moment) [kN]
1.	384.85	**9.**	364.67
2.	384.85	**10.**	625.15
3.	410.51	**11.**	360.99
4.	513.14	**12.**	360.99
5.	879.67	**13.**	385.06
6.	273.50	**14.**	481.32
7.	273.50	**15.**	825.12
8.	291.73		

To ensure a clear comparison of the results from Table 10, the results are depicted in a line chart in Figure 38. All results from one girder type are grouped via the same colour.

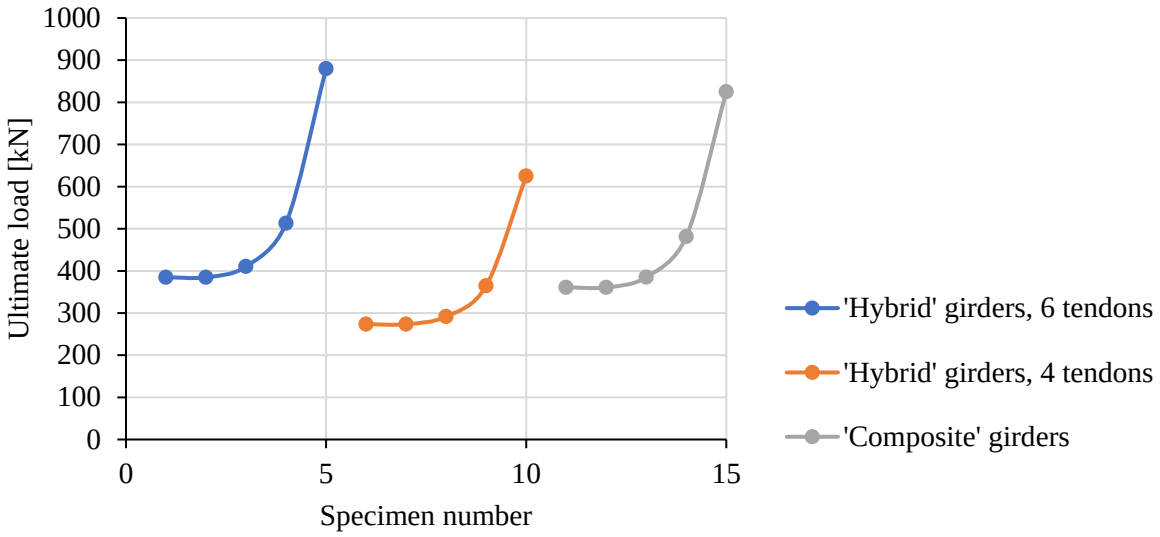

Figure 38: Ultimate loads of discussed specimens based on the moment capacities

The results of the *H6* girders are in general higher than the results for the other two types. This is a direct consequence of the larger moment capacity of the 'hybrid' girder with 6 tendons, what comes from the prestressing tendons. The combined tensile strength of the four tendons from the *H4* compositions is smaller than the tensile strength of the steel lower flange of the *CS* compositions, which in turn is less than the combined strength of the six tendons from the *H6* composition.

The shapes of the results-connecting lines for each girder type are very similar. Starting with the same moment capacity for all girders of one girder type, the ultimate loads are only dependent on the load position that comes with the load situation. Therefore, the shape of the connecting lines must be similar for each type.

3.3.3 Final ultimate loads

All values for the ultimate loads of the girders are calculated, based on the shear capacities, as on the moment capacities. Comparing the results found for these two bases and selecting the lowest value for each girder acquires the real ultimate loads provided by hand calculations (see Table 11). To highlight the lowest values (and thus the dominant values or final ultimate loads), these values are presented in bold.

Table 11: Comparing table of ultimate loads with selection of dominant capacities

Nr.	Ultimate load (shear) [kN]	Ultimate load (moment) [kN]
1.	775.96	**384.85**
2.	492.41	**384.85**
3.	**393.93**	410.51
4.	**328.28**	513.13
5.	**281.38**	879.66
6.	646.63	**273.50**
7.	340.37	**273.50**
8.	**272.30**	291.73
9.	**226.91**	364.67
10.	**194.50**	625.15
11.	969.95	**360.99**
12.	615.51	**360.99**
13.	492.41	**385.06**
14.	**410.34**	481.32
15.	**351.72**	825.12

For approximately half the specimens, the shear capacity is dominant. For the other half, the moment capacity is dominant. Also here, the results are depicted in a line chart (Figure 39):

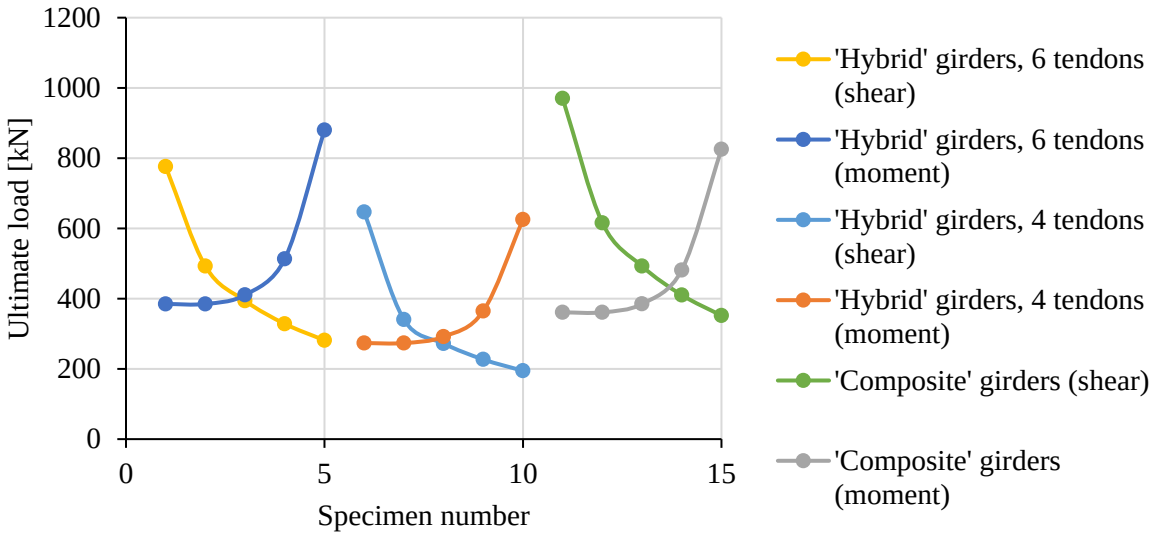

Figure 39: Ultimate loads of discussed specimens based on the shear and moment capacities

For each girder type, only the smaller and therefore dominant values of the ultimate load (based on shear or moment capacity) are important. The values based on the moment capacities increase each time when going over to the next load situation, while the values based on the shear capacities decrease. All three compositions start with a dominant moment capacity and switch after the second or third load situation to a dominant shear capacity. In Figure 40, solely the defining values (or lower values) are compared.

The final ultimate loads are used in chapter 4 (Finite element analysis) to estimate the maximum loads that have to be applied and to verify the obtained results. The final ultimate loads will also be used to determine the right experimental setups.

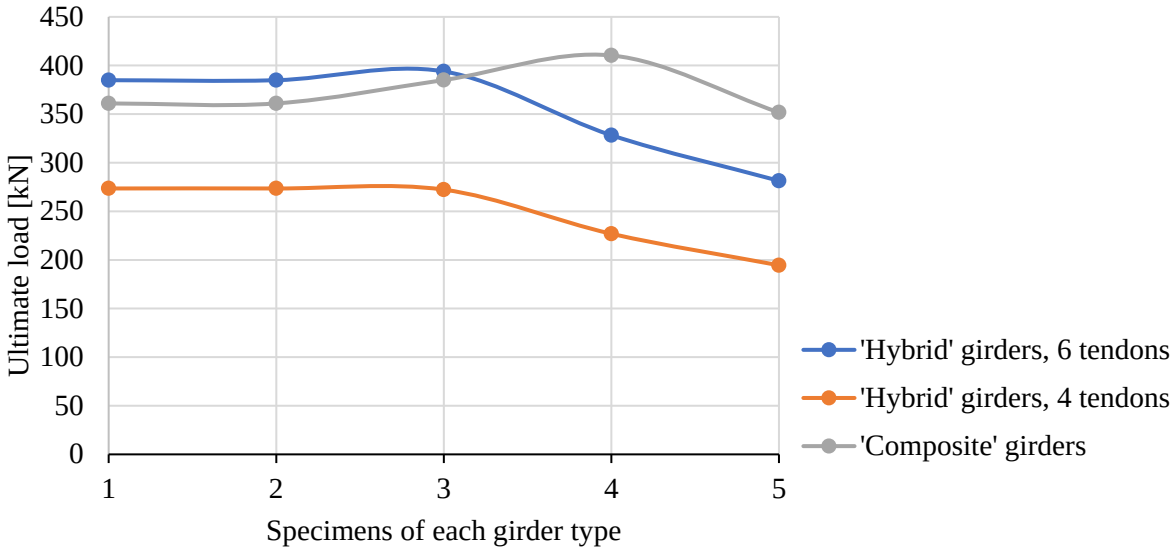

Figure 40: Final ultimate loads of all specimens

4 Finite element analyses

The aim of the finite element analysis is to give a preliminary estimate for the ultimate load carrying capacity and to investigate the structural behaviour of the experimental test specimens during the experimental tests. The created numerical models will also function in further research concerning the parameters of the compound girders. Therefore, in this section the previously presented steel-concrete compound girders with trapezoidal corrugated webs are modelled and analysed.

The chapter is divided into three sections: general information applicable for all analyses, numerical analyses using calculation software ANSYS 15.0 and numerical analyses using calculation software ATENA V5 in combination with pre and post processing software GiD 13.0.4.

The examination of the FE numerical models with respect to the pure ultimate load carrying capacities, namely the bending moment and shear capacities, have high importance in this research process. The validation of the FEM is performed by comparing the results with the hand calculated ultimate capacities. The evaluation of the comparison can be seen in chapter 6.

4.1 Generalities for the numerical analyses

In this section the attributes applicable for the simulation procedures executed with ANSYS and ATENA in combination with GiD, are presented. Approximations, limitations and assumption or discussed and the convergence study used for the meshing is explained.

Approximations, limitations and assumptions

In order to reduce in complexity and calculation time of the FE-analyses, some approximations are made during the modelling procedure. These approximations have almost no influence on the results, while the modelling can sometimes significantly be simplified. Due to limitations in information, other approximations can be necessary to produce working FE-models. These approximations however can sometimes considerably affect the results and are therefore important to be recognized. Following list presents various assumptions and approximations made during the analyses.

- The connection between the concrete flange(s) and the web is considered rigid. Therefore, the transverse connection bars are not modelled as their volume is neglectable compared to the concrete volume. Also, the holes in the web where the bars would cross are not created.
- In the FE-analyses (see section 4.2.1 and 4.3.1) all values of the material properties are mean values. These values can differ from the practice property values of the real girders made in the lab. The concrete for the experimental setups is tested and modified in the numerical models to closely approach the real values. This is an important measure taken to minimize the differences.
- The dimensions of the experimental specimens have certain differences with the ideal values presented in the specimen drawings and used for the FE-modelling and hand calculations. The casting of the concrete, the production of the steel plate, the folding of the plate, etc. have been performed as accurate as possible with the tools available.
- The variation in material properties in the folds of the webs due to strain hardening are not taken into account. Studies have shown that the effect of such variations do not affect the behaviour of the girders significantly. In spite of the fact that the girders in the tests, carried out by Lou and Edlund in 1994, have different properties, this conclusion can be extended to this project. How big the influence of this phenomenon is for the final results is not known, although it can be assumed that they are not big enough to form a problem [22].

- The extra stiffness under the load piston provided by the loading plate used during the experimental tests is not taken into account in the FE-analyses of ATENA. This might have some influence on the behaviour of the upper flange as the load distribution is different.
- Effects from welds are not taken into consideration. In the experimental girders, welds are made between the web and stiffeners, between various web parts and for the 'hybrid' girders to connect the steel web with the steel lower flange. If the welds are carried out properly, these variations will not produce any major differences.
- In experiments, regardless of trying to prevent, unexpected errors or complications can always occur. By working efficiently and attentively, these errors can be reduced to a minimum. If noted, some errors can be taken into account when comparing the results with the results of the FE-analyses.
- Some simplifications were made when modelling the rebars which prevent the transversal expansion of the concrete flanges. The curvatures that were made in the steel bars were modelled as corners each converged in one point.

Mesh convergence study

Mesh convergence study is executed to ensure the model accuracy. In finite element modelling, a finer mesh typically results in a more accurate solution. However, as a mesh is made finer, the computation time increases. The goal is to accomplish a mesh that satisfactorily balances accuracy and computing resources. One way to achieve this, is to perform a mesh convergence study. Performing a convergence study starts with creating a mesh with fewest, reasonable number of elements and analysing the model. Once results are obtained, the mesh using a denser element distribution is recreated, the model is re-analysed and the results found with both meshes are compared. The mesh density will continue to be increased and the model re-analysed until the results converge satisfactorily [25].

According to Moon et al. [25] one web fold should be modelled by minimum of 4-6 elements along the fold length to determine the capacity of the girder with adequate accuracy. Own investigation confirmed this statement. For meshing in ANSYS an GiD, this method was used in combination with the mesh convergence study to determine the best meshing size.

4.2 Numerical analyses using ANSYS

The behaviour of the composite girders with corrugated web under the discussed load situations is in the scope of investigation for this section. Only the composite girders are analysed using ANSYS because the cracking of concrete in ANSYS is not sufficiently developed. The lower flanges in the discussed models are always under tension but for the composite girders this flange is made of steel instead of prestressed concrete. Features necessary to analyse the composite structures are sufficiently accurate. Within the department where this study was conducted, there is a lot of knowledge about ANSYS and less about ATENA. For this reason, not all models were initially produced within ATENA. This chapter provides an explanation of the conducted numerical analysis using ANSYS. A subdivision is made between the numerical model development (section 4.2.1) and the FE-analysis results (section 4.2.2).

4.2.1 Numerical model development

The developed finite element models (geometry, materials, mesh, load and boundary conditions) produced in engineering software ANSYS 15.0 are introduced in this section. The chapter is divided into various topics, with names: geometric model, material model, finite element mesh, loads and boundary conditions, analysis type, applied imperfections and convergence study.

Geometric model

The geometrical models manufactured in ANSYS are modelled as full 3D structures. They consist of areas with material properties limited by surfaces, and surfaces limited by edges. Specimen number 15 is presented as a visualisation example in Figure 41. The full model, a detail with the middle stiffener (the position variating stiffener) and a detail without upper concrete flange are shown.

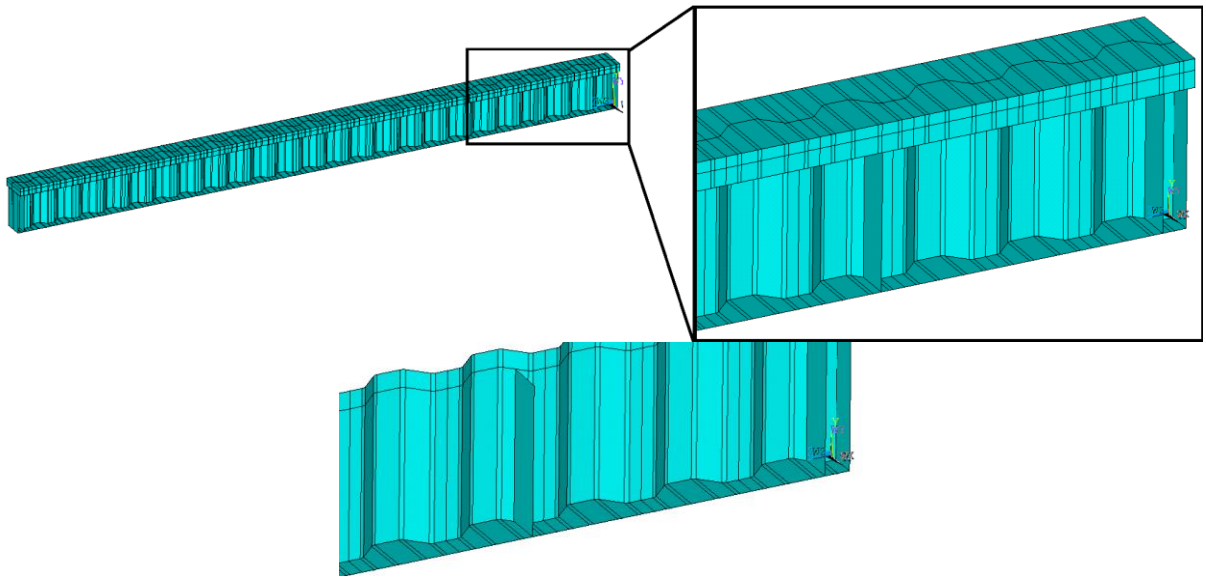

Figure 41: Geometric model of 'composite' girder specimen 15 modelled with ANSYS

Specimen number 15 can be recognized in Figure 41 because of its composition ('composite' girder type) and the positioning of the stiffeners. The middle stiffener is places at a distance of 1 m starting from the support stiffener. Therefore, this must be specimen number 15 that will be exposed to load situation 5.

Material model

In the FE-model two material models are used: one for the steel and one for the concrete volumes. For the steel material the character of the applied material model is a linear elastic - hardening plastic material model using von Mises yield criterion. This multilinear material model has in the plastic domain an isotropic hardening behaviour. The material is assumed to behave linearly elastic and to obey Hooke's law with a Young's modulus equal to 210000 MPa up to the assumed mean yield stress (f_y) of 280 MPa. The yield plateau is modelled up to 1% strains. Thereafter and until it reaches the assumed mean ultimate stress (f_u) of 460 MPa, the material is assumed to behave linear and strain harden with a reduced modulus. The ultimate strength is defined by 12% strains. The material is perfectly plastic when it reaches the ultimate stress.

For the concrete material the character of the applied material model is a linear elastic – softening plastic material model. For the sake of simplicity, the cracking and crushing are not considered in the analysis. This multilinear material model has in the plastic domain a kinematic hardening behaviour. The material is assumed to behave linearly elastic and to obey Hooke's law with a Young' modulus equal to 35000 MPa up to the assumed mean compressive stress (f_{cm}) of 50 MPa. The plateau is also modelled and after this, the material is assumed to linearly soften.

Finite element mesh

Figure 42 presents the finite element mesh of specimen number 15. In the finite element models the SHELL181 and SOLID65 elements are applied for the steel and respectively concrete parts. Both materials are given a certain colour and also the stiffeners have a different colour to clearly see the distinction of volumes. In the model, mapped mesh is applied for each part. The connection between the steel corrugated embedded web and the concrete upper slab is modelled rigid by having the same nodes for both parts.

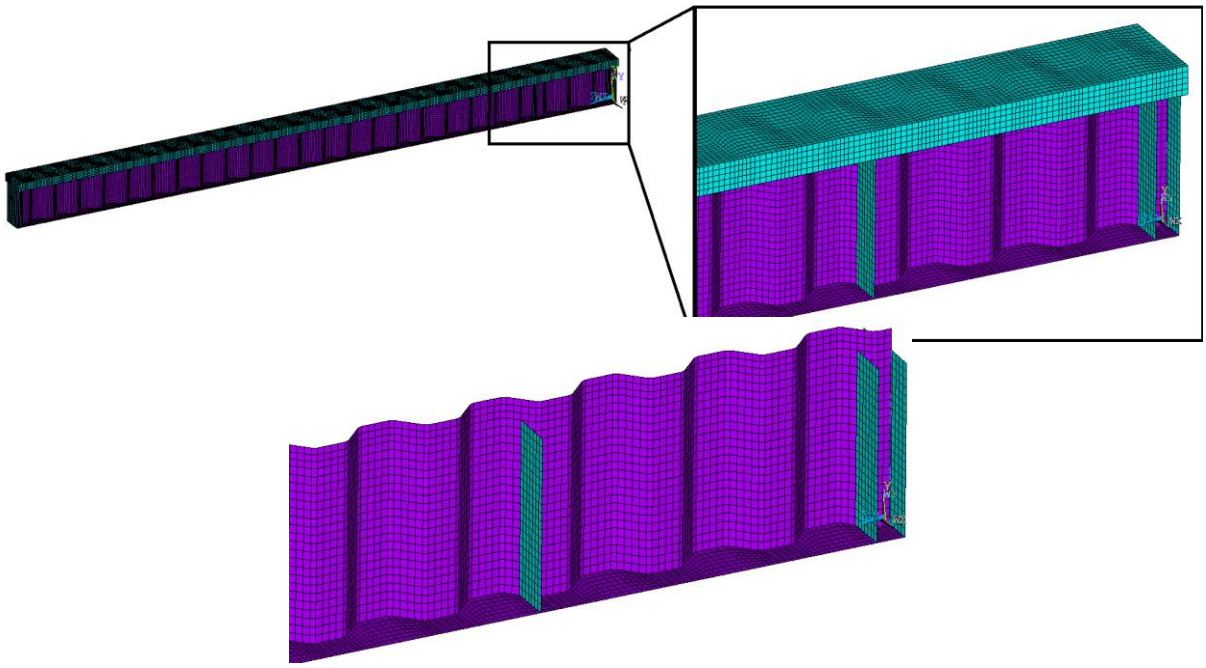

Figure 42: Finite element mesh of composite girder specimen 15 modelled with ANSYS

The attributes of the SOLID65 finite element are:

- eight-node solid element;
- three degrees of freedom at each node, translations in the nodal x, y and z direction;
- applicable for linear or nonlinear analyses.

Figure 43 provides a representation of SOLID65 element type used in the models for the concrete volumes.

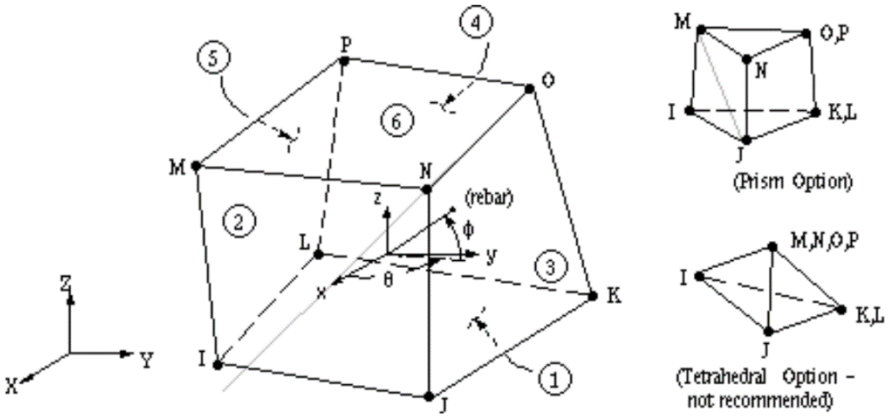

Figure 43: SOLID65 finite element [39]

The attributes of the SHELL181 finite element are:

- four-node thin shell element;
- bending and membrane (in-plane) capabilities, so both in-plane and normal loads are resisted;
- six degrees of freedom at each node, translations in the nodal x-, y- and z-direction and rotations around the nodal x-, y- and z-axis;
- large strain and large deflection capabilities are also included;
- it can be applicable for stability analysis (critical stress level determination);
- applicable for linear or nonlinear analyses;

Figure 44 provides a representation of SHELL181 element type used in the models for the steel volumes.

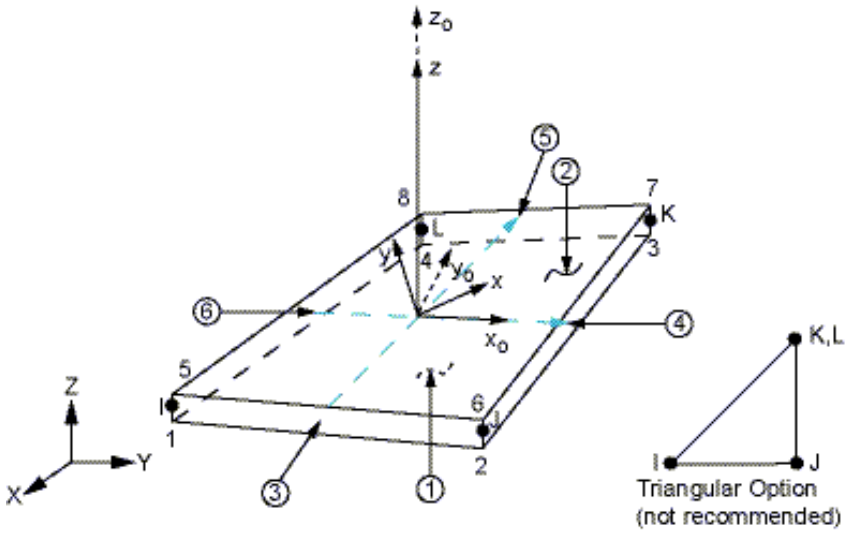

Figure 44: SHELL181 finite element [39]

Loads and boundary conditions

The different boundary and loading conditions of the finite element models modified for the investigation of the 'composite' girders in each load situation are presented. Figure 45 shows the situation when half of the girder is modelled: the right side of the girder is simply supported while on the left side symmetric conditions are prescribed. This model is applicable for load situation 1 and 2 (with different web thicknesses) as a result of the symmetrical characteristics of the setups. Only modelling half of the setup leads to a reduction in modelling data and therefore a shorter calculation time (with a constant mesh size).

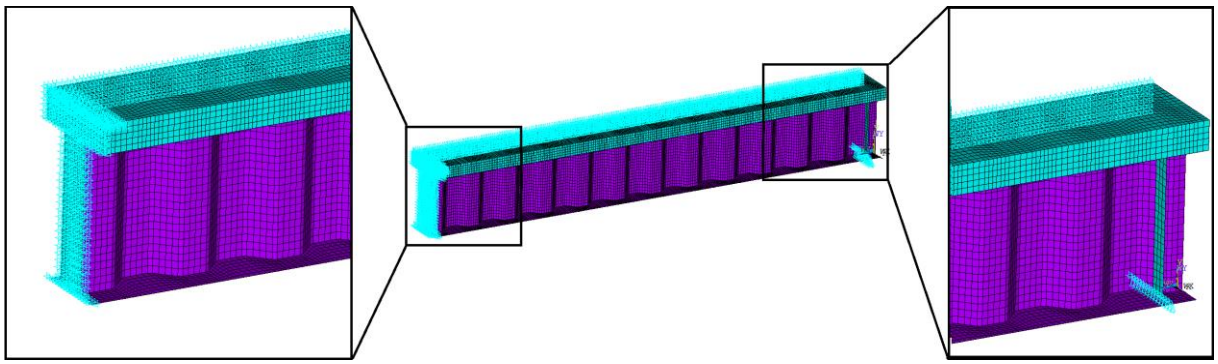

Figure 45: Boundary conditions for load situation 1 and 2

Figure 46 shows the situation when the whole girder is modelled: the girder is simply supported at the two ends and supported laterally along the whole girder to ignore lateral torsional buckling failure. This model is applicable for load situation 5 but also for 3 and 4 after repositioning the load and load stiffener conditions.

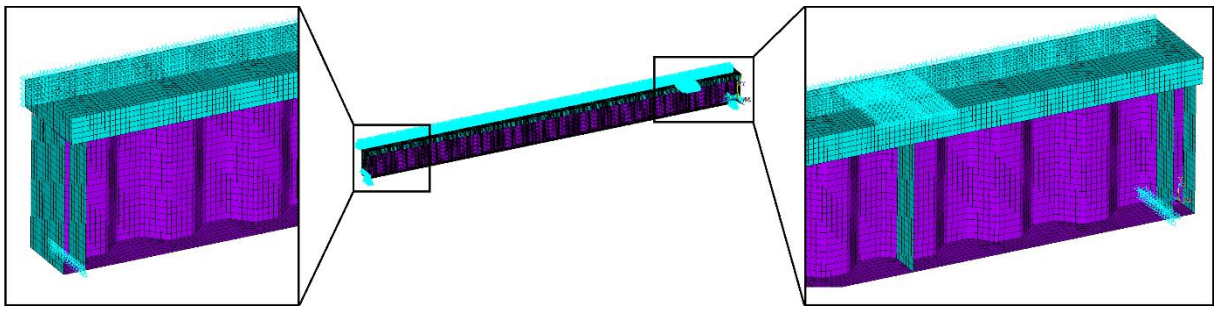

Figure 46: Boundary conditions for load situation 5

For the load, displacement magnitude is prescribed at the load introduction places. This indicates a displacement controlled instead of a force controlled analysis. The program stops its analysis if it is not able to converge in a displacement step or after reaching the prescribed displacement.

Analysis type

The analysed numerical FE-models in this chapter, namely the 'composite' girders, are developed using the finite element software ANSYS 15.0. The numerical modelling is based on the combination of shell and solid elements. The ultimate loads that form the combined load situations are determined by geometrical and material nonlinear analyses using equivalent geometric imperfections (GMNIA). The full Newton-Raphson approach is used in the nonlinear analyses since it is well-suited for handling large deformations. Working with the Arc-Length method would have given more precise results; this method is more suitable when doing research concerning collapse loads of structures. Because of the limited time for this project and the smaller calculation-time when working with the Newton-Rapson method, for the analyses of the 'composite' girders in ANSYS this method was chosen. This simplification is justified by the appropriat results obtained from the analyses performed with the Newton-Raphson approach. The nonlinear solver convergence was analysed using different time stepping attributes such as the time step size and maximum and minimum time step sizes. Due to the convergence study the time step sizes are set properly in the numerical simulations. During the simulations the default convergence criteria built in ANSYS are used. In the analyses displacement control is used.

Applied imperfections

The aim of this research is to determine the resistances of compound girders with corrugated web against pure and combined shear and bending forces. The shear strength is dependent on the probability of buckling, thus the initial introduced imperfection has an important role in the numerical calculation procedure. Initial imperfections are geometrical and/or structural imperfections (e.g. residual stresses). Both can be considered by equivalent geometrical imperfections. There are three different alternatives to define the equivalent geometric imperfection which are allowed according to the EN1993-1-5 [15].

1) The first possibility is to manually apply the frequently observed imperfection shapes after the fabrication processes. A possible imperfection shape is practically defined by a functional description such as a sine or other periodic functions. This approach is the most complex and very difficult to perform in practice.

2) The second possibility is to apply the critical plate buckling mode imperfections. The standard allows using the first eigenmode as an imperfection shape, which corresponds to the buckling shape of the analysed panel. The plate buckling modes have mathematical bases, therefore it is fully objective and the modelling technique has already been established. The main advantage of this technique is that the usage of the first eigenmode imperfection shape leads to a safe design.

3) The third option is the ultimate failure shape as a possible imperfection type, found by a primarily executed buckling analysis. In this case the applied imperfection shape comes from the previous geometrically perfect computation (GMNA[7]). The ultimate failure shape of the original perfect computation is then used to update the perfect geometry to an imperfect shape. This imperfection type is not a commonly used imperfection e.g. because it is time-consuming and may lead to a too conservative design approach.

What option 1 concerns: in most cases the initial imperfections of the specimens are not known during the modelling phase. On top of this, the measuring procedure is very time-consuming and does not contain the residual stresses. Using periodic functions as equivalent geometric imperfections can be a possible solution, but this leads to a very complex and slow approach which requires a high degree of attention. Therefore, it is not serviceable for parametric study and for combined loading situations.

For option 3: using the ultimate failure shape as equivalent initial imperfection is also a very time-consuming approach because all the nonlinear computations must be performed at least twice in order to primary determine the appropriate ultimate failure shape. Furthermore, it is very rare that the applied imperfection coincides with the ultimate failure shape imperfection, as a result this approach leads to the most conservative design.

Option 2: the application of the first eigenmode shape, is the most common option to use because it contains the relevant failure mode. In the current research work different failure modes are studied separately and in combination, the best and always a safe solution is ensured by using eigenmode imperfections. This imperfection type can handle the change of the failure mode in the interaction domain. Maybe the usage of the first eigenmode imperfection shape leads to a conservative design, but it can be assured that all of the calculations are on the safe side. As a result, all the numerical parametric studies are executed using the first eigenmode imperfection shape. The first eigenmodes due to pure shear force can be seen in Figure 47. Imperfections are introduced in the part most likely to fail, in this case next to the stiffener where the shear forces are greatest [15], [20].

[7] GMNA: Geometrically and Materially Nonlinear Analysis

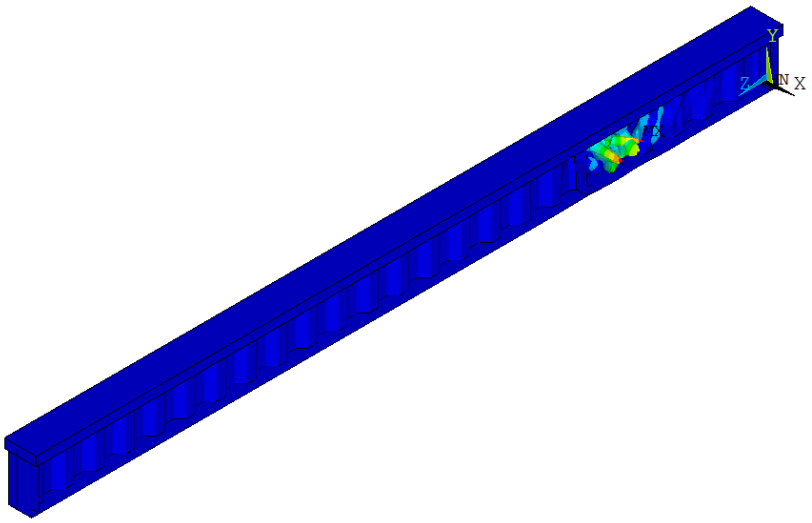

Figure 47: Shear buckling eigenmode introduced imperfection

For this imperfection implementation, there is no recommendation in the EN1993-1-5 for the imperfection amplitude of corrugated webs. However, imperfection sensitivity analysis has been also carried out by different researchers investigating the pure shear buckling resistance of corrugated web girders. Driver et al. [21] proposed that the magnitude of the applied imperfection amplitude can be taken as the thickness of the web which was confirmed by Hassanein et al. [22]. Another magnitude for the imperfection amplitude was proposed by Yi et al. [23], Nie et al. [24] and Jáger et al. [20]. They suggested using the web depth divided by the scaling factor 200, as equivalent initial geometric imperfection amplitude. The last one is used because in most of the cases it gives greater imperfection magnitudes and is therefore more conservative.

In the concrete volumes no imperfections must be implemented because these volumes are not slender and are not likely to buckle.

4.2.2 FE-analysis results

This section presents the preliminary FE-analysis results regarding the 'composite' test specimens. The examination and comparison of the results is based on four load step situations from the loading procedure of each girder. The first point (*a)* always regards the yield strength of the girder or in other words the situation were the girder stops obeying to Hooke's linearity law. The third point (*c*) belongs to the buckling of the web and the second point (*b*) is chosen close to the middle (in loading and deflection) between the first (*a*) and third (*c*) point. Depending on the shape of the load-deflection curve, points b and c can be chosen differently to more precisely clarify the behaviour of the beam member. The last point (*d*) indicates the end of the analyses, this is when the girder is considered failed.

To better understand the behaviour of the girders, colour maps of the internal stresses are used. The colour maps of the figures are limited by the ultimate strength of the two main materials, namely the mean compression strength of concrete and the mean yield strength of the steel material. The grey coloured surfaces in the figures represent the yielding of the steel or the crushing of the concrete. It is to be noted that due to the applied plastic-softening material model of concrete the crushed parts can become coloured again due to a smaller stress level, because of this the loading history (point *a*, *b*, *c* and *d*) has of importance. The simulation is terminated when it can not converge in a displacement step or after reaching the prescribed displacement. For all presented analyses, except the analysis of specimen 14, the prescribed displacements were not reached, what means that the full behaviours for all girders except specimen 14 are

examined until the deformations became too extensive. What specimen 14 concerns, here only a part of the post buckling range is obtained.

Specimen 11 exposed to load situation 1

Specimen 11 is the first 'composite' girder and is therefore exposed to load situation 1. It is a symmetric model with the increasing load imposed on the upper flange centrally located between the two supports and has a web thickness of 6 mm.

The results of the displacement controlled analysis are displayed in a load-deflection curve in Figure 48. The depicted deflection or vertical displacement is based on the part of the beam where the largest displacement occurs. This corresponds to the part on which the external force is applied, in this situation in midspan of the beam.

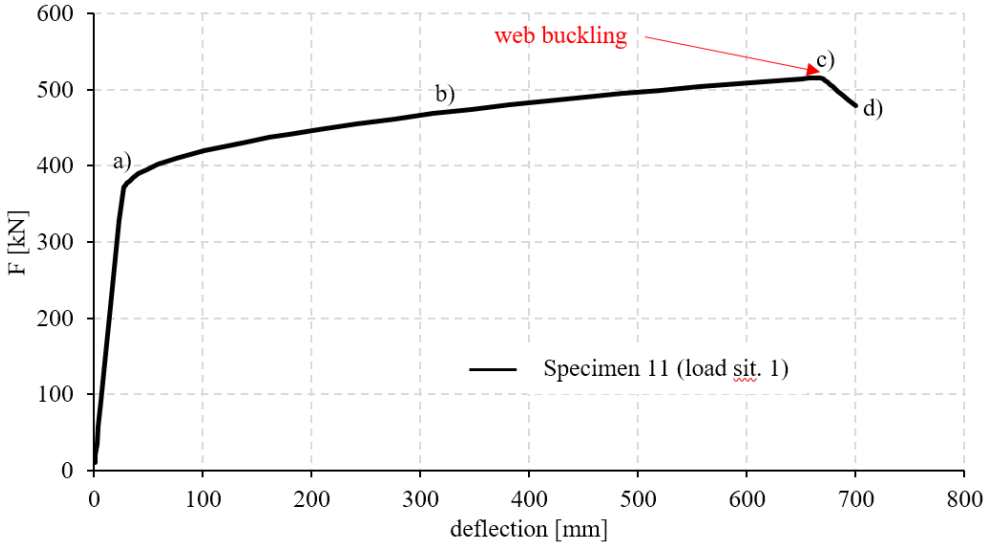

Figure 48: Load – vertical displacement curve of specimen 11 provided with ANSYS

From the found force-deflection results presented in Figure 48 the behaviour of the girder can be derived. The girder starts with an elastic behaviour based on Hooke's law with a Young's modulus equal to 21000 MPa. In point *a*, it then reaches the yield point and the structure begins to behave plastically. An explicit yield plateau is not formed, but from point *a* to *c*, a very linear hardening behaviour can be observed. Once the web starts to buckle in point *c*, the girder quickly loses its strength and fails in point *d*. The points (*a*,*b*,*c* and *d*) indicated on the curve presented in Figure 48 match the girder situations displayed in Figure 49.

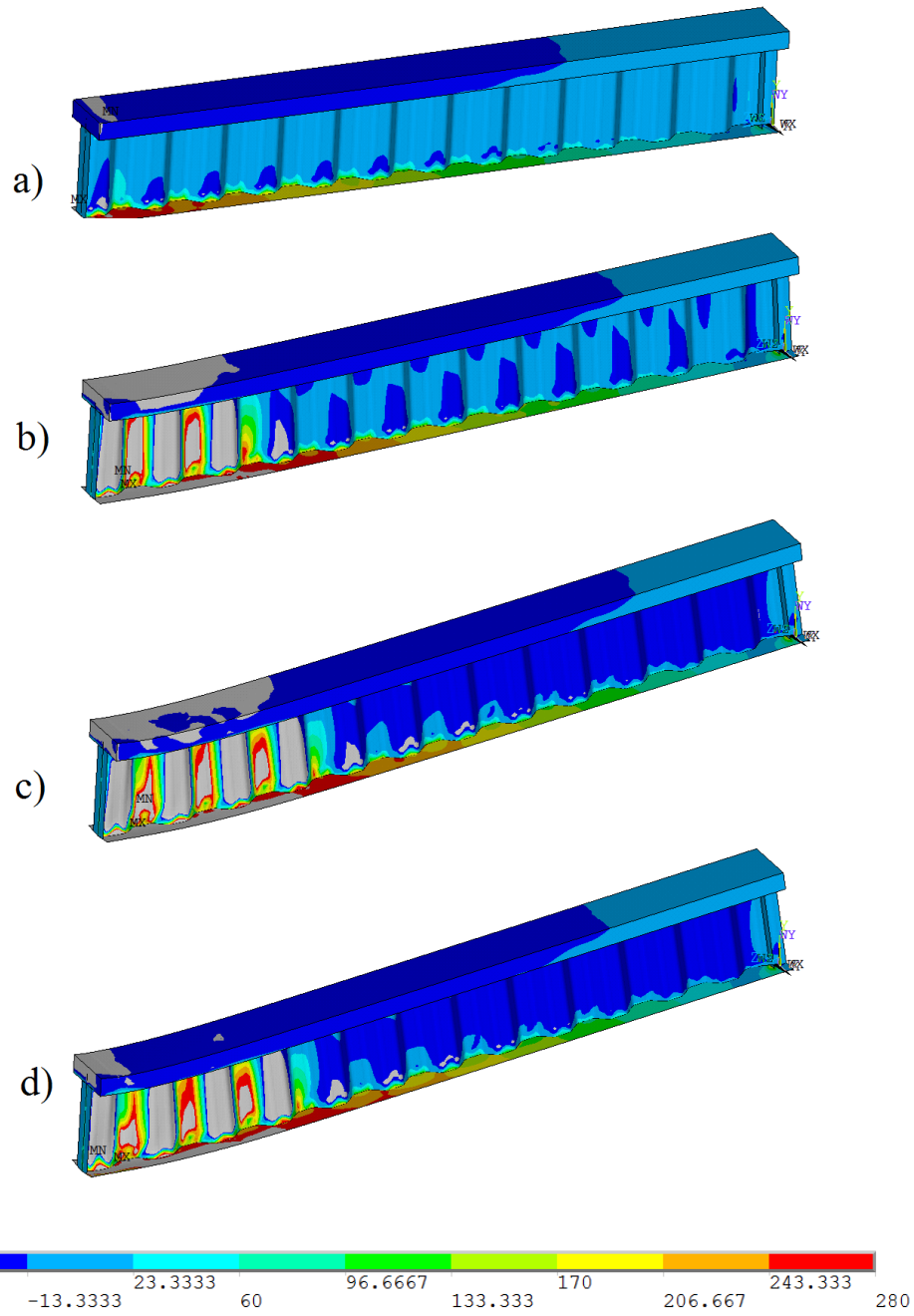

Figure 49: Longitudinal stress distributions in different load levels of specimen 11 modelled in ANSYS (see Figure 48)

The colour scaling in Figure 49 presents the stress distribution accompanying the force-deflection points from Figure 48. In the colour scale, the negative values refer to compression and the positive values to tension. As expected in the upper flange, the girder experiences compression, while in the lower flange mainly tension occurs. The grey colour locates the areas where the materials fail (crushing of concrete or yielding of steel). In this case the flanges determine the end of the simulation. In point *a*, both flanges reach their failure mode in the middle of the girder. The areas from the flanges in which the materials fail continue to increase until the girder is considered failed in point *d*. In the web, the rising shear forces starts introducing stresses that try to make the web buckle under local buckling mode. The stress colour areas mostly stay within one and the same fold. In the curve from Figure 48 and the stress distribution of Figure

49 can be seen that the structure is mostly exposed to bending forces. This was expected as the load is located in the middle of the girder, causing a situation where the bending moments are dominant.

Figure 50 presents the ultimate lateral displacement, or in other words the lateral displacement accompanying situation d from Figure 48 and Figure 49 of specimen 11.

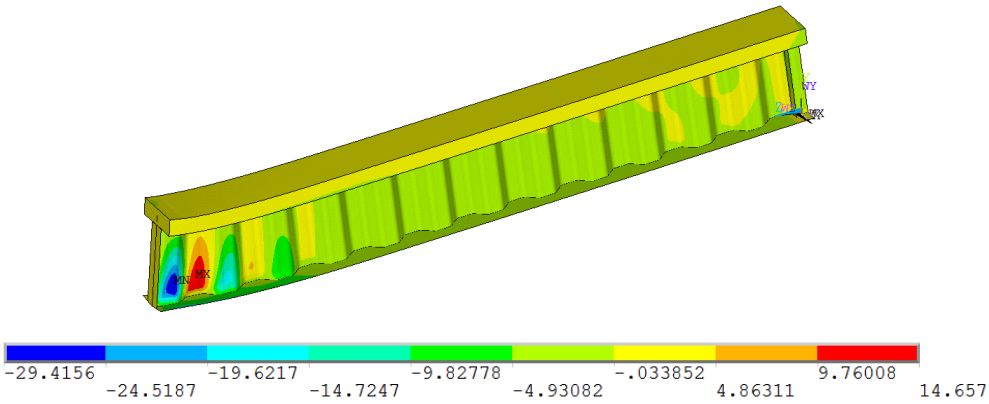

Figure 50: Ultimate lateral displacement of specimen 11 modelled in ANSYS

The colour scaling indicates that the web becomes most sensitive to buckling in the middle of the girder (in Figure 50 the left side of the model indicates the middle of the girder). Directly next to the middle stiffener and under the increasing load, the highest shear forces occur. Because of these shear forces the lateral displacements and buckling stresses are highest in this point.

Specimen 12 exposed to load situation 2

Specimen 12 is the second 'composite' girder and is therefore exposed to load situation 2 which has the same attributes as load situation 1. It is a symmetric model with the increasing load imposed on the upper flange centrally located between the two supports and has a web thickness of 4 mm. The results of the displacement controlled analysis executed in ANSYS are displayed in a load-deflection curve in Figure 51.

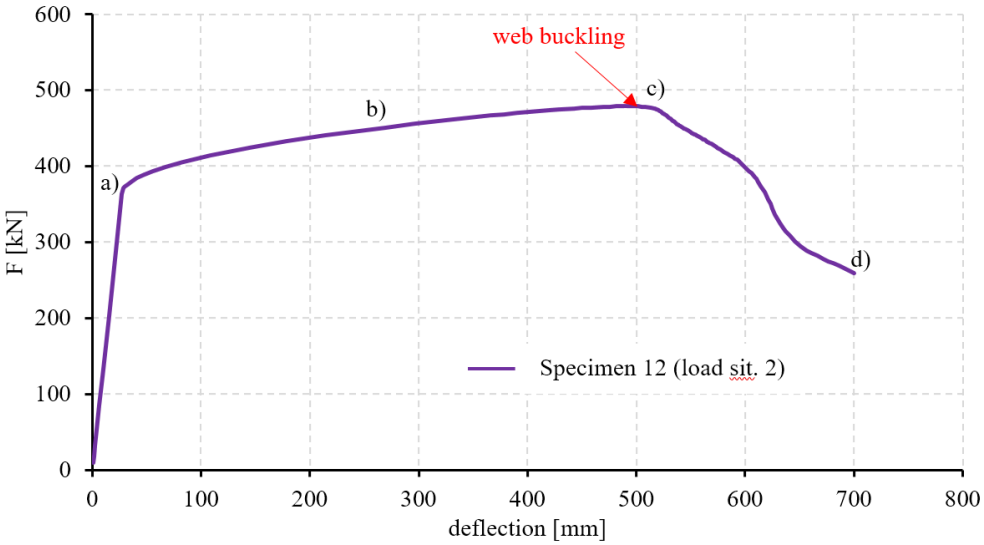

Figure 51: Load – vertical displacement curve of specimen 12 provided with ANSYS

The behaviour is expected to be similar to the behaviour of specimen 11 because the only difference (the web thickness) should not have a significant influence on the behaviour, as the girder is mainly subjected to bending moments. The load-deflection curve starts of the same as the curve of specimen 12 and reaches point *a* under the same load force with the same vertical displacement. That the two girders have the exact same ultimate loads is predicted in the hand calculations. After reaching point *a*, the girder starts its hardening process but does not reach the same values in *b* and *c* compared to the specimen 11. This a is then consequence of the difference in web thickness. The girder experiences more shear forces, because of the smaller web thickness it is less resistant to these forces and therefore the girder buckles in point *c* of the load-deflection curve, where it then loses its strength.

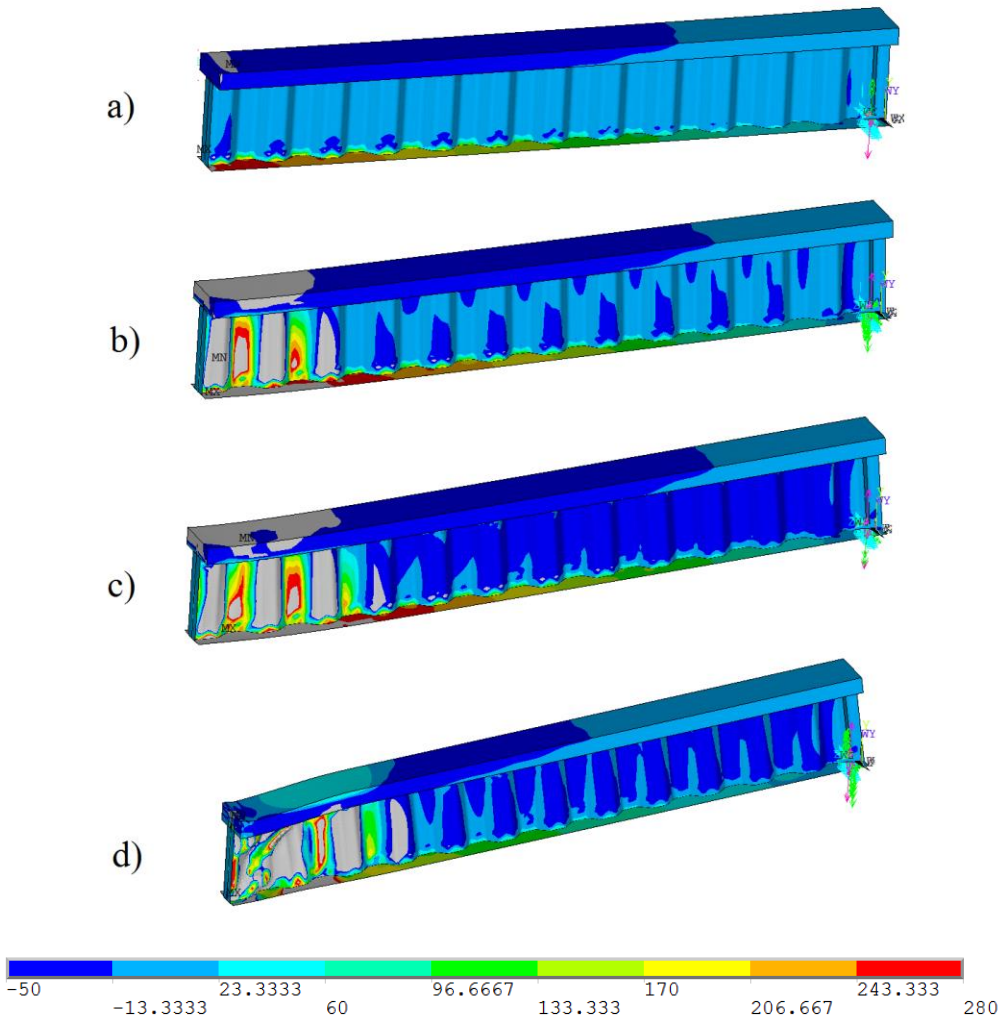

Figure 52: Longitudinal stress distributions in different load levels of specimen 12 in modelled in ANSYS (see Figure 51)

The colour scaling in Figure 52 presents the stress distribution accompanying the force-deflection points from Figure 51 concerning specimen 12 exposed to load situation 2. Also the progression of the longitudinal stress distribution in the girder, happens until point *a* practically in the same way as for the progression in specimen 11. The concrete upper flange and steel lower flange determine the end of the simulation. The stress colour areas mostly stay within one and the same fold, this indicates that the rising shear stress in the web introduces the local shear buckling mode. In the curve from Figure 51 and the longitudinal stress distribution progress shown in Figure 52 can be seen that the structure is mostly exposed to bending forces.

This was expected as the load is located in the middle of the girder, causing a situation where the bending moments are dominant.

Figure 53 presents the ultimate lateral displacement, or in other words the lateral displacement accompanying situation *d* (failure of the girder according to ANSYS).

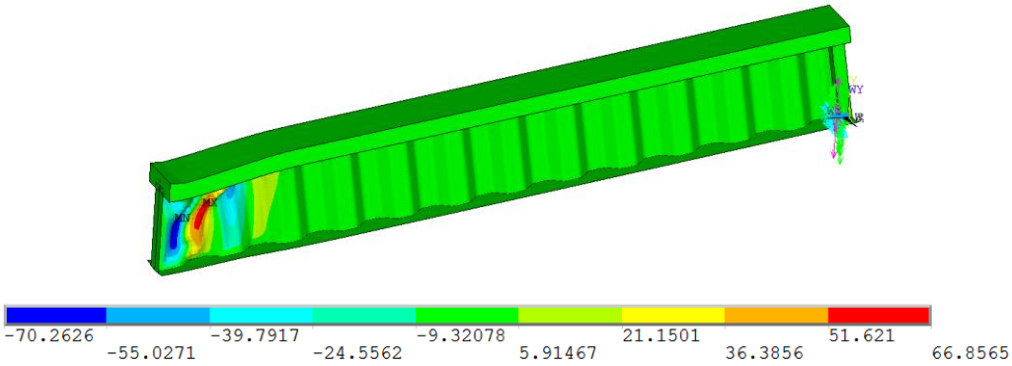

Figure 53: Ultimate lateral displacement of specimen 12 modelled in ANSYS

The colour scaling indicates that the web becomes most sensitive to buckling in the middle of the girder (the left side of the model indicates the middle of the girder). Directly next to the middle stiffener and under the increasing load, the highest shear forces occur. Because of these shear forces the lateral displacements and buckling stresses are highest in this point.

Specimen 13 exposed to load situation 3

Specimen 13 is the third 'composite' girder and is therefore exposed to load situation 3. It is an asymmetric model with the increasing load imposed on the upper flange at 3 m distance of the nearest support and has a web thickness of 4 mm. The results of the displacement controlled analysis are displayed in a load-deflection curve in Figure 54.

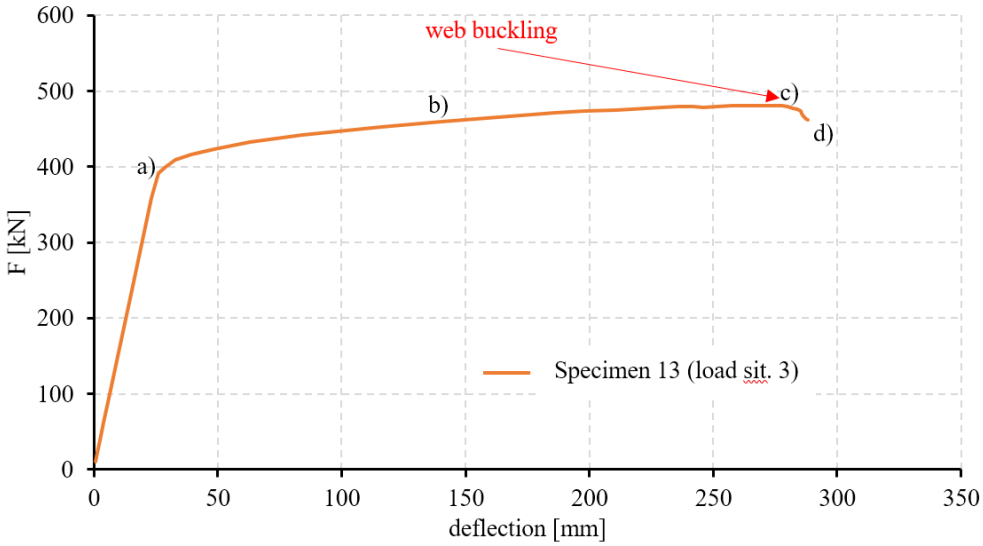

Figure 54: Load – vertical displacement curve of specimen 13 provided with ANSYS

The shape of the load-deflection curve depicted in Figure 54 is comparable to the load-deflection curves found for specimen 11 and 12. Starting with a similar composite Young's modulus, the girder reaches its yield point (*a*) under influence of a higher load force than the girders exposed to load situation 1 and 2. This

can be explained by examining the yielding process of the girder. The girder starts behaving plastically when the concrete upper flange starts crushing and/or the steel web start yielding, which results from the bending moment introduced by the load force (just like for specimen 1 and 2). The bending moment created by the same imposed load size, forms a smaller moment in the setup of load situation 3, than in load situation 1 and 2. Because the ultimate bending moment (moment where the girder start behaving plastically) of the girders should be the same, a greater load force can be applied before the girder reaches point *a*. The course from point *a* to point *c* in the load-deflection curve runs parallel for all three curves, but is for this girder stopped when reaching a much smaller deflection. This is because in this situation the same load force implies higher shear forces in the girder. Once the web starts to buckle in point *c*, the girder quickly loses its strength and fails in point *d*. The points (*a*,*b*,*c* and *d*) indicated on the curve presented in Figure 54 match the girder situations displayed in Figure 55.

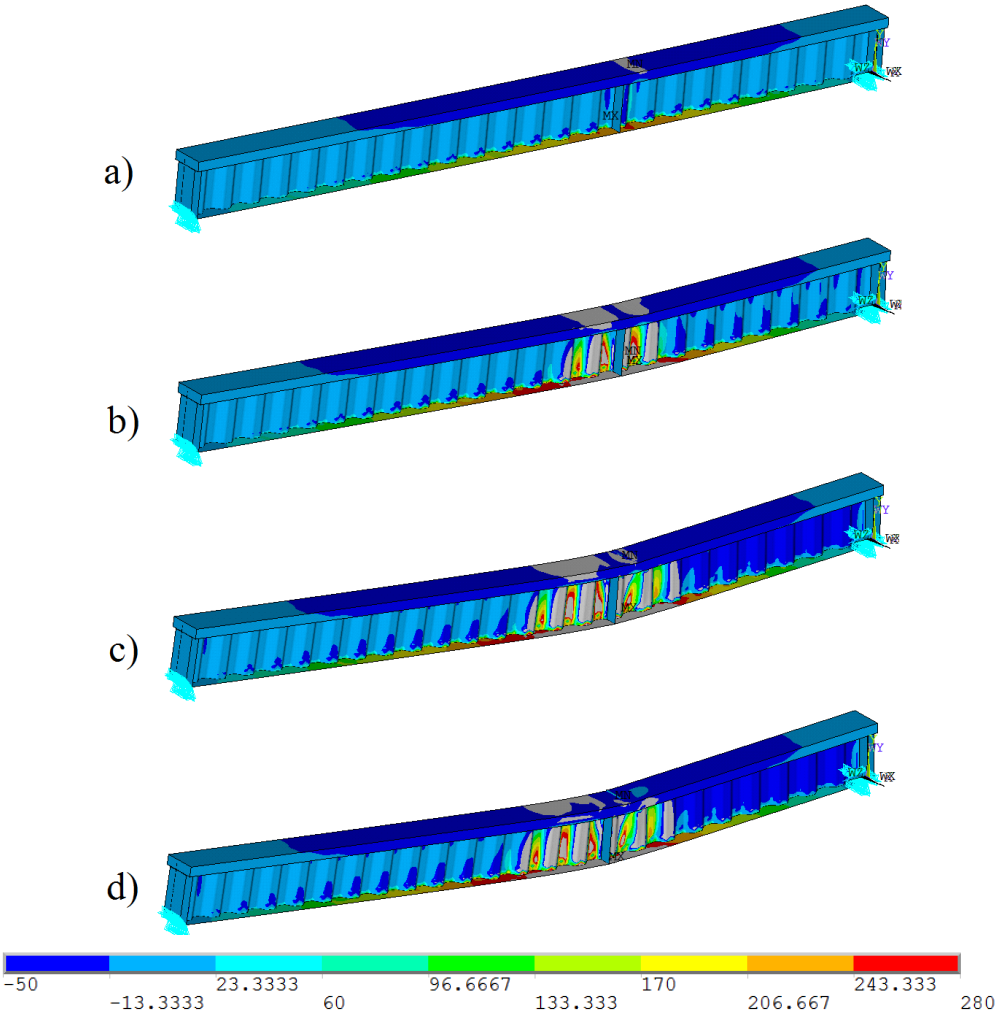

Figure 55: Longitudinal stress distributions in different load levels of specimen 13 in modelled in ANSYS (see Figure 54)

The colour scaling in Figure 55 presents the stress distribution accompanying the force-deflection points from Figure 54. The affected zone (under the applied load) originated more towards one of the supports compared to the symmetric setups. As a result of the arising bending moment, the concrete upper flange determines the end of the simulation. In the web, the rising shear stress introduces the interactive buckling mode (transitional phase between local and global buckling) and the development of the stresses in the web is associated with smaller deflections compared to specimen 11 and 12. Considering the internal forces as a result of the load situation, the bending moments are still dominant but the shear forces gain in importance.

Figure 56 presents the ultimate lateral displacement, or in other words the lateral displacement accompanying situation *d* (failure of the girder).

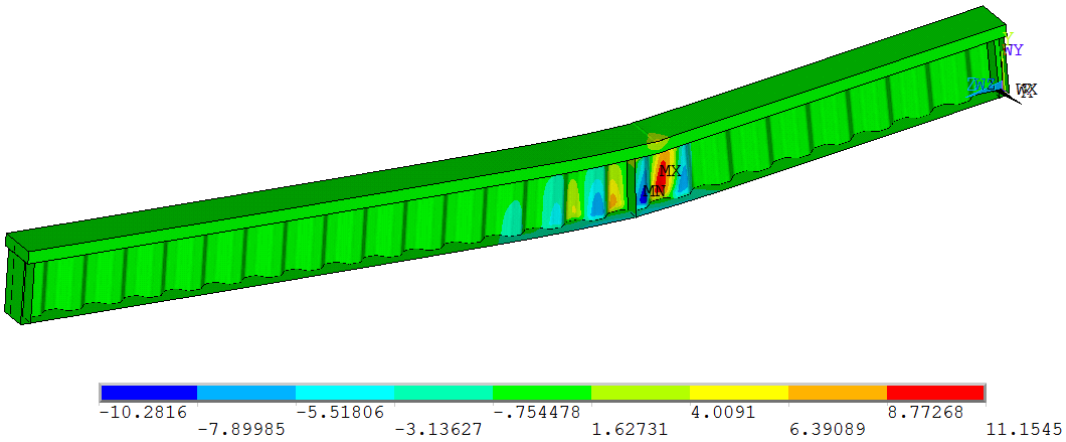

Figure 56: Ultimate lateral displacement of specimen 13 modelled in ANSYS

The colour scaling indicates that the web becomes most sensitive to buckling directly next to the middle stiffener and under the increasing load. Because of the load, the highest shear forces occur in this area and therefore also the highest lateral displacements and buckling stresses originate here.

Specimen 14 exposed to load situation 4

Specimen 14 is the fourth 'composite' girder and is therefore exposed to load situation 4. It is an asymmetric model with the increasing load imposed on the upper flange at 2 m distance of the nearest support and has a web thickness of 4 mm. The results of the displacement controlled analysis are displayed in a load-deflection curve in Figure 57.

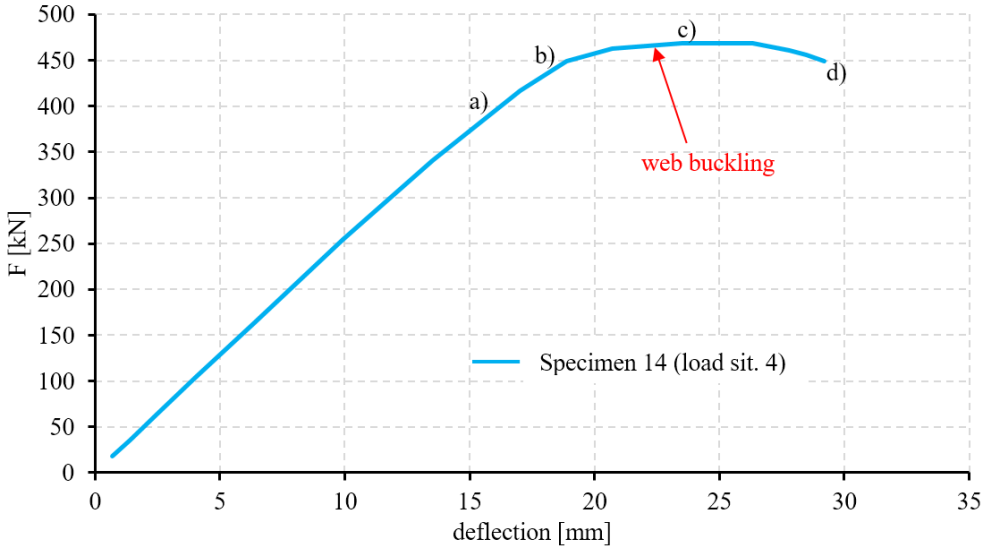

Figure 57: Load – vertical displacement curve of specimen 14 provided with ANSYS

The load-deflection curve depicted in Figure 57 has a different shape than the curves achieved for specimen 11, 12 and 13. Here the load is located closer to one of the supports and therefore introduces significantly higher internal shear forces. As predicted by the hand calculations, in the load situation applied to specimen 14, the shear capacity becomes more important than the moment capacity of the girder. Instead of crushing of the upper concrete flange or yielding of the steel lower flange, here point a is reached by the yielding of

steel web. After point a is reached, less than 10 mm extra deflection is needed for the web to buckle. After buckling (point *c*), only a part of the post buckling range is obtained. ANSYS terminated the analysis in point *d*, but a similar ending of the curve, as in the load-deflection curve of specimen 15 displayed in Figure 60 (see further), can be expected. The points (*a*,*b*,*c* and *d*) indicated on the curve presented in Figure 57 match the girder situations displayed in Figure 58.

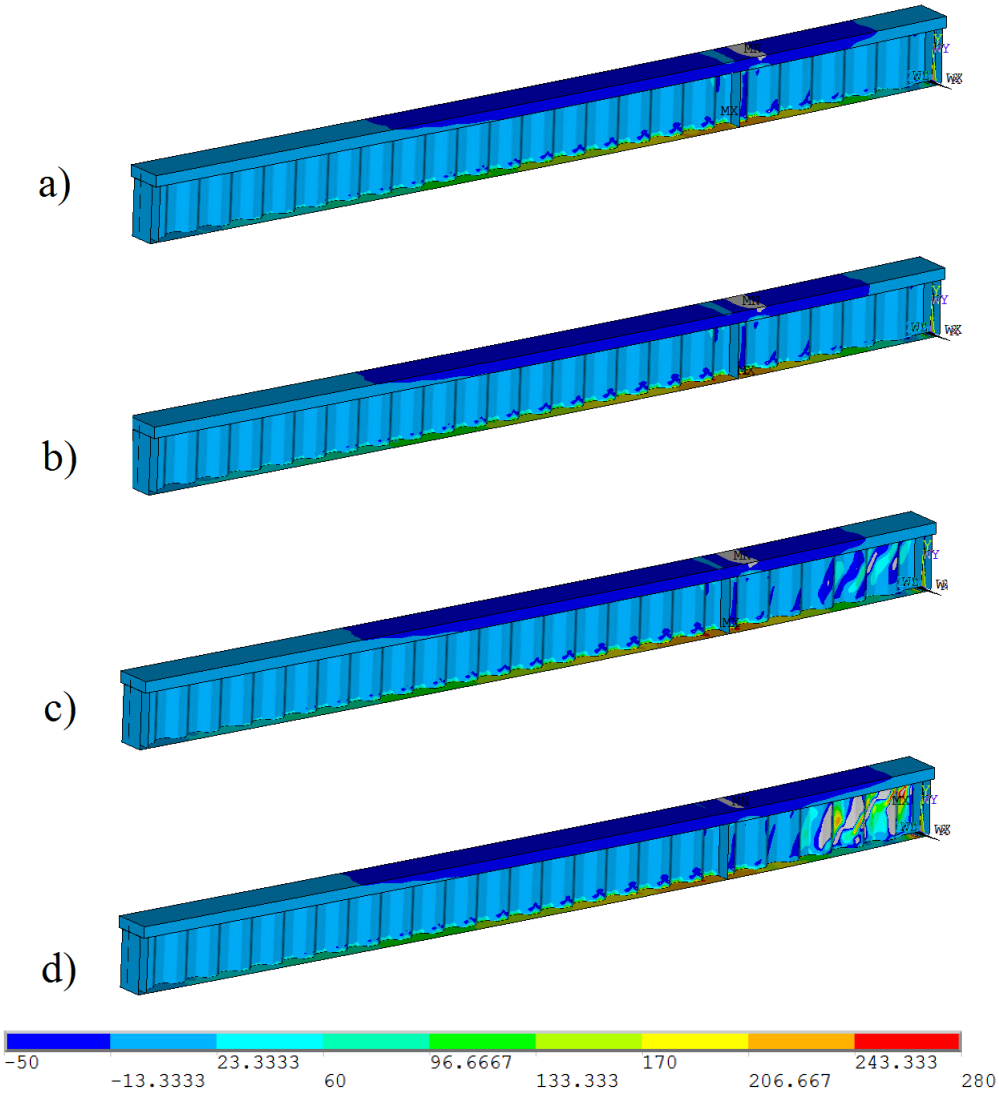

Figure 58: Longitudinal stress distributions in different load levels of specimen 14 in modelled in ANSYS (see Figure 57)

The colour scaling in Figure 58 presents the stress distribution accompanying the force-deflection points from Figure 57. The most affected zone in this case is the corrugated web between the middle stiffener and the nearest support exposed to shear stress. The arising bending moment will not be able to crush the concrete or yield the steel of the lower flange, before the web starts to yield. In point *a* (see Figure 58) the steel lower flange starts yielding after which in point *c*, the web starts to widely buckle in the area between the middle stiffener and the nearest support. In Figure 58 it is clear to see that the occurring buckling is of the global shear buckling sort. The colour areas do not stay within one particular fold but are spread over multiple folds.

Figure 59 presents the ultimate lateral displacement, or in other words the lateral displacement accompanying situation *d* (failure of the girder).

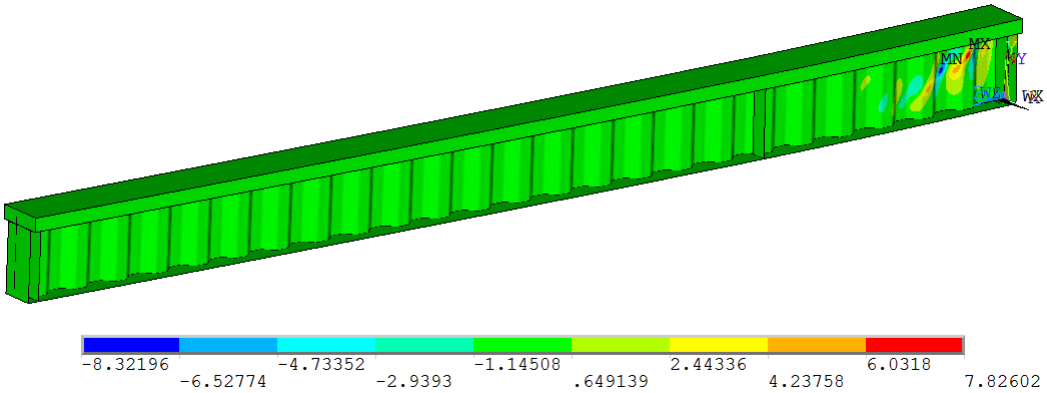

Figure 59: Ultimate lateral displacement of specimen 14 modelled in ANSYS

The colour scaling indicates that the web becomes most sensitive to buckling directly next to the nearest support (relative to the load). The long colour areas indicate the that the type of buckling corresponds to global shear buckling.

Specimen 15 exposed to load situation 5

Specimen 14 is the last 'composite' girder and is therefore exposed to load situation 5. It is an asymmetric model with the increasing load imposed on the upper flange at 1 m distance of the nearest support and has a web thickness of 4 mm. The results of the displacement controlled analysis are displayed in a load-deflection curve in Figure 60.

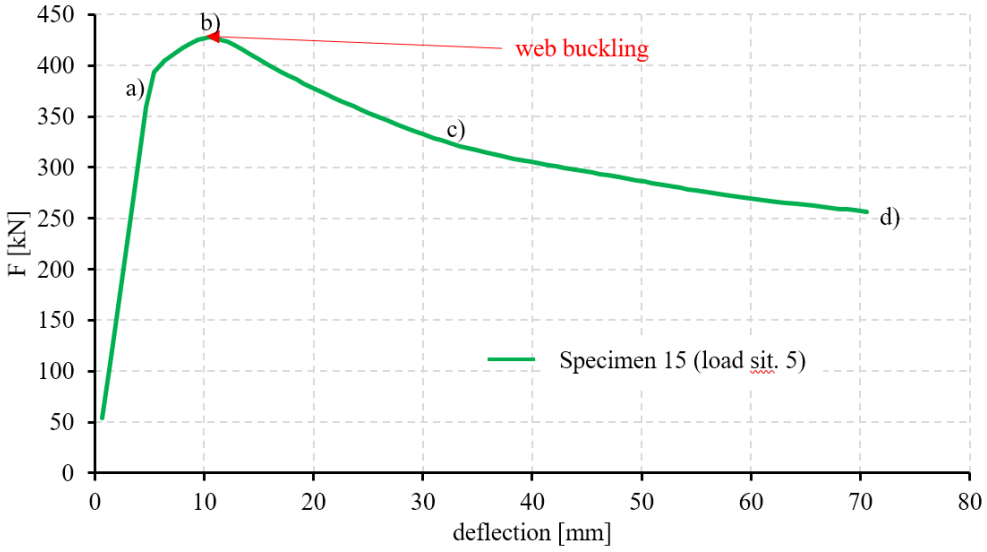

Figure 60: Load – vertical displacement curve of specimen 15 provided with ANSYS

The load-deflection curve depicted in Figure 60 has a similar course as the curve achieved for specimen 14. In load situation 5 (implemented for the discussed specimen) the load is located closer to one of the supports and therefore introduces significantly higher internal shear forces. Point *a* is reached with a smaller load level than for specimen 14 but the composite Young's modulus is the highest of the composite girders. Less deflection is achieved for the composite girders when the shear forces are dominant over the bending moment. The load is applied 1 m from one of the supports and produces therefore almost solely shear forces and almost no bending moment in the girder. After web buckling in point *b*, the girder loses strength until it is considered failed. The points (*a*,*b*,*c* and *d*) indicated on the curve presented in Figure 60 match the girder situations displayed in Figure 61.

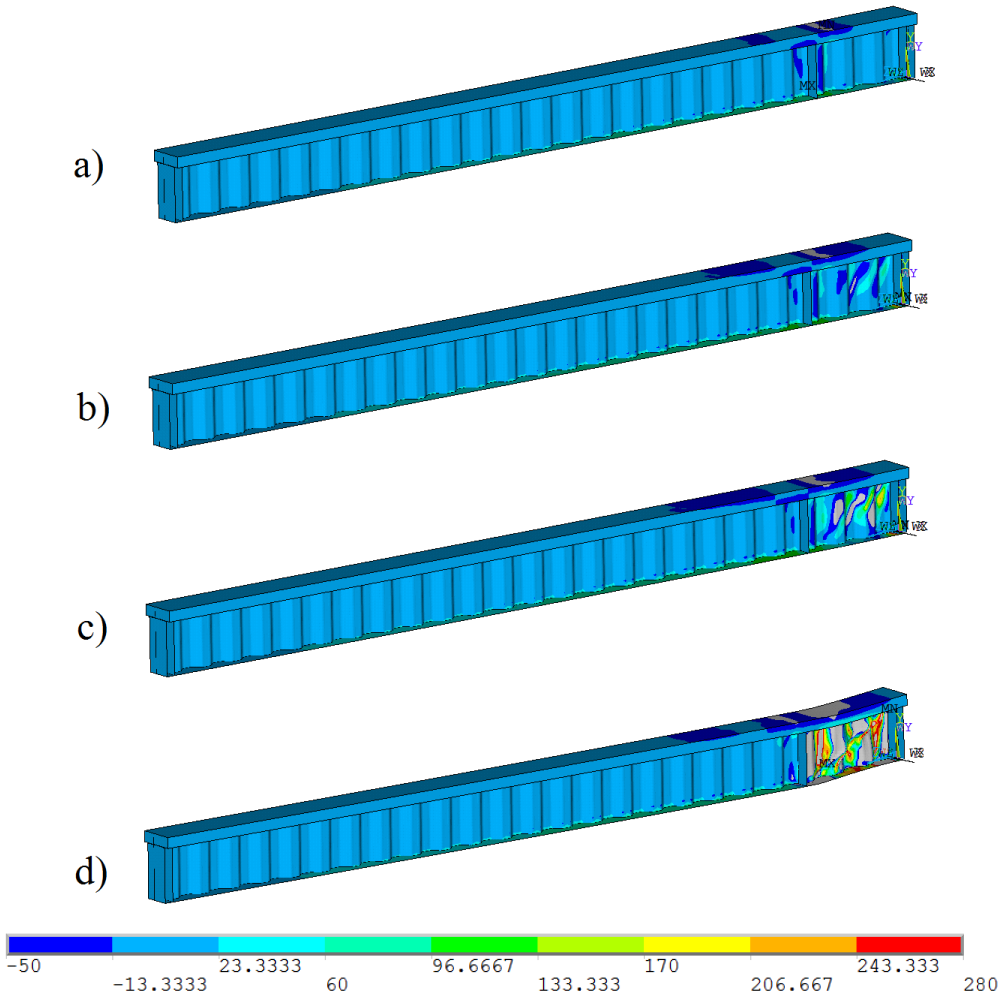

Figure 61: Longitudinal stress distributions in different load levels of specimen 14 in modelled in ANSYS (see Figure 60)

The colour scaling in Figure 61 presents the stress distribution accompanying the force-deflection points from Figure 60. The most affected zone in this case is the corrugated web between the middle stiffener and the nearest support, which is exposed to shear stress. The arising bending moment will not be able to crush the concrete or yield the steel lower flange before the web starts to yield. In point *a* (see Figure 60 and Figure 61), the web around the stiffener starts yielding after which in point *b*, the web starts to buckle in the area between the middle stiffener and the nearest support. Further, expanding of the yielding areas of the web ensures that the girder strength continues to decrease (point *c*) until the end of the simulation in point *d*. In Figure 61 it is clear to see that the occurring buckling is of the global shear buckling sort. The colour areas do not stay within one particular fold but are spread over multiple folds.

Figure 62 presents the ultimate lateral displacement, or in other words the lateral displacement accompanying situation *d* (failure of the girder).

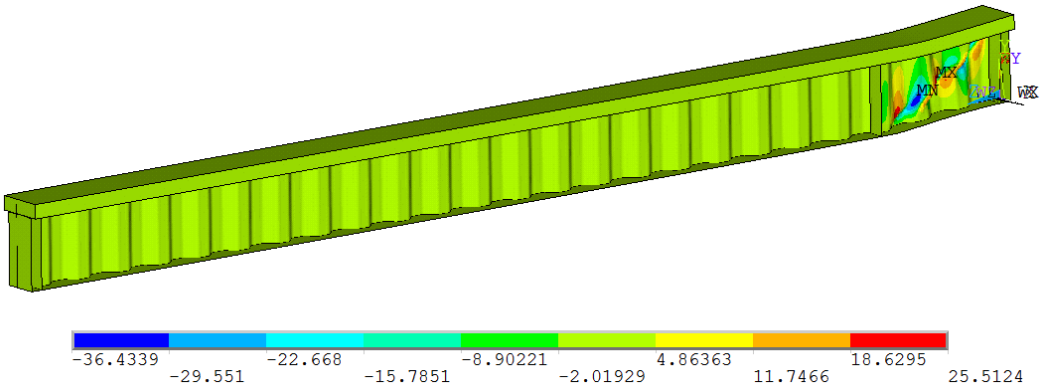

Figure 62: Ultimate lateral displacement of specimen 15 modelled in ANSYS

The colour scaling and the deformed web indicate that the web becomes most sensitive to buckling between the nearest support and the middle stiffener. The long colour areas indicate the that the type of buckling corresponds to global shear buckling. Compared to the specimens that fail because of insufficient bending resistance instead of shear resistance, the elongated shapes of the colour areas turned 45 degrees.

Evaluation of the FE-analysis results

Evaluating and comparing the results of the finite element analyses estimates the accuracy of the results and provides an insight into the behaviour of the girders. The results are validated through comparison with the hand calculation results (found in chapter 3) which are based on the Eurocode standards. Table 12 compares the results obtained in the hand calculations and the results found with the simulation software ANSYS.

Table 12: Overview FEM and hand calculation results of the 'composite' girders

Nr.	$F_{R,FEM}$ [kN]	$V_{R,FEM}$ [kN]	$M_{R,FEM}$ [kNm]	$F_{R,EC}$ [kN]	$V_{R,EC}$ [kN]	$M_{R,EC}$ [kNm]
11.	372.35	186.18	744.71	360.99	484.97	721.98
12.	363.83	181.92	727.67	360.99	307.76	721.98
13.	391.69	244.81	734.42	385.06	307.76	721.98
14.	462.87	347.16	694.31	410.34	307.76	721.98
15.	393.32	344.15	344.15	351.72	307.76	721.98

All values in Table 12 refer to previous discussed point 'a' which stands for crushing of the concrete flange and yielding of the lower steel flange, or yielding of the steel web, whichever occurs first. The references found in the overview table explained, are listed below.

$F_{R,FEM}$: FEM based ultimate load

$V_{R,FEM}$: FEM based shear force resistance

$M_{R,FEM}$: FEM based bending moment resistance

$F_{R,EC}$: EC based ultimate load

$V_{R,EC}$: Shear buckling resistance of the web based on EC3

$M_{R,EC}$: Bending moment resistance provided by the flanges based on EC2.

In table 12 certain values for the internal maximum forces (V_R and M_R) based on FEM and EC, have large differences. These can be explained by the fact that in the hand calculations, both maximum values for the shear and moment resistances are calculated while in the FEM calculations, the shear and moment resistances are derived from the same ultimate load. Calculating the resistances from the ultimate loads makes, that the non-dominant force capacities of the girders undervalued are because they did not reach their ultimate value during the simulation. These undervalued resistances are not relevant to this project and are therefore not equated.

To clarify the differences between the values achieved via FEM and in the hand calculations, Table 13 with the multiplication factors for the total ultimate loads, maximum shear forces and maximum bending moments, shows the percentage differences.

Table 13: Multiplication factors between the resistances calculated by FEM and hand calculations for the 'composite' girders

Nr.	$F_{R,FEM}$ / $F_{R,EC}$	$V_{R,FEM}$ / $V_{R,EC}$	$M_{R,FEM}$ / $M_{R,EC}$
11.	1.03	0.38	**1.03**
12.	1.01	0.59	**1.01**
13.	1.02	0.80	**1.02**
14.	1.13	**1.13**	0.96
15.	1.12	**1.12**	0.48

The multiplication factors of the shear and moment resistances which are relevant for the factors of the ultimate loads are set in bolt. All multiplication factors presented in Table 13 are shown in the graph depicted in Figure 63.

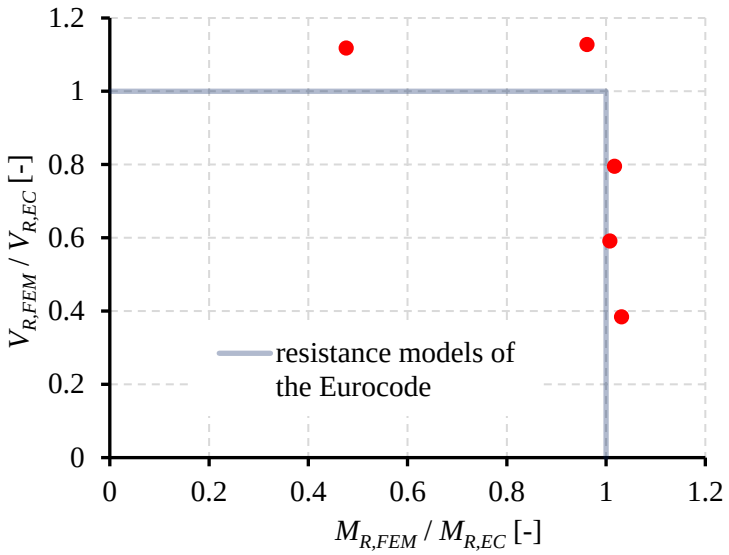

Figure 63: Comparision scatter plot of the obtained FEM and Eurocode based capacities

Based on all the relevant multiplication factors there can be concluded that, the values calculated by numerical analyses are greater than the values obtained with the hand calculations based on the standard

(see Table 13). This indicates the safety of the calculations based on the standard. The differences of the shear capacities are overall greater than the differences of the moment capacities. A cause responsible for a large part of this difference is the made conservative assumption, that only the web resists to shear forces. In reality, the flanges also absorb a part of these shear forces (see further). In general, it can be concluded that the values, obtained with the two calculation methods, do not differ much and that therefore both procedures are validated.

The load-deflection curves created in ANSYS are used to understand the behaviour of the girders when subjected to their accompanying load situation. Figure 64 collects the different behaviours of the girders. The first two girders (specimen 11 and 13) experience a more ductile behaviour, while the fourth and the fifth girder (specimen 14 and 15) possess a more brittle behaviour. Girder specimen 13 has a less distinct behaviour; the composition does not strongly act brittle or ductile under the applied load situation.

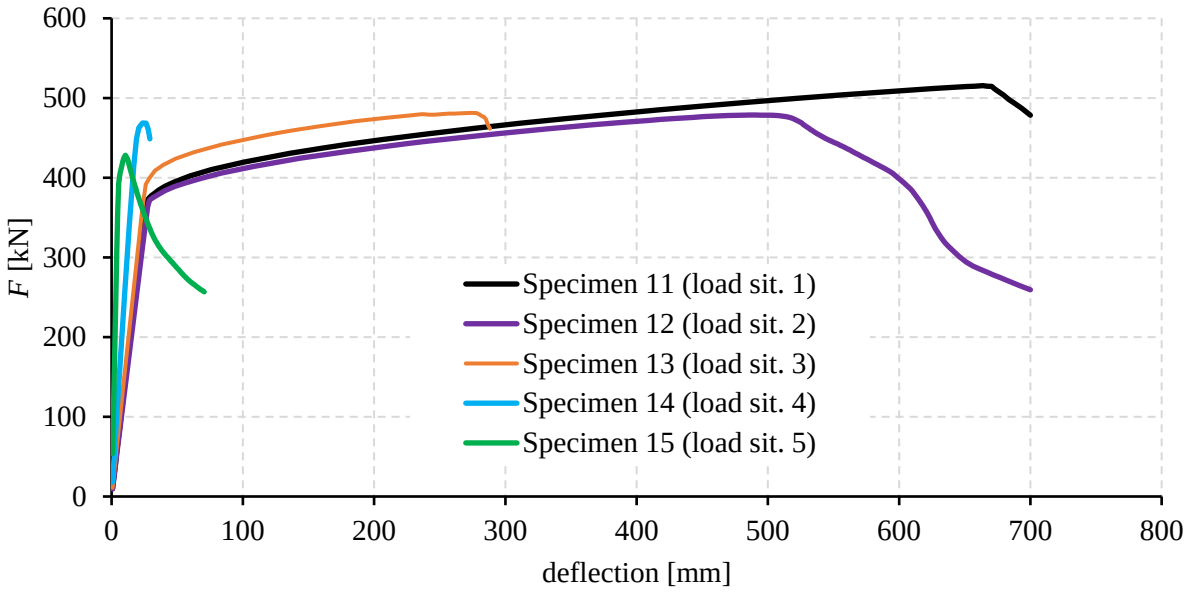

Figure 64: Combinatorial load – deflection curve for the 'composite' girders created in ANSYS

On the basis of these results of the FE-analyses, the shear-bending interaction in the 'composite' girders can be checked. Within the hand calculations, it is assumed that the bending moments are completely resisted by the flanges, while the shear forces are resisted by the corrugated web. To examine the accuracy of this assumption, all ultimate bending moments obtained in ANSYS are divided by a certain reference value: $M_{R,ref}$. Because in load situation 1 the beam is mainly loaded by bending moments, the ultimate bending moment ($M_{R,FEM}$) of specimen 11 is used as the reference value for the ultimate bending moments. This reference value ($M_{R,ref}$) can be found in Table 12 and is equal to 744.71 kNm. When dividing all ultimate bending moments by $M_{R,ref}$, the results listed in the second column of Table 14 are obtained.

Table 14: Bending moment and shear force divided by their reference value to determine the degree of interaction

Nr.	$M_{R,FEM}$ / $M_{R,ref}$ [-]	$V_{R,FEM}$ / $V_{R,ref}$ [-]
11.	1.00	0.40
12.	0.98	0.53
13.	0.99	0.71
14.	0.93	1.01
15.	0.46	1.00

The exact same thing is done for the shear capacities, these values are divided by the shear capacity of the girder that is exposed to the highest shear force divided by bending moment ratio, namely the 344.15 kN shear capacity of specimen 15 (see Table 12). These values are listed in the third column of Table 14. A scatter plot, to clearly see the interaction of the shear and bending forces in the discussed girders, is drawn up and presented in Figure 65.

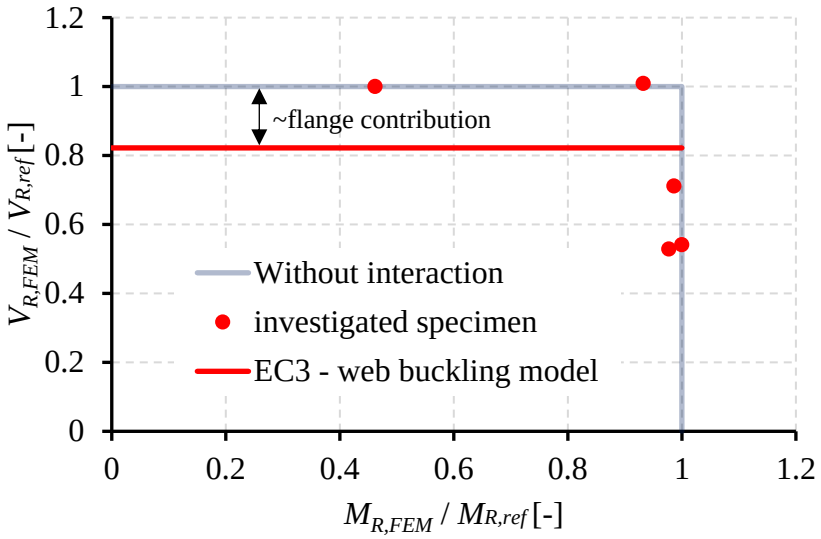

Figure 65: Shear force-bending moment interaction scatter plot of the 'composite' girders

The blue line in Figure 65 indicates the reference value (for bending the bending resistance of specimen 11 and for shear the shear resistance of specimen 15) divided by itself and represents the girders without shear-bending interaction. All results found during the FE-analyses of the girders, more or less follow the course of this line and therefore, it can be concluded that there is no shear-bending interaction in the girders. Because no interaction occurs, the bending moment situation and the shear force situation of the girders can be assessed separated from each other (as assumed during the hand calculations). This phenomenon can significantly simplify investigations.

A comparison is also made with the ultimate shear force hand calculations (solely based on the web) made according to the Eurocode. In Figure 65, the red line represents the shear buckling resistance of the web based on the Eurocode, divided by the shear force capacity of specimen 15 in point *a* based on the FE-analysis. During the hand calculations, only the shear resistance of the web is taken into consideration. As can be seen from the difference between the red and blue horizontal lines in Figure 65, the flanges also provide a resistance to shear. More precisely, the resistance of the flanges represents almost 20%.

4.3 Numerical analyses using ATENA

The behaviour of the 'hybrid' girders under the discussed load situations is in the scope of investigation for this section. The 'hybrid' girders (with 4 or 6 tendons) are analysed using ATENA because the cracking of concrete in this software is more accurately developed then in ANSYS. The lower flanges in the discussed models are always under tension and in the 'hybrid' girders this flange is made of prestressed concrete instead of steel. The program has the capacity to simulate the real behaviour of concrete and reinforced concrete structures including concrete cracking, crushing and reinforcement yielding. This chapter provides an explanation of the conducted numerical analysis using ATENA. A subdivision is made between the numerical model development (section 4.3.1) and the FE-analysis results (section 4.3.2).

4.3.1 Numerical model development

The developed finite element models (geometry, mesh, load and boundary conditions) produced in the pre and post processing software GiD 13.0.4 and analysed in calculation software ATENA V5 are introduced in this section. The chapter is divided into various topics, with names: geometric model, material model, finite element mesh, loads and boundary conditions, analysis type, applied imperfections and convergence study.

Because of the limited time frame in which this thesis is conducted, only a part of the developed models is analysed. All fabricated models are stored for the further elaboration of the overarching project that this thesis is part of.

Geometric model

The geometrical models manufactured in GiD 13.0.4 (and to be calculated by ATENA V5) are modelled as 3D structures. The properties of the models are given in chapter 2. All girders are modelled in full to avoid mistakes and speed up the composition process of the different models. Volumes are first made: they consist of areas with material properties limited by surfaces, and surfaces limited by edges. A model that can be used for specimen 2, 3, 4 and 5 is presented as a visualisation example in Figure 66. The full model in normal and flat rendering are both shown with a detail of the left end of the girder.

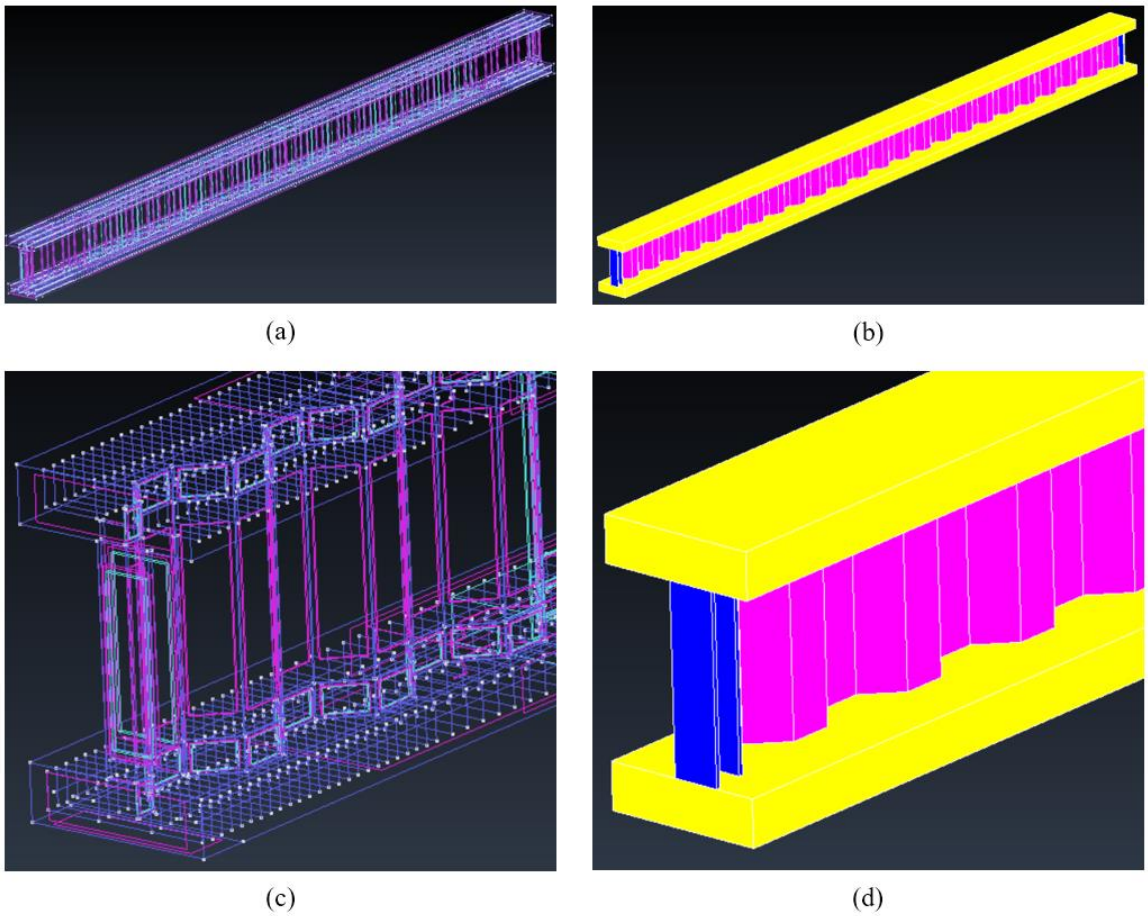

Figure 66: Geometrical model for specimen 1 and 2 created in with GiD: left in normal rendering, right in flat rendering

This model can be used for specimen 2 to 5 on condition that the middle stiffener is placed correctly (under the load of the applicable loading situation). Different web geometry must be implemented for all other

specimens and the number of stiffeners modified for the 'hybrid' girders with 4 tendons (specimen 6 to 10) Figure 66 clearly shows the internal transverse rebars in the concrete slabs. The figure also shows the two end stiffeners of one side. Due to all the lines from the internal rebars, the longitudinal tendons are not clearly visible. When the rebars are turned off, the tendons become more visible, as seen in Figure 67.

Material parameters

Step two includes the assignment of the material parameters to the corresponding volumes. Chapter 2 presents the introduced material parameters of the girders. It is important to always set the safety formats to 'Mean' for every assigned material. This because the values are not used for designing a structural element or structure, but for research concerning the behaviour and ultimate strength of girders. The default parameters accompanying the materials in GiD are predefined according to Eurocode 2 [30].

In the steel-concrete compound specimens of this project the parameters of concrete class C40/50 for all concrete slabs are used. Other attributes aside from the concrete class and the safety format are left as default. The material model for concrete used in ATENA is the 'Concrete EC2' model which is logically

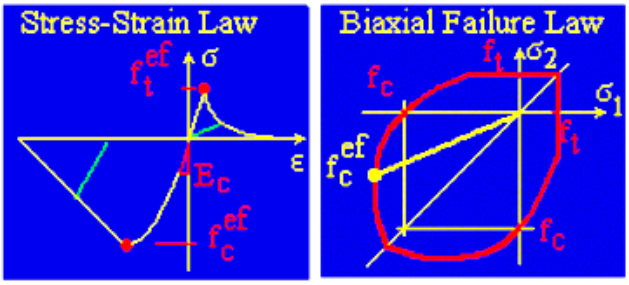

Figure 68: Stress-strain and biaxial failure curves of the material model used for concrete

based on the standard Eurocode 2. It is a fracture-plastic constitutive material model implemented in ATENA and is suitable for brittle materials, such as concrete. The material model includes the behaviour of concrete in non-linear behaviour under compression, fracture of concrete under tension, biaxial strength failure criterion, reduction of compressive strength after cracking, tension stiffening effect[8] and reduction of the shear stiffness after cracking. In the material model, two crack models were used: fixed crack direction and rotated crack direction. In order to simulate cracking of the concrete, Rankine failure criterion, exponential softening and rotated or fixed crack model based on the smeared crack concept, were adopted. In the girder models, the strains for the smeared crack models are calculated for each element separately followed by the application of the crack-opening law. The material model is based on elastic, plastic and fracturing strain components. The compressive behaviour for the crushing of concrete is modelled using a plasticity-based model. The stress-strain and biaxial failure laws governed by the model are shown in Figure 68 [29].

[8] Tension stiffening: the effect of concrete acting in tension between cracks due to the stress of steel reinforcement. At a crack, all the internal tensile force is carried by the reinforcement, whereas between cracks some amount of the tensile force is transferred to the surrounding concrete, which results in a reduction in the reinforcement stresses and strains, and causes the reinforcement strain at uncracked zone to be less than the reinforcement strain at the cracked sections [38].

Going over to the properties of the steel corrugated web: the material of the web is assigned under the criterion of Von Mises. The default settings of steel are adopted, except for the yield strength. The yield strength has been set to 280 MPa since, as stated earlier, the steel quality for the body is equal to S235 and the mean yield strength for this class is 280 MPa. The stress-strain and biaxial failure laws governed by the model are presented in Figure 69 [29].

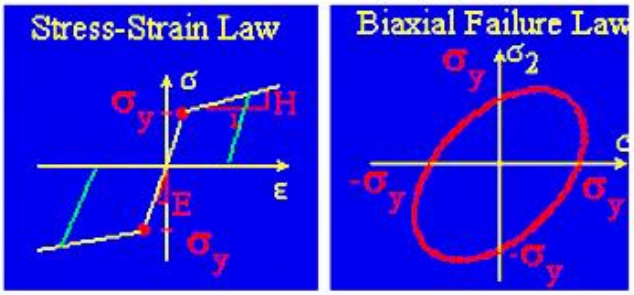

Figure 69: Stress-strain and biaxial failure curves of material model used for the steel corrugated web

Also here, '1D Reinforcement' is used to create the assigned material. In the main menu the type of reinforcement is set to tendon instead of reinforcement. Reinforcement or tendons can be modelled in two forms: discrete and smeared. In this study, discrete reinforcement was used to model the tendon and reinforcement materials. Discrete reinforcement is in form of reinforcing bars and is modelled by truss element. The type of tendons (Fp1150/1860) requires a multi-linear law for the stress-strain behaviour. In ATENA this consist of four lines as shown in Figure 70.

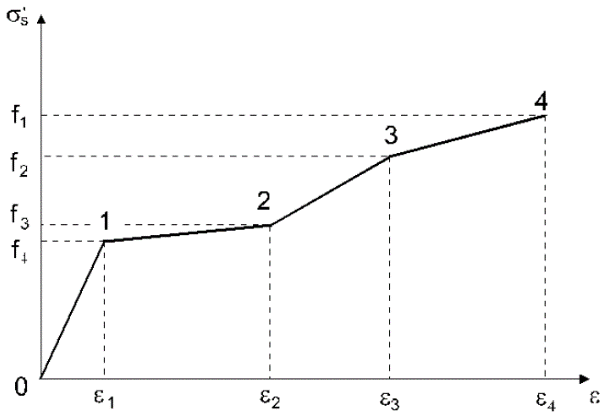

Figure 70: The multi-linear stress-strain law for reinforcement and tendons

This law allows the modelling of four stages of steel behaviour: elastic stage, yield plateau, hardening and fracture. The multi-line is defined by four points, which can be specified by input. As required by the used tendon type, bilinear law with hardening is used for the material stress-strain behaviour of the tendons. The multilinearity for the stress-strain reinforcement function is set to 2. The Young's modulus of the elastic part is set to 195 GPa and the characteristic yield strength (f_{xk} or f_1) equals 1580 MPa. For the second part in the function (after reaching the yield strength of 1580 MPa), the maximum stress of the yielding phase is set to 1860 MPa, here the tendons rupture. All these values are specific to the Fp150/1860 type tendons. The tendons have a real diameter of 15.7 mm, but because each tendon is made of 7 part-tendons the nominal diameter, namely 12.9 mm, is filled in. After assigning the material parameters of the tendons, the prestressing force of 1475 MPa is applied. The basic property of the reinforcement bond model with the concrete slabs is the bond-slip relationship. This relationship defines the bond strength (cohesion) depending on the value of current slip between reinforcement and surrounding concrete. The laws are generated based on the concrete compressive strength, reinforcement diameter and reinforcement type [29].

Next, the material of the rebars, to withstand the expansion of the concrete, is defined. The longitudinal place-keeping bars of the rebars are disregarded as they offer neglectable structural utility. The reinforcements of the 'hybrid' girders are created in a similar way as the previous discussed process concerning the prestressed reinforcement or tendons. In GiD, material type '1D reinforcement' is chosen, the material properties are set to default and the class of reinforcement is set to class B. The assigned class has an influence on the rupture of the bars. Additionally, the Young's moduli are changed from a default 200 GPa to 205 GPa and the characteristic yield strength is set to 500 MPa to match the properties of the B500B steel bars used in the experimental compositions. The reinforcement bars (just as the tendons) have a bilinear law for the reinforcement stress-strain function (see Figure 70), but here the default settings can be used for the further course of the curve [29].

As last material group: the contact surfaces between the steel web and concrete flanges are created. The interface material model from GiD can be used to simulate contacts between two materials and is based on Mohr-Coulomb criterion. All properties are left in their default setting except for the tension strength. As a safe consideration, the tension strength is set to zero. This means that if the concrete moves away from the contact surface with the steel embedded web, the interface will not have any ability to prevent this movement except for the cohesion between the two materials.

Finite element mesh

Figure 71 presents the meshed finite element model of specimen number 4 as a mesh example.

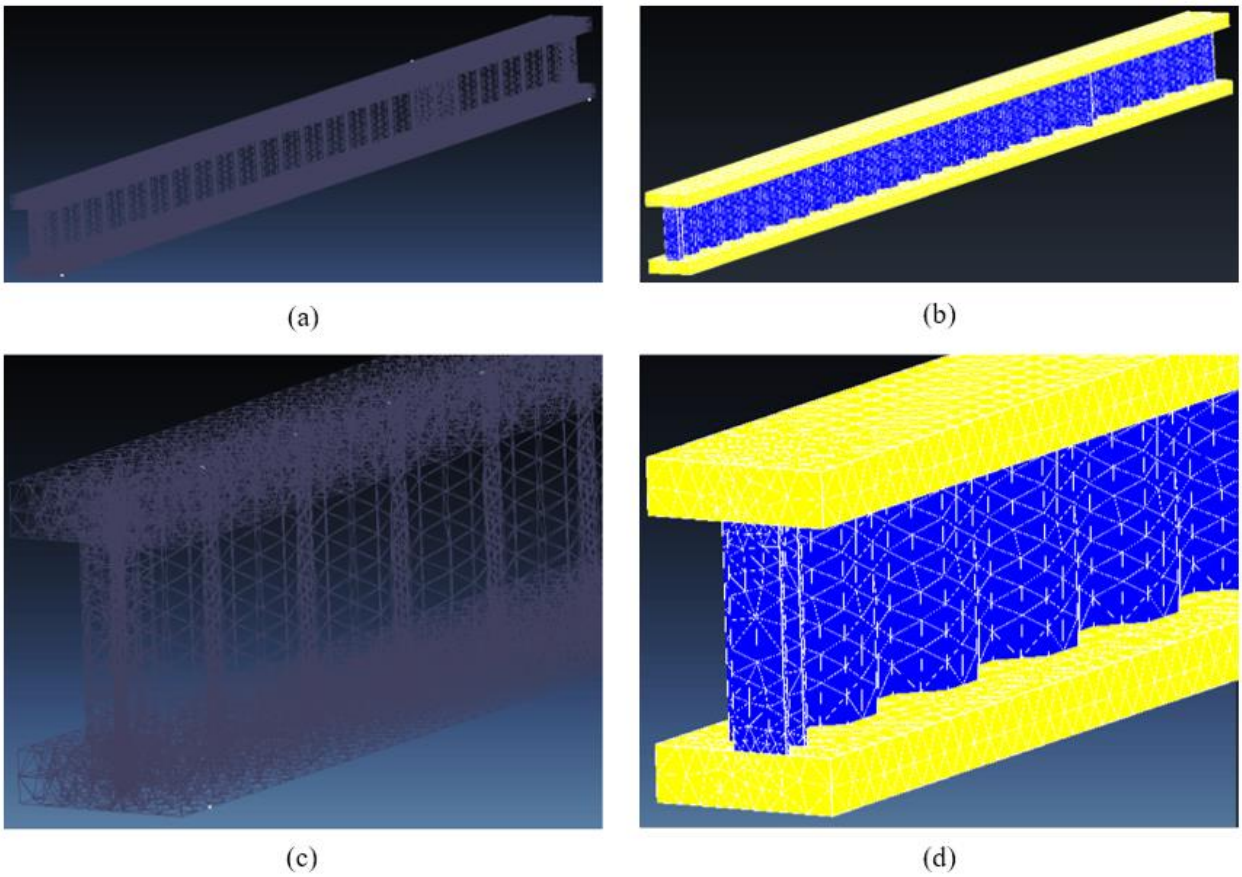

Figure 71: Example finite element mesh: (a) full girder in normal rendering, (b) full girder in flat rendering, (c) detail of girder end from in normal rendering, (d) detail of girder end in flat rendering

A mapped mesh is chosen for the finite element models, more specifically a tetrahedra element mesh is used as 3D mapped mesh. Tetrahedra elements are chosen over hexahedra elements when a rather complex structure (e.g. a lot of angles) is under investigation. The convergence study to find the right mesh, could not be completed. As a result of the magnitude of the model (geometry, materials, mesh, load and boundary conditions) the fineness of the mesh is limited by the RAM capacity of the used computer. The most precise mesh and therefore the mesh used for all analyses has a precision of 0.05 m.

Loads and boundary conditions

Most properties of the 'hybrid' girders stay the same for the different specimens. Not all girders are symmetrical and because most elements could be copied for the modelling of the different girders, all girders are modelled in full. This saves time and minimizes the risk of mistakes.

What the load concerns: displacement magnitude is prescribed at the load introduction places. This indicates a displacement controlled instead of a force controlled analysis. The program stops its analysis if it is not able to converge in a displacement step or after reaching the prescribed displacement.

Analysis type

The analysed numerical FE-models in this chapter, namely the 'hybrid' girders, are developed using the finite element software ATENA V5. The numerical modelling is based on the combination of different volume elements. In ATENA, Arch length method is chosen as numerical iteration solver. Next to the Newton-Raphson method, the Arc-length approach is the most widely used iteration solver method in ATENA. Because of its excellent performance, the Arc-length method is quite well established for geometric non-linearity and for material non-linearity. The main reason for the popularity of this method is its robustness and computational efficiency which assures good results even in cases where traditional Newton-Raphson methods might fail. This is possible due to the changing load conditions during iterations within an increment. The main idea of this method is well explained by its name, Arc-length. The primary task is to observe complete load-displacement relationship rather than applying a constant loading increment as it is in the Newton-Raphson method. Hence this method fixes not only the loading but also the displacement conditions at the end of a step. During the simulations the default convergence criteria built in ATENA are used. In the analyses displacement control is used.

Applied imperfections

ATENA is a software that often gets chosen for its concrete applications, while ANSYS is more used when steel is the most important material. Imperfections have effect on slender elements such as steel plates. The concrete slabs in these load situations are (unlike the steel corrugated webs) not likely to buckle due to axial forces. The concrete slabs will experience mainly bending moments and because of their dimensions unexpected failures will not occur. For this reason, no imperfections are necessary to be implied in the models.

4.3.2 FE-analysis results

This section presents the FE-analysis results regarding the 'hybrid' test specimen. The examination and comparison of the results is based on the load-deflection curves and the Von Mises stresses in the deformed girders at the end of the analyses. Colour maps are used to indicate the Von Mises stresses in the girders. In the colour scales, no distinction is made between the areas under compression and tension stresses. The cracks in the concrete flanges of the girders are also presented and assessed.

Unfortunately, only two of the 'hybrid' girders were fully analysed, namely specimen 2 and 3. The behaviour of the other 'hybrid' girders are therefore only discussed by used of the hand calculated ultimate loads. The two analysed specimens are modelled without stiffeners. After the analyses of both models, the results were checked to see the see if this simplification had significant influence on the results. Omitting the stiffeners was necessary because the required mesh size had to be set so small, to correctly model the intersection, that the calculations became too sizeable for the program to properly analyse the model. For certain other models this simplification is not an option as the shear forces become more dominant in the applied load situations.

Specimen 2 exposed to load situation 2

Specimen 2 is the second 'hybrid' girder with 6 tendons, and is therefore exposed to load situation 2. It is a symmetric model with the increasing load centrally located on the upper concrete flange, and a web thickness of 4 mm. This 4 mm thickness of the corrugated web is the only difference with above presented specimen 1. The results of the displacement controlled analysis are displayed in a load-deflection curve in Figure 72.

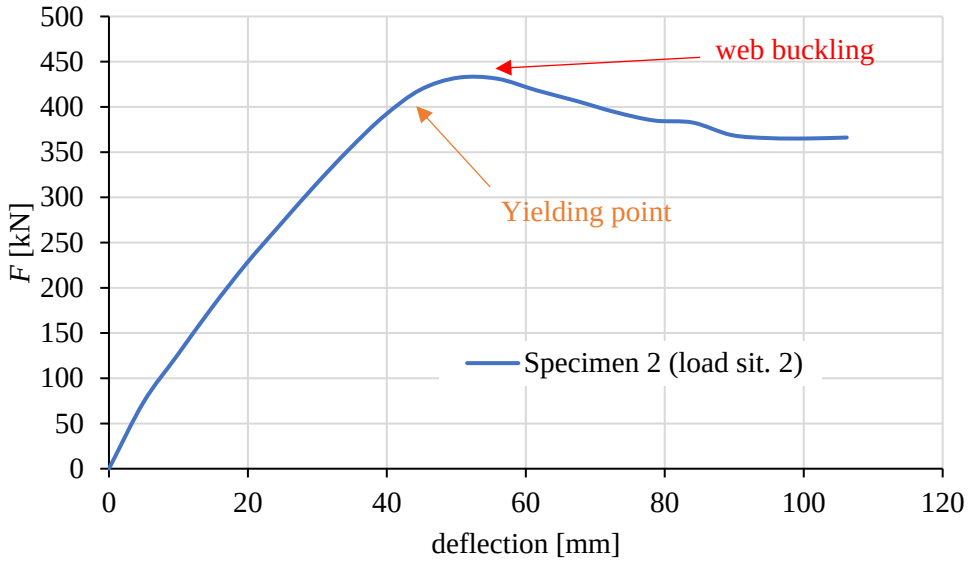

Figure 72: Load – vertical displacement curve of specimen 2 provided with ATENA

The yielding and the buckling of the web happen almost at the same position in the L-D curve (both are indicated on the curve in Figure 72), the hardening process is very short.

The stress distribution of the girder at the end of the simulation is assessed with use of the colour mapping of the Von Mises stress in the girder, this is presented in Figure 73.

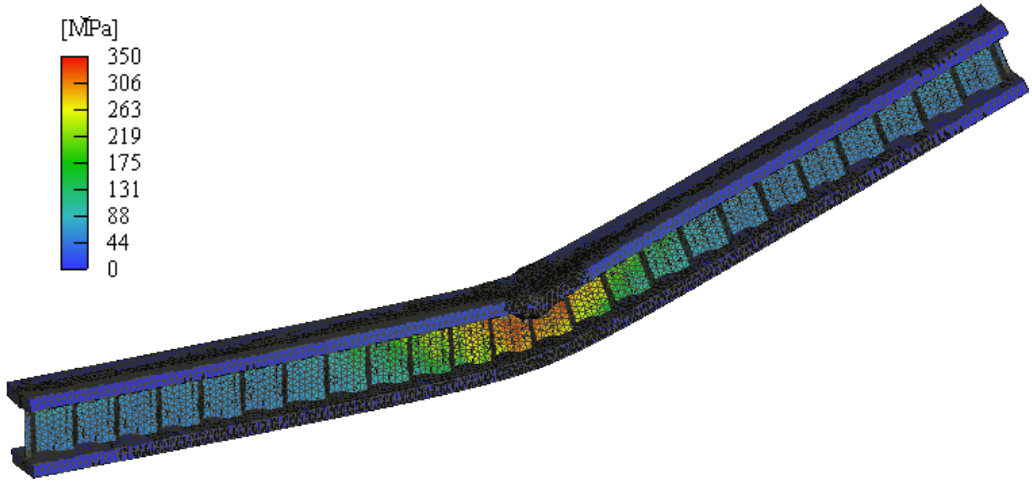

Figure 73: Specimen 2 at the end of the analysis with cracks and colour mapped Von Mises stress

The concrete reaches its maximum compression strength in the middle of the girder, this can be seen by the cracks and the deformation of the upper flange in the area under the load force. For the concrete, no tensile strength is considered, therefore the lower flange is full of cracks but does not contain any stress levels.

What the web concerns, in the middle of the girder (where the load is positioned) the yield strength of the steel web is achieved, this proves the web buckling. Going further away from this point, the stress decreases.

Specimen 3 exposed to load situation 3

Specimen 3 is the third 'hybrid' girder with 6 tendons and is exposed to load situation 3. It is an asymmetric model with the increasing load imposed on the upper flange at 3 m distance of the nearest support and a web thickness of 4 mm.

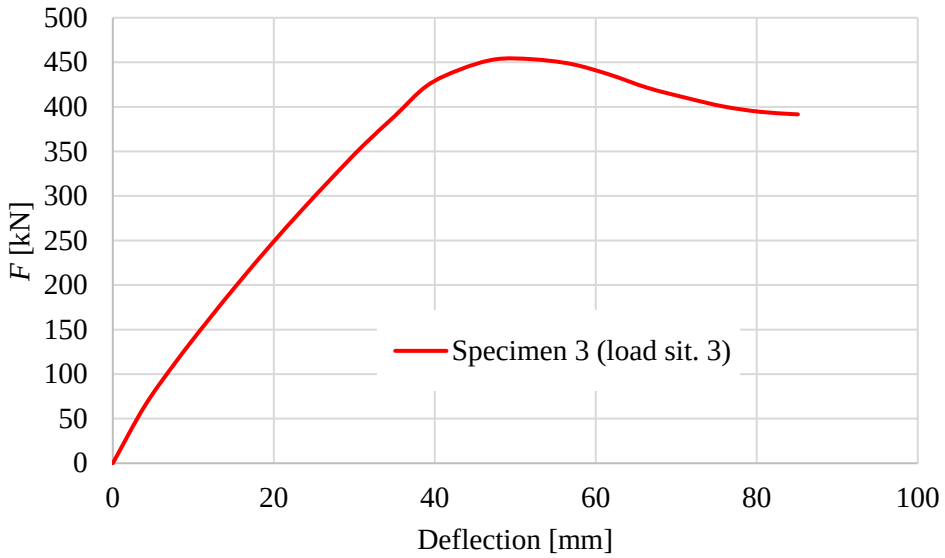

Figure 74: Load – vertical displacement curve of specimen 3 provided with ATENA

The load-deflection curve for specimen 3, depicted in Figure 74, has a similar course as the curve achieved for specimen 2. In load situation 3 (implemented for the discussed specimen) the load is located closer to one of the supports and therefore introduces higher internal shear forces. This means a higher yield point of the compound girder and a higher deformation resistance (steeper elastic zone), compared to the girders exposed to a symmetric load situation.

The analysis is terminated when the deformations in the concrete flanges become too extensive for the program to converge in a new displacement step. Figure 75 depicts the status of the girder at the end of the analysis, when the girder is considered failed.

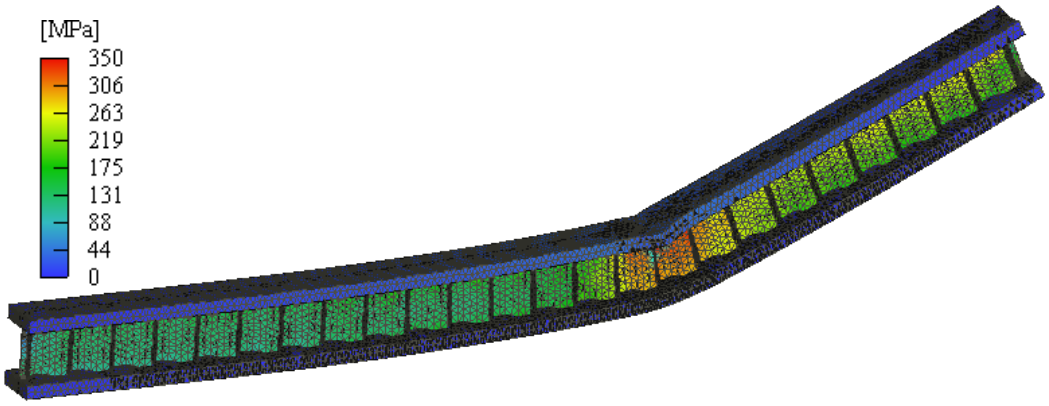

Figure 75: Specimen 3 at the end of the analysis with cracks and colour mapped Von Mises stress

Next to the deformations of the girder, Figure 75 also shows the distribution of the Von Mises stresses and the cracks formed in the concrete flanges. What the web concerns, the highest forces are found right underneath the load force position and reduce going further away from this point.

When the maximum Von Mises stress is set to 50 MPa which is the crushing strength of the used concrete, the web vanishes. All stress in the web is higher than 50 MPa, this makes it easier to assess the stress in the flanges with a more precise colour scale. All material under stress in the range between 0 and 50 MPa (concrete flanges) is shown in Figure 76.

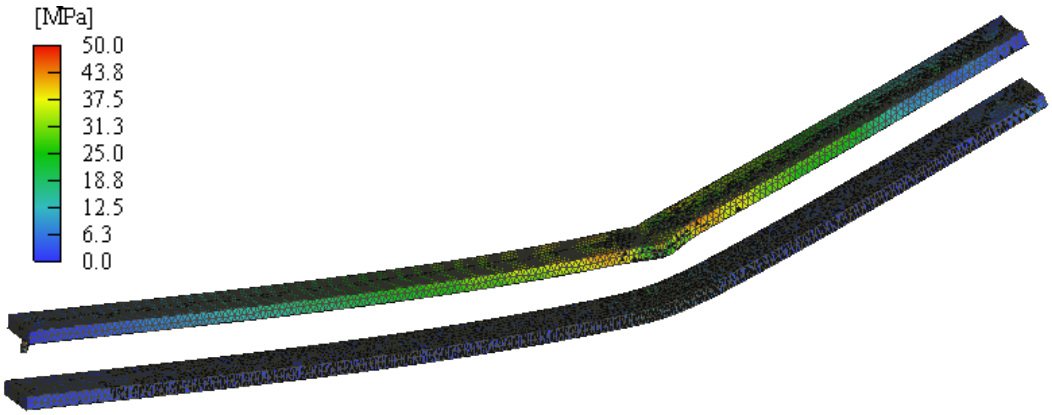

Figure 76: Specimen 3 at the end of the analysis with cracks and calour mapped Von Mises stress in the range of 0-50 MPa

The stress in the upper flange starts at zero at the supports and gradually increases until the loading point, where it reaches its maximum value and crushes. In the lower flange, te stress does not increase because the concrete is not able to withstand any tensile stress. The cracks are displayed by elements of the mesh which are coloured black. Most black elements are located in the bottom flange, these cracks are a result of the extensive tension created as a result of the large bending moments that the load introduces in the girder. In the area underneath the load force, the most cracks can be found because the bending stress is highest this area. Also in the upper flange black elements can be seen. These represent the areas where the concrete is crushed. This again mostly in the area around the load force.

Evaluation of the FE-analysis results

Evaluating and comparing the results of the finite element analyses estimates the accuracy of the results and provides an insight into the behaviour of the girders. The results are validated through comparison with the hand calculation results (found in chapter 3) which are based on the Eurocode standards. Table 15 compares the results obtained in the hand calculations and the results found with the simulation software ATENA.

Table 15: Overview FEM and hand calculation results of the analysed 'hybrid' girders

Nr.	$F_{R,FEM}$ **[kN]**	$V_{R,FEM}$ **[kN]**	$M_{R,FEM}$ **[kNm]**	$F_{R,EC}$ **[kN]**	$V_{R,EC}$ **[kN]**	$M_{R,EC}$ **[kNm]**
2.	390.37	195.18	780.73	384.85	246.21	769.71
3.	423.51	264.69	794.08	393.93	246.21	769.71

All values in Table 15 refer to previous discussed 'yield' point of the girder, which stands for crushing of the concrete flange and yielding of the lower steel flange, or yielding of the steel web, whichever occurs first. The references found in the overview table explained, are listed below.

$F_{R,FEM}$: FEM based ultimate load

$V_{R,FEM}$: FEM based shear force resistance

$M_{R,FEM}$: FEM based bending moment resistance

$F_{R,EC}$: EC based ultimate load

$V_{R,EC}$: Shear buckling resistance of the web based on EC3

$M_{R,EC}$: Bending moment resistance provided by the flanges based on EC2.

In Table 15 the values for the internal maximum shear forces (V_R) based on FEM and EC of specimen 2 and the values of the internal maximum moments (M_R) of specimen 3, might have big differences. The difference can be explained by the fact that in the hand calculations, both maximum values for the shear and moment resistances are calculated while in the FEM calculations, the shear and moment resistances are derived from the same ultimate load. Calculating the resistances from the ultimate loads makes, that the non-dominant force capacities, in this case the shear capacities, of the girders undervalued are because they did not reach their ultimate value during the simulation. These undervalued resistances are not relevant to this project and are therefore not equated.

To clarify the differences between the values achieved via FEM and in the hand calculations, Table 16 with the multiplication factors for the total ultimate loads, maximum shear forces and maximum bending moments, shows the percentage differences.

Table 16: Multiplication factors between the resistances calculated by FEM and hand calculations for the 'hybrid' analysed girders

Nr.	$\boldsymbol{F_{R,FEM} / F_{R,EC}}$	$\boldsymbol{V_{R,FEM} / V_{R,EC}}$	$\boldsymbol{M_{R,FEM} / M_{R,EC}}$
2.	1.01	0.79	**1.01**
3.	1.08	**1.08**	1.03

Multiplication factor 1.03 of specimen 3 for the moment capacity calculations is very close to one, or in other words, the calculated moment capacities based on FEM in ATENA and based on EC are very close to each other, and this while the moment capacities are not relevant for the ultimate loads. This has to do with the fact that specimen 3 in combination with load situation 3 is very close to the transition point where the dominance of the shear or moment capacity switches. The multiplication factors of the shear and moment resistances which are relevant for the factors of the ultimate loads are set in bolt.

The load-deflection curves created in ATENA are used to understand the behaviour of the girders when subjected to their accompanying load situation. Figure 77 collects the different behaviours of the two girders analysed with ATENA.

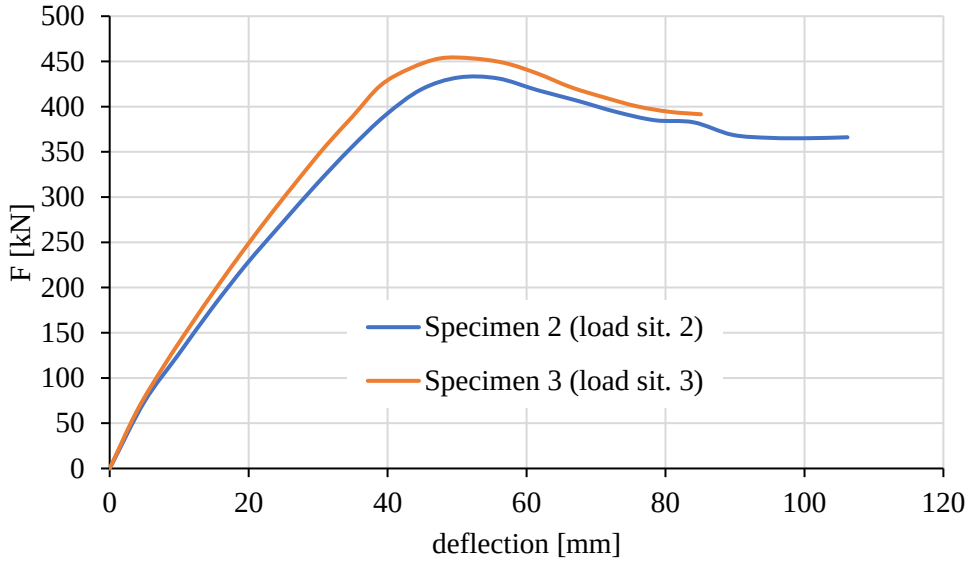

Figure 77: Combinatorial load – deflection curve of specimen 2 and 3

As only two specimens are analysed, the conclusions that can be made for the behaviour of these two can not be extended for all 'hybrid' girders with 6 tendons. What can be seen in the curve of Figure 77 is that the resistance against load force in the elastic phase is higher for specimen 3. Specimen 3 experiences more shear forces and less bending moment at the same load force value (within the elastic phase) so that the deformations remain smaller. The deformations caused by shear forces are in fact smaller than the deformations due to the bending moments in the discussed girder setups.

5 Experimental phase

Based on the results obtained during the calculations of this project, the cross-sectional dimensions of the girders and the setup of the applied load situations were modified to be able to clearly determine the influence of certain parameters on the load bearing capacity and load-deflection behaviour of steel-concrete compound girders. The specific parameters under investigation are the web thickness, the girder type and the load situation (or influence of the longitudinal position of the load force) on the capacity and behaviour of the girders exposed to a transverse load. After determining the correct compositions, the shop-drawings of the test specimens are created and the manufacturing of the girders is started. Following explanation presents some main steps of the fabrication process of the experimental girders. The fabrication of the experimental specimens is executed by Rutin Kft.

The corrugated webs (conform chapter 2: 'Research setup') are manufacture starting from identical corrugated web plates, which are welded together in longitudinal direction. Some of these original plates are depicted in Figure 78.

Figure 78: Initial corrugated steel plates

In these original plates of Figure 78, the holes made for the passing through of the connectivity bars can be seen. After welding the plates together, the total web length is reached and the webs are manufactured. For visualisation, the steel corrugated web for load situation 1 or 2 of the 'hybrid' girders is presented in Figure 79.

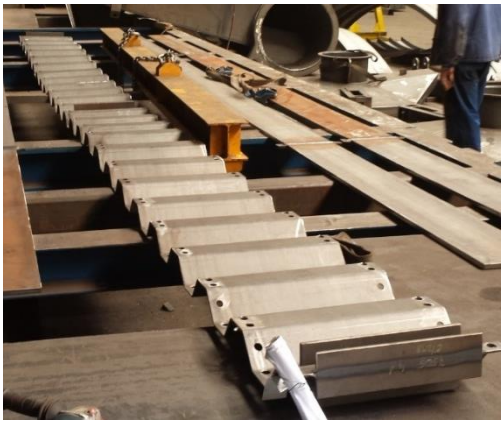

Figure 79: Steel corrugated web for load situation 1 or 2

That this web is specifically made for a girder composition which will be exposed to load situation 1 or 2 can be seen by the location of the middle stiffener. The middle stiffener is centrally located, what means

that the load force will also be centrally placed during the test. The corrugated web has a height of 520 mm, which means that it is fabricated for one of the 'hybrid' girders. In Figure 79 can be seen that the webs are welded against the steel web.

Once the webs are constructed, the next step is to create a setup that ensures a proper and easy to implement manner of compiling the web-flange connections. The casting of the upper and lower slabs shall be performed in one time with the same mix and the steel corrugated web will be greased to avoid adhesion between the steel and concrete surfaces throughout the production phase. Avoiding adhesion is necessary to ensure that there are as less residual stresses in the girders as possible. Unfortunately, the workers in the lab did not get this far in the composition process to include the pictures in this project. The rebars, needed to keep the concrete from expanding in the transverse direction, also still need to be fabricated. In a previous work within BME (Budapest University of Technology and Economics), similar rebars, with the corresponding longitudinal bars to hold the transverse rebars in place, were created. These are shown as a comparative arrangement in Figure 80.

Figure 80: Comparative rebar arrangement for all concrete slabs of the specimens [20]

The project for which these compositions were made was called 'Experimental analysis of prototypes' and had as biggest difference with this project, a different composition of the cross-section of the girders (load situations and experimental setup are similar). Instead of I-girders with two flanges, this project conducted research about composite T-girders with a flat steel web and one concrete slab. The test setup, of this previously executed project, is comparable to the one needed in this project. As a result, also the composition of the test set-up is used as a comparable arrangement for this project (see Figure 81) [20].

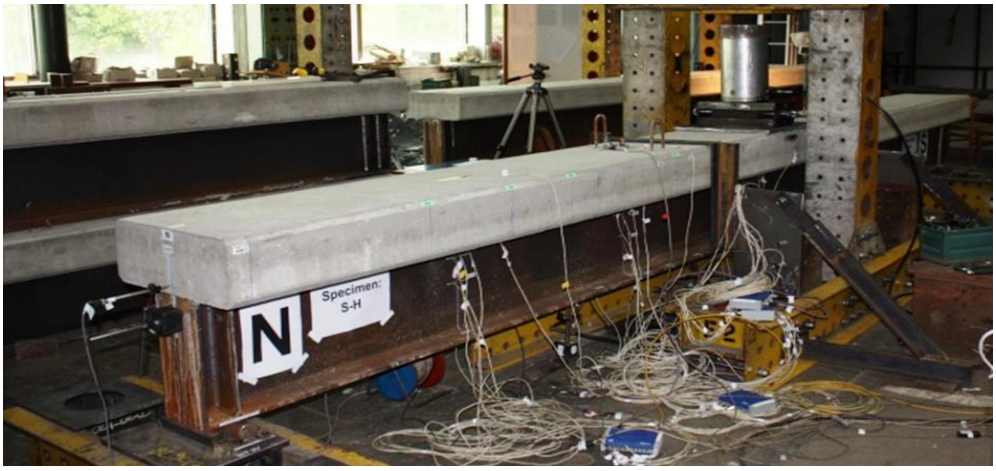

Figure 81: Comparative test setup (picture) [20]

In the setup the girder is placed on two supports and exposed to an increasing load that can be applied anywhere between the two supports. Therefore, this setup can also be used to test all discussed specimens of this thesis. Notice that in the girder of Figure 81 similar end stiffeners are used. Also the support conditions of the experimental setup are comparable [20].

As can be seen in Figure 82, where a sketch of the setup of the comparable study is presented, in this project not only the cross-section composition is different but also the span (6.00 m instead of 8.20 m).

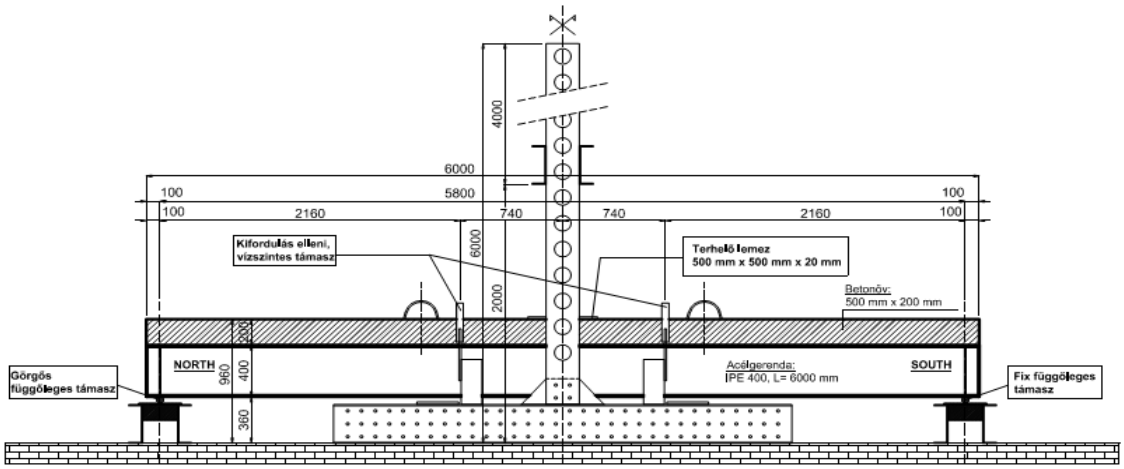

Figure 82: Comparative test setup (drawing), dimensions in mm [20]

These two main differences are the only two that will be pointed out. Because the setup is not composed yet, the specifications are not fully known. During the composition, less influential changes can still be made. The conclusion of this setup representation is to show the possibilities of the laboratory. The needed test setup can be created in the lab. The most important question is, whether the load piston can produce a load force that is high enough to investigate the hole load-deflection behaviour of the test specimens. Both the yielding and buckling point are to be determined. To this question, an answer is given by using the calculations made in this project. Also the behaviour of the girders during the tests is predicted to know what to expect during the tests.

6 Discussion

This chapter discusses the resulting girder capacities found by hand calculation (chapter 3) and by numerical analysis (chapter 4 and 5). The results are presented in different sections, the subdivision is based on the changing parameter: load situation, girder type and web thickness. Furthermore, the results in each section are discussed in relation to the ultimate load and the load-deformation relationship. In addition, a chapter devoted to the discussion of the capacity of the Structural Laboratory of the Department of Structural Engineering in relationship with the planned research program is created.

6.1 Interaction of the shear and moment stress in the girders

At the beginning of the project it was assumed that the shear capacity and bending moment capacity of the girder can be examined separated from each other and that the two have no interaction whatsoever. By comparing the results found in ANSYS (composite girders) this assumption is justified. To discuss this phenomenon, the interaction curve found in chapter 4.2 is again presented in Figure 83.

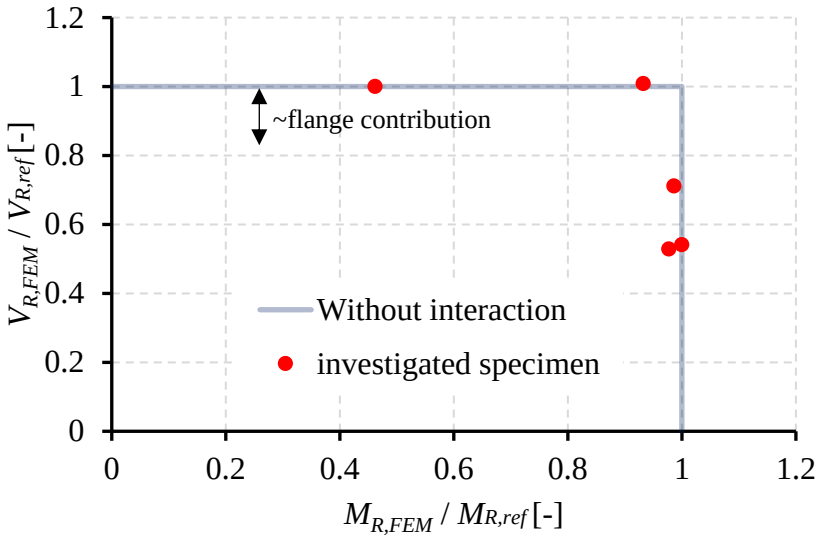

Figure 83: Shear force-bending moment interaction scatter plot of the composite girders

The curve represents the ultimate loads of the 'composite' girders divided by their reference value to show that there is no interaction between the shear stress and the moment stress. The reference values of the shear and moment capacity are based on the situations where the shear stress respectively the moment stress is dominant. In the interaction curve it can be seen that the relative values of the ultimate loads, follow the line of no interaction quite well. Knowing this, in this chapter the shear and moment capacity are considered as two completely separate entities for the discussion of the various parameters.

6.2 Influence of load situation

As a reminder, the load situations are presented in Figure 84.

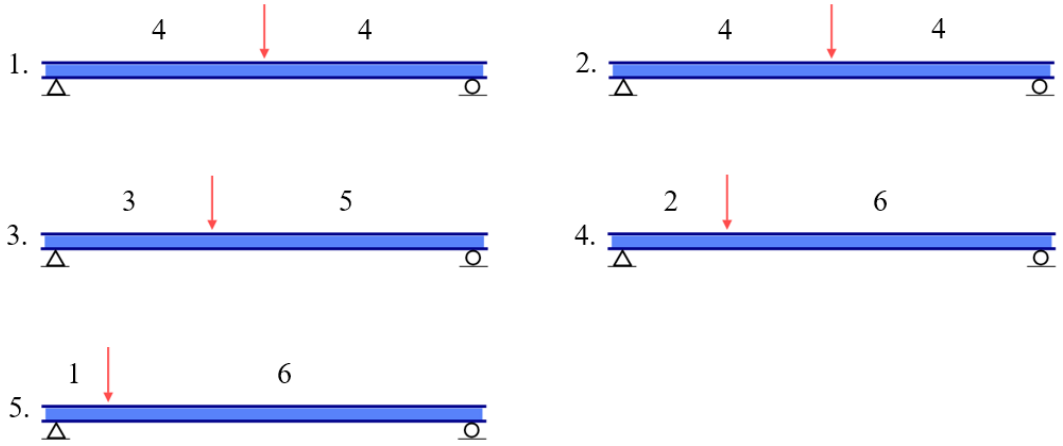

Figure 84: All load situations used for one girder type, dimensions in meters

The difference in load situation is solely based on the position of the applied load. For situation 1 and 2 (which have the same setup), the load is centrally located in the middle of the girder and therefore also in the middle of the span. For situation 3 up until 5, the applied load is shifted towards one of the supports in steps of one meter per load situation.

In this section, the load situation is the only relevant variating parameter. To neglect the influences of the 'girder type' parameter, only the behaviour of one girder type is discussed at once. From the five specimens of one girder type, only the second until fifth girder have the same composition. To neglect the web thickness parameter, the specimens exposed to load situation 1 are omitted from this chapter. Omitting these specimens for the discussion concerning the load situations, will not lead to a reduction in data since the first and second load situations are the same.

Because all ultimate loads for the different specimens of one girder type were calculated by the executed numerical analyses in ANSYS, namely the 'composite' girders, these values are used to assess the influence of the load situation on the ultimate load of a girder. The combined curve found in chapter 4 that includes the ultimate loads for all 5 'composite' specimens is again presented in Figure 85 but here only the results of the four relevant specimens (without specimen 11) are depicted.

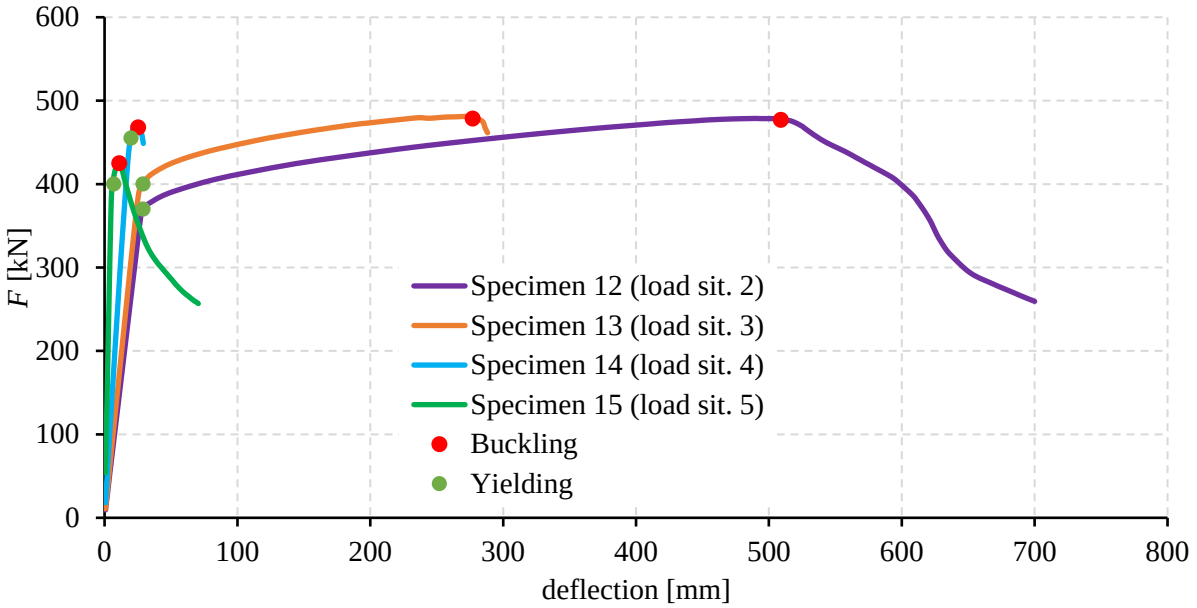

Figure 85: combinational load-deflection curve for the 'composite' girders

To clearly see where the girders yield (concrete crushing/steel yielding of flanges) and where the web of the girders buckles, these places are located and indicated with dots. Discussing the load situations comes down to discussing the distribution of the load force in shear and moment stress in the girder. If the load force is positioned in the middle of the girder, more moment stress will occur. On the other hand, if the load force is positioned near one of the supports, the load is almost solely distributed in shear stress.

One of the phenomena that can be seen in the curve of Figure 85 is, the more dominant the shear stresses in the girder become, the smaller the hardening phase becomes and the closer the buckling point moves towards the yield point. In specimen 14 and 15 which are almost solely exposed to shear stress, the yielding and buckling practically happen at the same time. Here the girder has a more sudden failure, while the girder subjected to higher moment stress, experience a more ductile behaviour. The second phenomenon concerns the elastic parts of the curves. When the force is position more towards one of the supports, and thus the more dominant the shear forces are, the overall deformations of the beam become smaller. This can clearly be seen in Figure 85 by examining the changing steepness of the elastic part. Shear forces positioned more towards the ends of the beam, bring less vertical deformation to the beam than moments in the middle of the span do. A third aspect that can be established from Figure 85 is that for the 'composite' girders the yield strength increases when the load does not introduce a dominant force type (shear force or bending moment). A setup where the load force is located somewhere between 1 meter (specimen 15) and 3 meters (specimen 13) distance from the nearest support will probably give the highest yield strength for the 'composite' composition. Which point this is can not be established based on the results found in this project. This last aspect can be examined for the other girder types based on the hand calculated ultimate loads. The hand calculated ultimate loads, with the exception of the first specimen of each girder type, are presented in Figure 86.

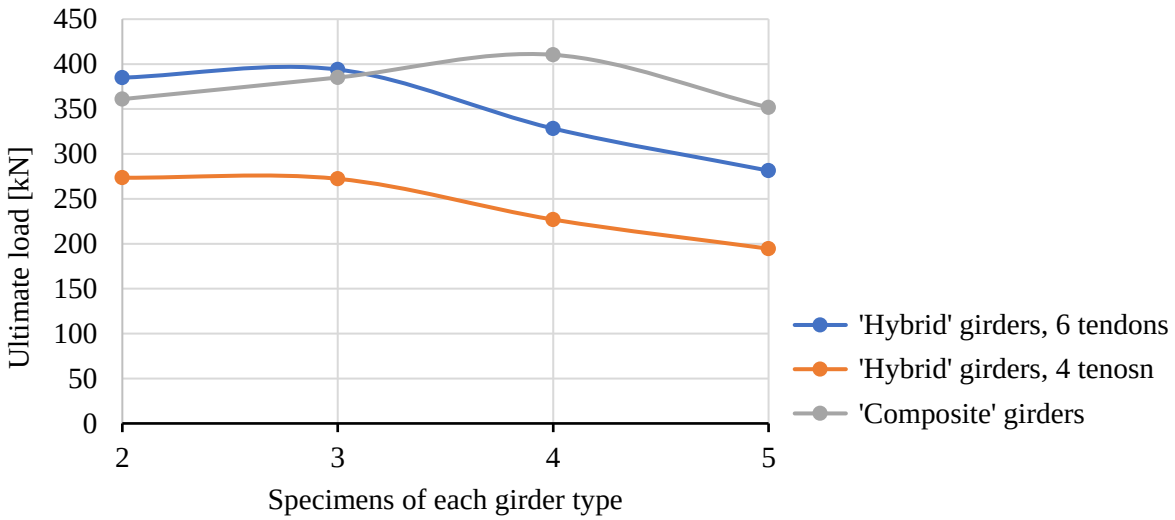

Figure 86: Final ultimate loads of all specimens except the specimens exposed to load situation 1, calculated by hand

The greatest ultimate load implemented that can be implemented on a girder will have to reach the shear capacity of the girder and the moment capacity at the same load level. On bases of the ultimate load results found in Figure 86, an estimate can be made of the location were the load force should be applied to be able to implement the greatest load level that the specific girder type can bear. As stated in chapter 4.2 'Numerical analyses using ANSYS', the hand calculated moment capacities correspond well with the simulated values, while the shear capacities are underestimated by about 20%. Taking into account the fact that the values of the shear capacities are underestimated as a result of the assumption that the web withstands all shear forces, it can be assumed that the greatest load can be placed on approximately 2 meters distance from the support for all 3 the beam types.

6.3 Influence of girder type

For the sake of clarity of the examination, the influences of the girder types are subdivided into two categories: ultimate load and load-deflection relationship. As a reminder in Figure 87 the different girder types are presented.

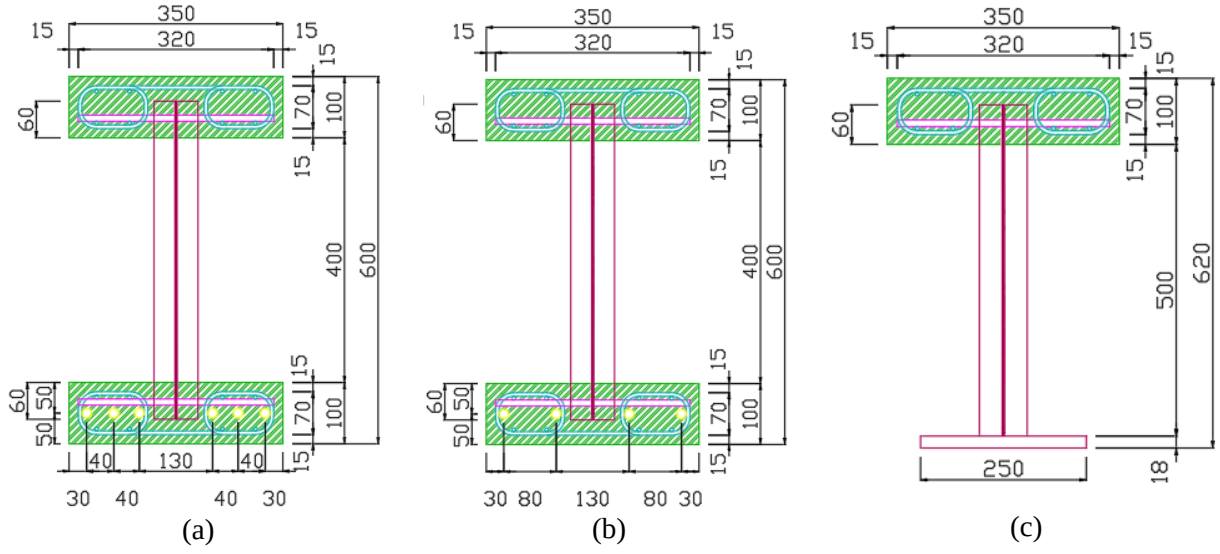

Figure 87: Cross-sectional properties of the three different girder types, dimensions in mm: (a) 'hybrid' 6 tendons, (b) 'hybrid' 4 tendons, (c) 'composite' girder type

Ultimate load

By examining the hand calculation results found in chapter 3, it can be noted that the difference in girder compositions (girder types) has a significant influence on the load bearing capacity of the girders. Figure 88 is a copy of the obtained hand calculated ultimate loads for all girders. The girders of one girder type are grouped by the same colour.

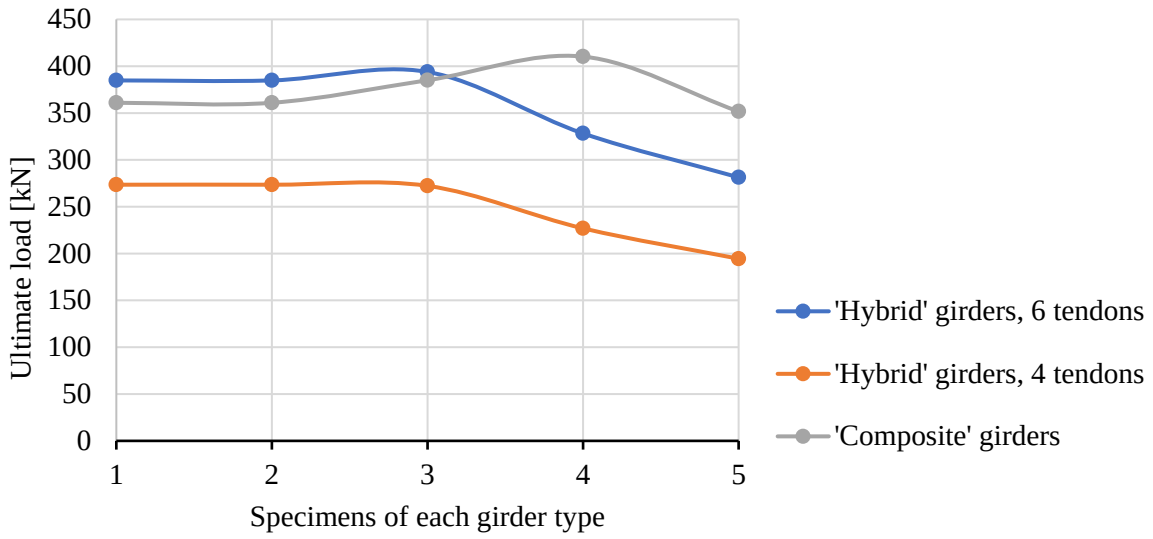

Figure 88: Final ultimate loads of all specimens calculated by hand

The influence of the ‘girder type’ parameter ensures generally lower values for the ultimate loads of the 'hybrid' girders with 4 tendons. This is due to the smaller tensile capacity of the lower flange for the first specimens. For the last ‘hybrid’ girders with 4 tendons specimens, the lower values are more a result of the web thickness which is one millimetre thinner than the corresponding specimens of the other girder types. It proves from the ultimate load results that the 'hybrid' girders with 6 tendons have approximately the same capacities as the 'composite' girders. The differences that still exist can be explained by the difference in web height and tensile capacity of the bottom flange. For the first specimens, which fail due to a too sizeable bending moment, the values of the ‘hybrid’ girders with 6 tendons are larger due to a greater tensile capacity of the lower flange. If the shear force capacity of the girder becomes important due to the imposed load situation, the ultimate loads of the 'composite' girders become larger. This is the result of a larger web. A larger web of the 'composite' beams allows for more slender folds, which increases the shear force capacity.

Load-deflection relationship

By comparing the load-deflection curves of the ‘composite’ girders (made in ANSYS) with the curves of the ‘hybrid’ girders with 4 and 6 tendons (made in ATENA), the influence of the girder type on the load-deflection relationship can be assessed. Unfortunately, not all ‘hybrid’ girders are numerical analysed. The girders with the same web thickness and load situation must be examined to clearly see the influence of the girder type on the course of the L-D curve. Specimen 2 and specimen 12, but also specimen 3 and 13 can be compared. In the curve below, see Figure 89, the L-D curve of specimen 2 and 12 are can be found.

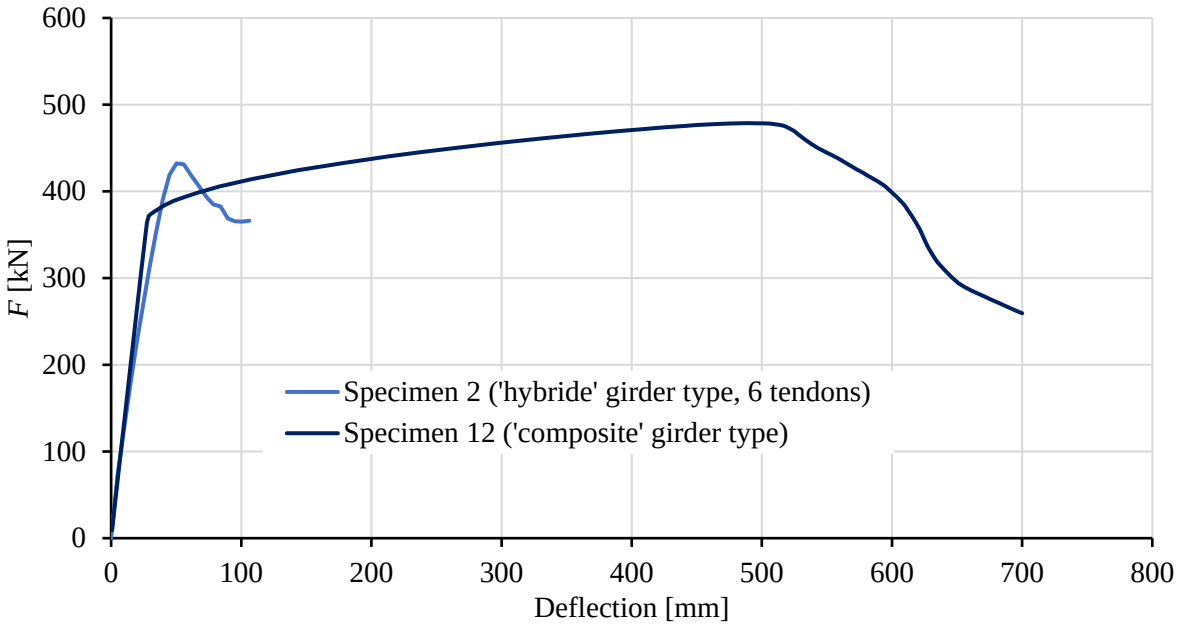

Figure 89: Comparison curve of specimen 2 and 12 both under the influence of load situation 2

Based on the different courses of specimen 2 and 12 in the load-deflection curve, it is expected that the 'hybrid' composition with 6 tendons has less resistance against deformations in the elastic phase than the 'composite' composition. The elastic phase of specimen 2 in Figure 89 is less steep than for specimen 12. The elastic phase of the 'hybrid' girder type with 6 tendons might be less steep, but it is also longer. This means a greater force load is needed to reach the yield point of the girder. After reaching the yield point, the girder with the 'hybrid' composition buckles and loses its strength, while the 'composite' composition experiences a considerably long hardening phase and buckles accompanying a higher load force. A similar constatation can be found for specimen 3 and 13 with the exception that the hardening phase is much shorter. The comparison curve of specimen 3 and 13 is given in Figure 90.

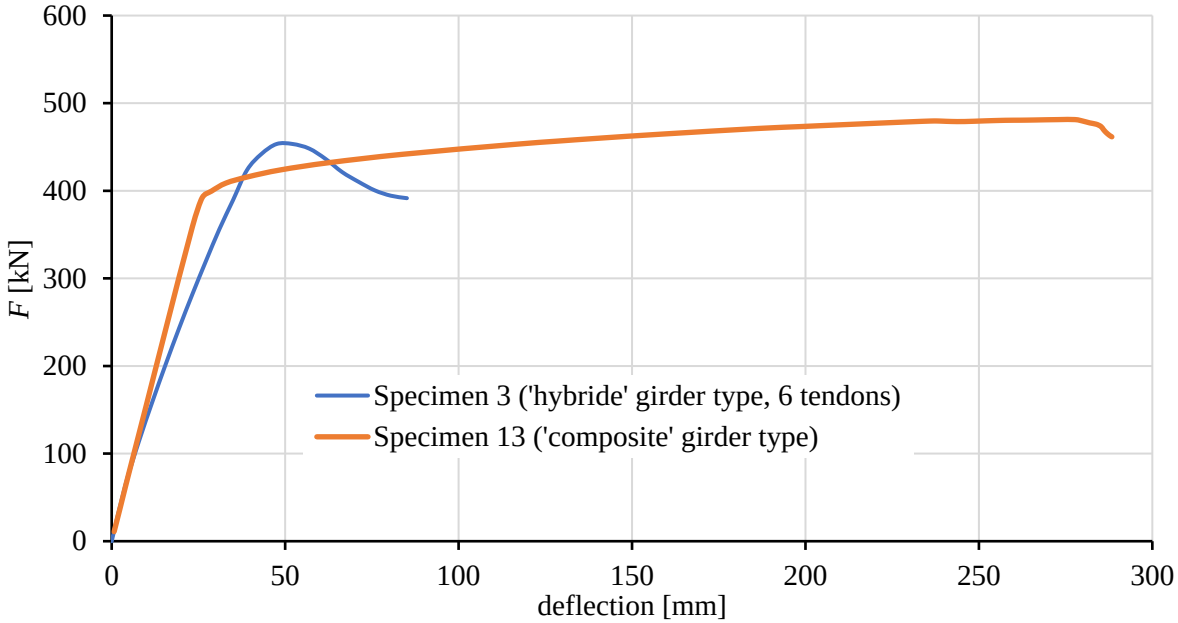

Figure 90: Comparison curve of specimen 3 and 13 both under the influence of load situation 3

6.4 Influence of web thickness

The web thickness of the corrugated steel web has an influence on the shear capacity of the girder. Because for each girder type, the first and the second specimen are exposed to the same load situation but have another web thickness, these two specimens of each girder type are used for the evaluation of the web thickness influence on the girders. For the sake of clarity a subdivision is made to between the ultimate load and the load-deflection curve.

Ultimate load

The ultimate loads for the first and second specimens of the girder types always have the same ultimate loads found via hand calculation. The web has no influence on the ultimate loads of the girders that fail due to a too large bending moment. But the behaviour can be discussed by use of the shear capacities of theses specimens. In the table below (Table 17) the hand calculated shear capacities of the first two specimens of each girder type are presented. The web thicknesses are also included in the table.

Table 17: Shear capacities of the first two girders of each girder type

'Hybrid' girder, 6 tendons

Nr.	Web thickness [mm]	Shear capacity [kN]
1.	6	387.98
2.	4	246.21

'Hybrid' girder, 4 tendons

Nr.	Web thickness [mm]	Shear capacity [kN]
6.	5	323.32
7.	3	170.19

'Composite' girder

Nr.	Web thickness [mm]	Shear capacity [kN]
11.	6	484.97
12.	4	307.76

As expected, all first specimens have a greater shear capacity than the second. The web properties are exactly the same with the exception of the web thickness. To be able to discuss the relative differences, the multiplication factors are given in Table 18. These factors have been achieved by dividing the shear capacity of the first specimens by the capacity of the second specimens for all girder types.

Table 18: Multiplication factors of the shear capacities of the first two girders of each girder type

'Hybrid' girder, 6 tendons		'Hybrid' girder, 4 tendons		'Composite' girder	
	$V_{R,EC} / V_{R,EC}$		$V_{R,EC} / V_{R,EC}$		$V_{R,EC} / V_{R,EC}$
Nr.1/nr.2	1.58	**Nr.6/nr.7**	1.90	**Nr.11/nr.12**	1.58

The multiplication factors of the 'hybrid' girder with 6 tendons and the 'composite' girder are the same. It seems like the web height does not have an influence on the percental change of the shear capacity. To better compare the influence of the web thickness on the shear capacity, the four webs of the 'hybrid' girders are compared in a line chart (see Figure 91).

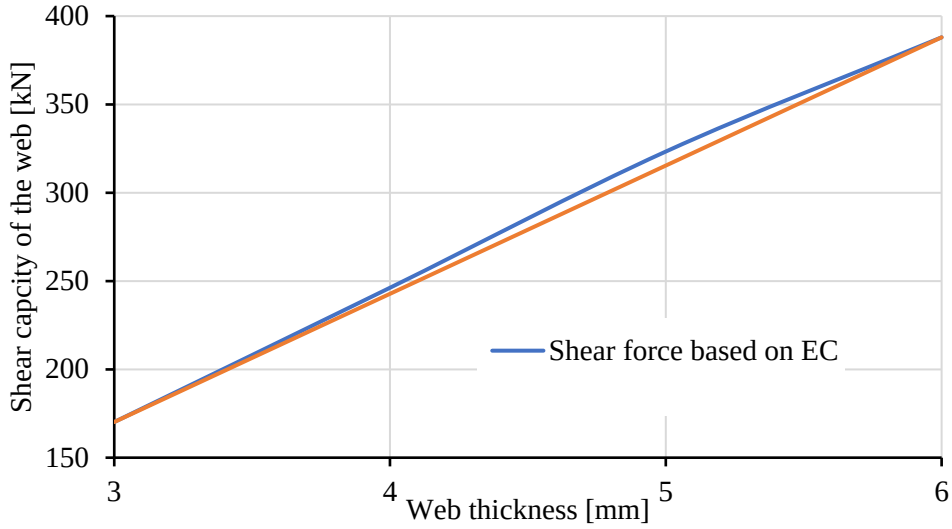

Figure 91: Shear capacity of the first two specimens of the two 'hybrid' girder types

With these results the further course of the graph can not be predicted. The results are not sufficiently accurate to form a correct formula for the further course of the curve based on these small differences. What can be concluded is that the shear will increase less with higher web thicknesses.

Load-deflection relationship

To discuss the influence of the web thickness on the load-deformation relationship, the curves of specimen 11 and 12 are compared. They have the same load situations applied and the only difference in composition is the web thickness of the girders. To compare the course of the load-deflection curves, both curves are presented in Figure 92.

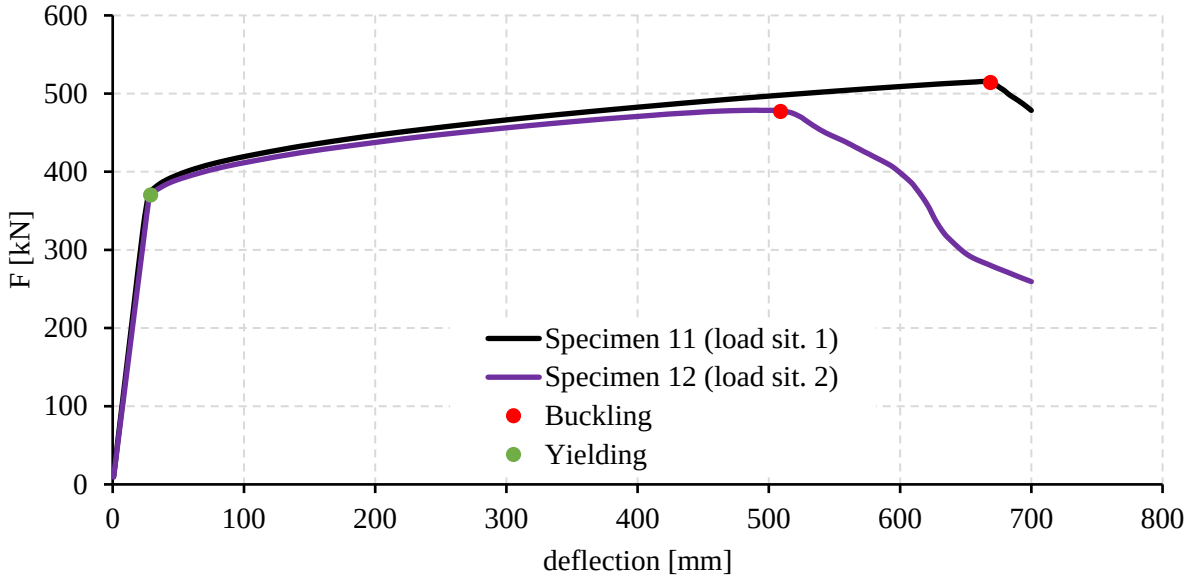

Figure 92: Load – vertical displacement curve of specimen 11 and 12 provided with ANSYS

The web thickness does not have an influence on the ultimate load of the girder. As the load is centrally located on the girder, it mainly imposes bending moments in the girders and the yielding therefore occurs at the same loading point (or in the same displacements step). Going further in load-deflection course, the buckling of the web (which is a result of mainly shear forces) occures at a lower load level and a smaller deflection.

6.5 Capacity validation of the Structural Laboratory

A main goal of this project is to investigate if the capacity of the Structural Laboratory at the Department of Structural Engineering at BME is sufficient for the planned research program. In chapter 4 is established that the elements needed to create the experimental setup are available in the lab. The already completed comparable study 'Experimental analysis of prototypes' at BME had almost the exact same setup that is needed for the experimental tests presented in this project.

The piston available in the lab has a maximum force load of 1000 kN. Based on the calculations of the girder capacities and the behaviour of the girders (L-D curves) in the presented load situations, it can be checked whether the piston is strong enough to map the full load-deflection curve of the girders. The highest force in the conducted load-deflection curves is found for specimen 11 under load situation 1. This value is equal to almost 510 kN. If taken in consideration that in the hand calculations the curve presented in Figure 93 of the ultimate loads is obtained, there can be concluded that specimen 11 will acquire the highest load force for the course of the load-deflection curve.

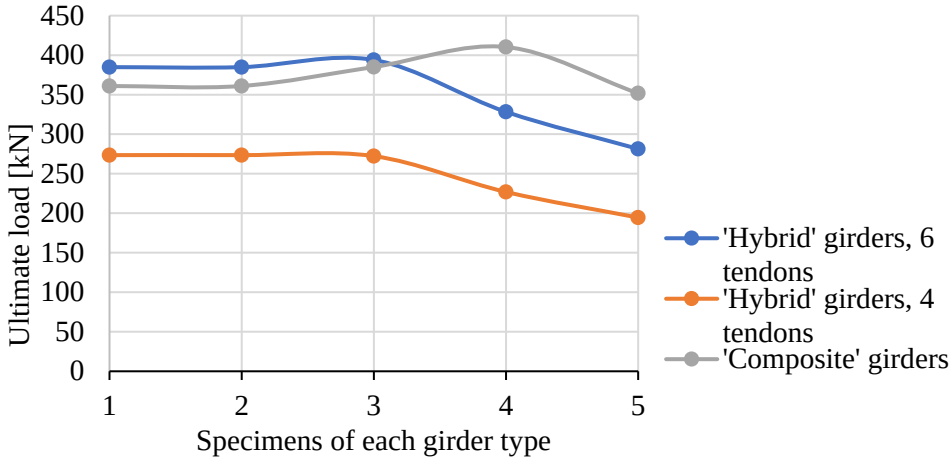

Figure 93: Final ultimate loads of all specimens based on hand calculations

In the curve presented in Figure 93 it can be noted that for the first load situation, not specimen 11 but the first specimen of the 'hybrid' girders with 6 tendons (specimen 1) will acquire the highest load force to reach the yield point or 'ultimate' load of the girder. Therefore, chances are that this girder will acquire the greatest load force to reach the point of web buckling. The ultimate force load of specimen 1 provided by hand calculation is equal to 384.85 kN and for specimen 11 this is 360.99 kN. Value 384.85 of specimen 1 is 6.61% higher than 360.99 kN of specimen 11. If this difference of 6.61% is taken into account for the 510 kN maximum reached value of specimen 11, a value of 543.71 kN is obtained. This is an estimation of the maximum needed load force in the experimental lab. Knowing that specimen 12 reaches higher values in the L-D curve than specimen 2 (see Figure 94), and specimen 1 and 2, and 11 and 12, have the same hand calculated ultimate loads (see Figure 93) this is a save consideration.

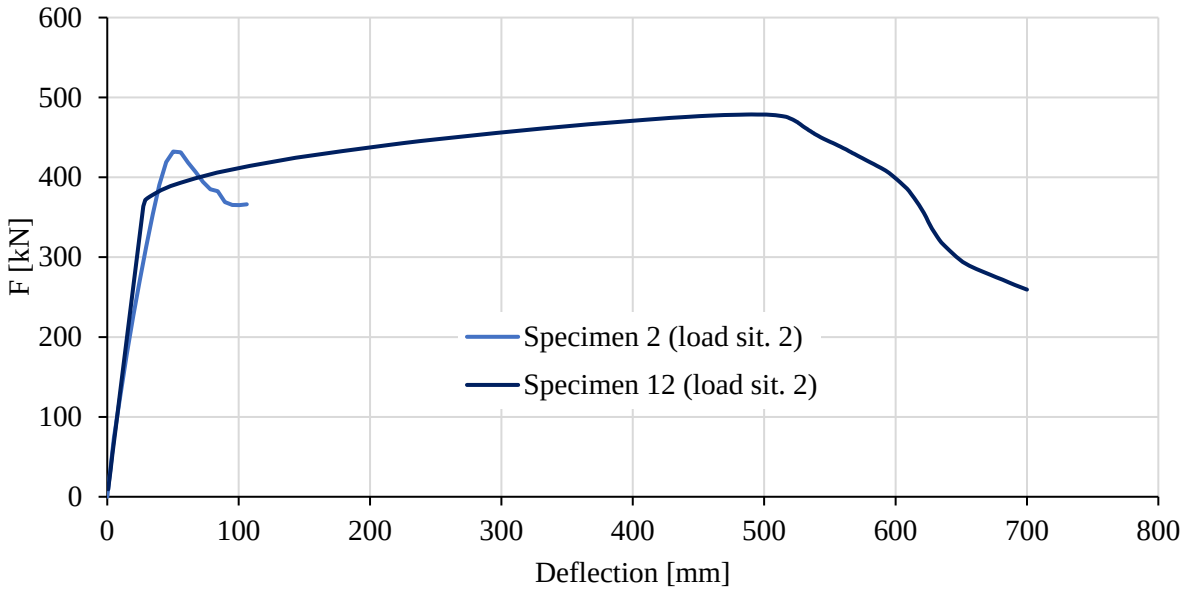

Figure 94: Comparison curve of specimen 2 and 12

If 543.71 kN is taken as the maximum load according to the calculations of the girders, then the maximum pressure force of the piston has a buffer of 456.29 (1000-543.71) kN. There can be concluded that the piston will most likely be sufficient for the purpose of the overarching research of this project.

7 Conclusion

Compound box and I-girders with a corrugated steel web are innovative developments that are often used for bridge constructions. A lot of research is being conducted concerning the best compositions in relation with certain load cases and the implementation of new composition possibilities. Various parametric studies are under investigation regarding the potential of these different configurations. This thesis is part of an overarching research concerning the load bearing capacity of compound girders with trapezoidal corrugated webs and the behaviour of the girders exposed to certain loading situations. Current project focuses on the design of an experimental phase of the overarching research program and investigates if the designed girders fit to possibilities (maximum loading) within the Structural Laboratory of BME. The main goal of the thesis is to develop the numerical models for the test specimens and to determine their load carrying capacities. In addition, the structural behaviour and M-V interaction of the investigated girders exposed to the accompanying load situations is studied. The advantages of the corrugated webs are acknowledged and discussed. During the investigations, following results are obtained:

1) A detailed literature review on the behavioural aspects of corrugated web girders is conducted and presented in section 1. Numerous papers are studied dealing with stress distributions, strength, stability and also the current developed connection techniques of compound girders with a steel corrugated web and concrete flange(s).
2) Numerical models are developed to investigate the structural behaviour of composite and hybrid girders, and the load bearing capacities are determined by FE simulations. Different software programs are used to model the composite and the hybrid girders depending on their modelling capabilities and features.
3) Concepts concerning the M-V interaction within a girder have been discussed and for the ‘composite’ girder composition it has been proven that the interaction between the stress of the shear and bending moment can be neglected.
4) The calculation methods of the Eurocode are labelled as conservative, but well approximated to the computed results obtained by FEM calculations.
5) The assumption that all bending moment is resisted by the flanges has been proven to be a valid assumption using the moment-shear interaction curve made for the ‘composite’ girders. With this curve, it has also been established that the assumptions that only the web resists to shear forces, is rather conservative and that nearly 20% underestimation of the capacity follows.
6) Which influences the three changing parameter categories of the discussed girders have on the load-deflection behaviour, the failure modes and the maximal load force values that can be resisted by the girders, are determined for the ‘composite’ girders and ‘hybrid’ girders.
7) The behaviour and the maximum tolerable loads of the specimens during the experimental tests are predicted. The experimental setup has been checked and the possibilities of the Structural Laboratory at BME have been identified as sufficient.

The present knowledge regarding the load bearing capacity and behaviour of compound girders with corrugated webs and the influence of certain composition parameters is limited. Further research is necessary in order to obtain reliable design models. Experimental tests on the behaviour of girders with corrugated webs with a large variation of properties should be performed. These experimental tests and tests specimens should not differ too much in order to best assess the influence of the composition parameters. Starting all research from a specific starting composition and only varying one or two parameters per study would be idealistic. This way the different results could more easily be compared. In the further development of the overarching project where this thesis is part of, a basis to this principle

will be made. For the experimental phase (that will be performed in the end of August 2018) I will be present in the laboratory in Budapest.

References

[1] J. P. Pederson, International Directory of Company Histories, California: Gale, 1999.

[2] R. J. Jiang, F. T. K. Au and a. Y. F. Xiao, "Prestressed Concrete Girder Bridges with Corrugated Steel Webs: Review," *International Journal of Steel Structures,* 2015.

[3] Y. L. A. C. a. T. Y. Jun He, "Mechanical Behavior and Analysis of Composite Bridges with Corrugated Steel Webs: State-of-the-Art," *International Journal of Steel Structures,* vol. 12, no. 3, 2012.

[4] E. Y. Sayed-Ahmed, "Composite Bridges Contructed With Corrugated," 2003.

[5] E. Y. Sayed-Ahmed, "Behaviour of steel and (or) composite girders with," *NRC Research Press Web,* 2001.

[6] B. Kövesdi, "The patch loading resistance of corrugated steel webs used in bridge building," Budapest University of Technology and Economics Department of Structural Engineering, Universit[at Stuttgart Institute of Structural Design, Budapest, 2007.

[7] VSL, "Incremental launching method," [Online]. Available: http://en.vsl.cz/incremental-launching-method/. [Accessed 15 May 2018].

[8] J. J. J. Pitroda, "A SHORT STUDY ON LAUNCHING TECHNIQUES," S.N. Patel Institute of Technology & Research Centre, Umrakh, India, 2015.

[9] WSP, "BRIDGE CONSTRUCTION METHODS," 2018. [Online]. Available: https://www.wsp.com/en-GL/services/bridge-construction-methods. [Accessed 15 May 2018].

[10] The Constructor, "Span by Span Casting method of Bridge Construction," 2017. [Online]. Available: https://theconstructor.org/structures/span-by-span-casting-method-of-bridge-construction/6129/. [Accessed 17 May 2018].

[11] B. Sward, "Segmental Bridge Construction Techniques," 7 May 2012. [Online]. Available: http://www.post-tensioning.org/Uploads/Conference/2012%20Convention/Segmental%20Bridge%20Constructin%20Techniques.pdf. [Accessed 19 May 2018].

[12] Y. L. A. C. D. W. T. Y. Jun He, "Bending behavior of concrete-encased composite I-girder with corrugated steel web," *Elsevier,* 2012.

[13] Y. L. Z. L. A. C. T. Y. Jun He, "Shear behavior of partially encased composite I-girder with corrugated," *Journal of Constructional Steel Research,* 2012.

[14] O. K. N. Ljungstrom, “Girders with Trapezoidally Corrugated,” *CHALMERS UNIVERSITY OF TECHNOLOGY,* 2010.

[15] BSI, “Eurocode 3 - Design of steel structures - Part 1-5: Plated,” *EUROPEAN STANDARD,* 2006.

[16] J. Linder, “Zur Bemessung von Trapeztegträgern,” vol. 10, no. 61, 1996.

[17] B. J. L. D. B. Kövesdi, “Girders with trapezoidally corrugated webs subjected by combination of bending, shear and path loading,” *ResearchGate,* 2015.

[18] R. M. G. S. C. M. D. B. B. Johansson, “COMMENTARY AND WORKED EXAMPLES TO EN 1993-1-5 “PLATED STRUCTURAL ELEMENTS","” *JRC Scientific and Technical Reports,* 2007.

[19] J. Raichle, “Randnahe Kopfbolzen im Brückenbau,” *Institut für Konstruktion und Entwurf; Stuttgart,* 2015.

[20] P. M. J. R. M. E. M. H. Prof. Dr.-Ing. Ulrike Kuhlmann, “NEW DEVELOPMENTS OF STEEL AND COMPOSITE BRIDGES”.

[21] BSI, “Eurocode 2: Design of concrete structures - Part 1-1 : General,” *EUROPEAN STANDARD,* 2004.

[22] B. E. R. Luo, “Ultimate Strength of Girders with Trapezoidally Corrugated Webs Under Patch Loading,” *Thin-Walled Structures,* no. 24, 1996.

[23] Autodesk Support, “How to Perform a Mesh Convergence Study,” 26 May 2016. [Online]. Available: https://knowledge.autodesk.com/support/simulation-mechanical/learn-explore/caas/sfdcarticles/sfdcarticles/How-to-Perform-a-Mesh-Convergence-Study.html. [Accessed May 26 2018].

[24] L. N. H. L. H. E. Moon J., “Moment gradient correction factor and inelastic flexuraltorsional,” *Thin-walled Structures,* no. 62, 2013.

[25] B. Jáger, “INTERACTING STABILITY BEHAVIOUR OF STEEL I-GIRDERS,” BUDAPEST UNIVERSITY OF TECHNOLOGY AND ECONOMICS, Budapest, Hungary, 2014.

[26] A. H. S. R. Driver RG., “Shear behaviour of corrugated web bridge girder,” vol. 132, no. 2, 2006.

[27] K. G. Hassanein M.F., “Behaviour of bridge girders with corrugated webs: (II) Shear strength and design,” *Engineering Structures,* no. 57, 2013.

[28] G. H. Y. K. L. H. Yi J., “Interactive shear behaviour of trapezoidally corrugated,” *Engineering Structures,* no. 30, 2008.

[29] Z. L. T. M. T. L. Nie J.G., “Shear strength of trapezoidal corrugated steel,” *Journal of Constructional Steel Research,* no. 85, 2013.

[30] Červenka Consulting s.r.o., *ATENA Program Documentation Part 4-6,* Prague, 2016.

[31] Červenka Consulting s.r.o., "ATENA Program Documentation Part 1," Prague, 2018.

[32] D. László, *10. feladatrész: Prototípusok kísérleti analízise,* Budapest: Budapest University of Technology and Economics, 2016.

[33] SkyCiv, "Beam," [Online]. Available: https://platform.skyciv.com/dashboard. [Accessed 2 May 2018].

[34] Structurae, "Pont de Maupré," [Online]. Available: https://structurae.info/ouvrages/pont-de-maupre. [Accessed 30 April 2018].

[35] Bridge Design & Engineering, "Force of nature," 22 March 2016. [Online]. Available: https://www.bridgeweb.com/Force-of-nature/3938. [Accessed 15 May 2018].

[36] p.s. mitsubishi construction co. ltd , "Works : Civil Engineering," [Online]. Available: http://www.psmic.co.jp/ps_english/works/award/000539.html. [Accessed 15 May 2018].

[37] Mooser, "BRIDGE CONSTRUCTION," 2016. [Online]. Available: https://www.mooser.net/en/construction-references/bridge-construction/litjesundbruecke-e.html. [Accessed 15 May 2018].

[38] Western Mechanical Electrical Millwright Services Ltd., "Equipment: Railway Span Replacement Gantry," Western, 2018. [Online]. Available: http://www.westernmechanical.net/equipment/railway-span-replacement-gantry/. [Accessed 17 May 2018].

[39] A. v15.0, Canonsburg, Pennsylvania, USA.

[40] M. S. G. E. A. S. Said M.Allam, "Evaluation of tension stiffening effect on the crack width calculation of flexural RC members," *Alexandria Engineering Journal,* 2013.

[41] R. M. G. S. C. M. D. B. B. Johansson, "COMMENTARY AND WORKED EXAMPLES TO EN 1993-1-5 "PLATED STRUCTURAL ELEMENTS"," JRC EUROPEAN COMMISSION, 2007.

List of appendices

Appendices

Appendix A: Geometric notations of corrugated web [15] p.50

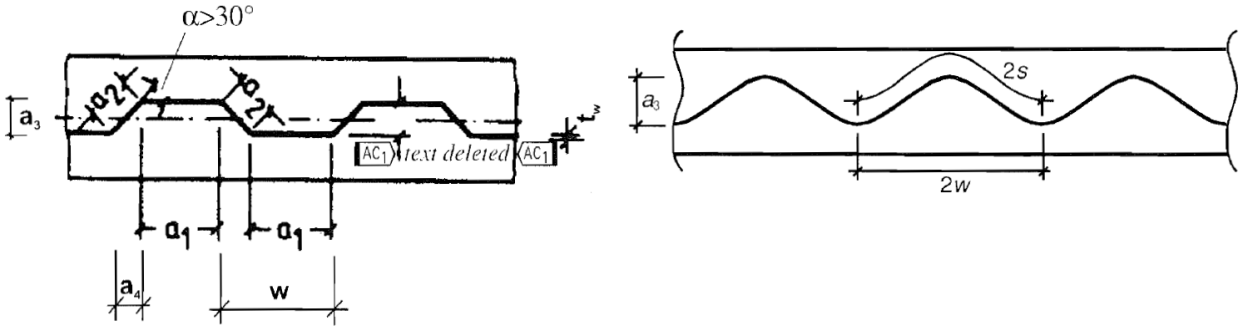

Appendix B: AutoCAD drawing of specimen 1

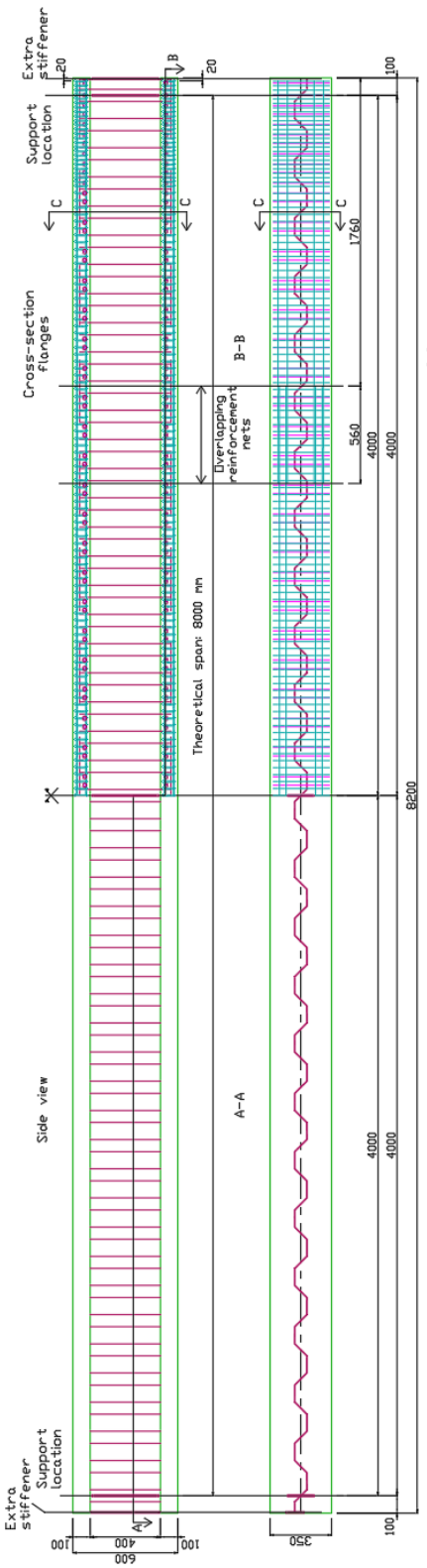

Notes:

1. All dimensions are in [mm].
2. Prestressing tendons: nominal diameter of 12.9mm with 7 strands, applied: 6 pcs 6x8.2m=49.2m, weight: 38.62kg
3. Stress level in the tendons shall be 1475MPa in the time instant of prestressing.
4. For each tendon the instand prestressing means 221.4kN (total 6x221.4kN=1328kN).
5. Material properties: concrete: C40/50-XC1-8-KK, rebars: B500B, lifting hooks: B240B, mesh reinforcement shall be used.
6. Concrete cover thickness: 15mm.
7. Concrete volume to be casted: 0.58 m3.
8. Weight of the specimen (around): 8.2x0.18=1.48 tons.
9. Bowing of the specimen (negative deflection) in the time instant of prestressing: -16.4mm.
10. The hardening of concrete can be subserved by heating or chemical procedures - according to the manufacturer's quality assurance policy.
11. The dismantling shall not be performed at least 8 hours after casting.
12. The concrete quality shall be tested by 6 test cubes from each mix according to the MSZ 4715/4 and MSZ 4020/2 standards.
13. The concrete strenth must be at least 38 MPa before prestressing (regarding the cube test having 15cm widths).
14. The bending radius of rebars are external dimensions and shall be at least 4*fi (fi=diameter of rebar).
15. The steel corrugated web shall be greased to avoid adhesion between the steel and concrete surfaces in the production phase.
16. The casting of the upper and lower slabs shall be performed in one time with the same mix.

Appendix C: AutoCAD drawing of specimen 6

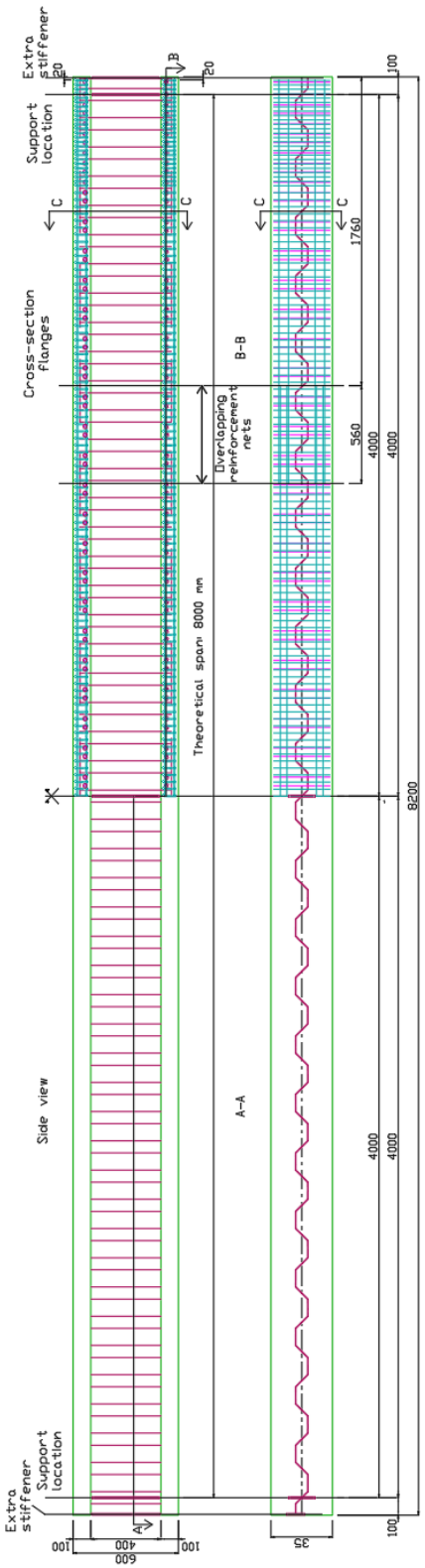

Notes:

1. All dimensions are in [mm].
2. Prestressing tendons: nominal diameter of 12.9mm with 7 strands, applied: 4 pcs 4x8.2m=32.8m, weight: 25.75kg
3. Stress level in the tendons shall be 1475MPa in the time instant of prestressing.
4. For each tendon the instand prestressing means 221.4kN (total 6x221.4kN=1328kN).
5. Material properties: concrete: C40/50-XC1-8-KK, rebars: B500B, lifting hooks: B240B, mesh reinforcement shall be used.
6. Concrete cover thickness: 15mm.
7. Concrete volume to be casted: 0.58 m3.
8. Weight of the specimen (around): 8.2x0.18=1.48 tons.
9. Bowing of the specimen (negative deflection) in the time instant of prestressing: -11.2mm.
10. The hardening of concrete can be subserved by heating or chemical procedures - according to the manufacturer's quality assurance policy.
11. The dismantling shall not be performed at least 8 hours after casting.
12. The concrete quality shall be tested by 6 test cubes from each mix according to the MSZ 4715/4 and MSZ 4020/2 standards.
13. The concrete strenth must be at least 38 MPa before prestressing (regarding the cube test having 15cm widths).
14. The bending radius of rebars are external dimensions and shall be at least 4*fi (fi=diameter of rebar).
15. The steel corrugated web shall be greased to avoid adhesion between the steel and concrete surfaces in the production phase.
16. The casting of the upper and lower slabs shall be performed in one time with the same mix.

Appendix D: AutoCAD drawing of specimen 11

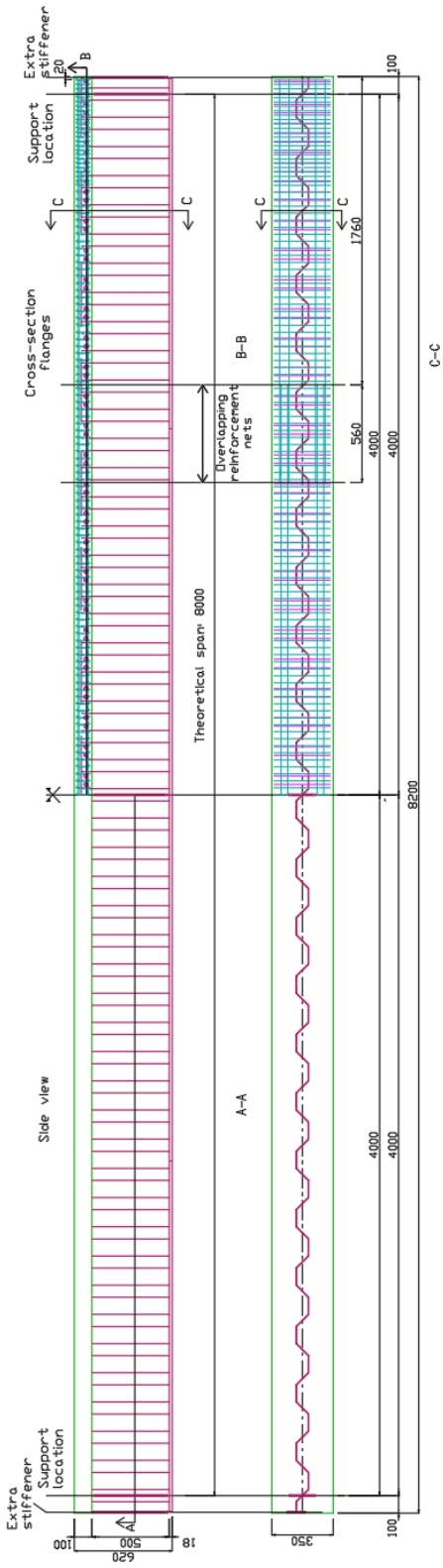

Notes:

(1) Dimensions in mm.
(2) Material quality: Concrete: C40 / 50-XC1-8-KK.
(3) Concrete steel: B500B (B60.50.)
(4) Lifting tab: B240B (B38.24.)
(5) Welded mesh is made.
(6) Concrete cover thickness: 15mm.
(7) Concrete volume to be casted: 0.58m3.
(8) Weight of of the specimen (ground): 8.20 x 0.18 = 1.48 tonnes.
(9) The solidification of concrete shall be accelerated by means of a heat treatment and chemical process, as regulated by the manufacturer's quality system.
(10) The dismantling shall not be performed at least 8 hours after casting.
(11) The concrete quality shall be tested by 6 test cubes from each mix according to the MSZ 4715/4 and MSZ 4020/2 standards.
(12) Then bending radius of rebars are external dimensions and shall be at least 4*fi (fi=diameter of rebar).
(13) The steel corrugated web shall be greased to avoid adhesion between the steel and concrete surfaces in the production phase.

Appendix E: Hand calculation results for the shear capacities

	t_w [mm]	h_w [mm]	alpha [°]	a1 = a2 [mm]	a3 = a4 [mm]	f_{yw} [MPa]	$\tau_{cr,1}$ [MPa]	λ_{rel} [-]	χ_{rel} [-]	D_X [N/mm]	D_Z [N/mm]	$\tau_{cr,g}$ [MPa]	$\lambda_{rel,g}$ [-]	$\chi_{rel,g}$ [-]	χ_{min} [-]	$V_{Rk,Ec}$ [kN]
1.	6	400	45	97.6311	69.0356	280	3830.8295	0.2054	1	3545.5295	1172558.9361	9279.9378	0.1320	1	1	387.9794
2.	4	400	45	97.6311	69.0356	280	1702.5909	0.3081	0.9519	1050.5272	781705.9574	7577.0375	0.1461	1	0.9519	246.2063
3.	4	400	45	97.6311	69.0356	280	1702.5909	0.3081	0.9519	1050.5272	781705.9574	7577.0375	0.1461	1	0.9519	246.2063
4.	4	400	45	97.6311	69.0356	280	1702.5909	0.3081	0.9519	1050.5272	781705.9574	7577.0375	0.1461	1	0.9519	246.2063
5.	4	400	45	97.6311	69.0356	280	1702.5909	0.3081	0.9519	1050.5272	781705.9574	7577.0375	0.1461	1	0.9519	246.2063
6.	5	400	45	97.6311	69.0356	280	2660.2983	0.2465	1	2051.8110	977132.4467	8471.3854	0.1381	1	1	323.3162
7.	3	400	45	97.6311	69.0356	280	957.7074	0.4108	0.8773	443.1911	586279.4680	6561.9069	0.1570	1	0.8773	170.1860
8.	3	400	45	97.6311	69.0356	280	957.7074	0.4108	0.8773	443.1911	586279.4680	6561.9069	0. 1570	1	0.8773	170.1860
9.	3	400	45	97.6311	69.0356	280	957.7074	0.4108	0.8773	443.1911	586279.4680	6561.9069	0. 1570	1	0.8773	170.1860
10.	3	400	45	97.6311	69.0356	280	957.7074	0.4108	0.8773	443.1911	586279.4680	6561.9069	0. 1570	1	0.8773	170.1860
11.	6	500	45	97.6311	69.0356	280	3830.8295	0.2054	1	3545.5295	1172558.9361	5939.1602	0.1650	1	1	484.9742
12.	4	500	45	97.6311	69.0356	280	1702.5909	0.3081	0.9519	1050.5272	781705.9574	4849.3040	0.1826	1	0.9519	307.7578
13.	4	500	45	97.6311	69.0356	280	1702.5909	0.3081	0.9519	1050.5272	781705.9574	4849.3040	0. 1826	1	0.9519	307.7578
14.	4	500	45	97.6311	69.0356	280	1702.5909	0.3081	0.9519	1050.5272	781705.9574	4849.3040	0. 1826	1	0.9519	307.7578
15.	4	500	45	97.6311	69.0356	280	1702.5909	0.3081	0.9519	1050.5272	781705.9574	4849.3040	0. 1826	1	0.9519	307.7578

Appendix F: Shear force diagram of specimen 1 imposed by load situation 1 with the ultimate load value based on the ultimate shear force achieved in chapter 3 (scheme obtained with SkyCiv [23])

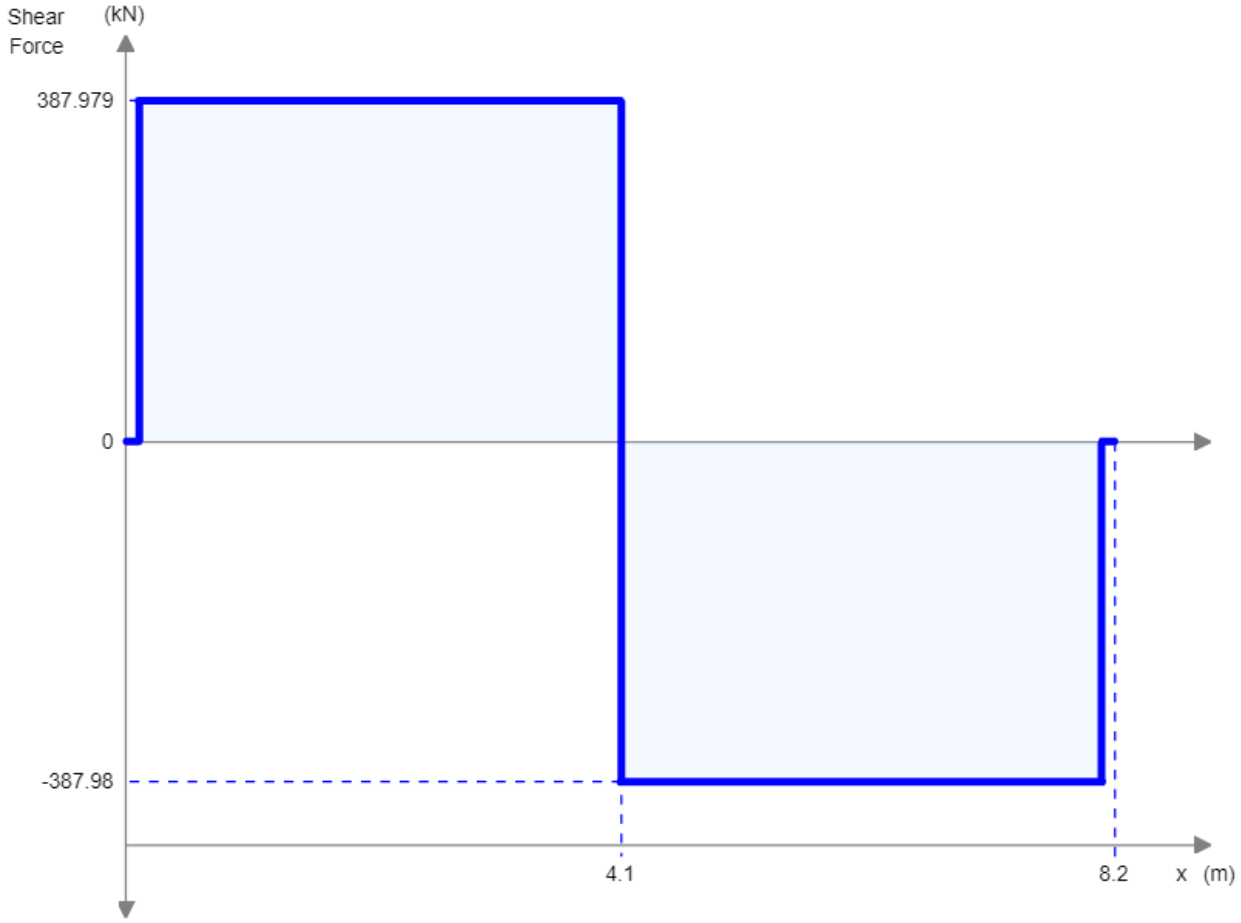

Appendix G: Shear force diagram of specimen 3 imposed by load situation 3 with the ultimate load value based on the ultimate shear force achieved in chapter 3 (scheme obtained with SkyCiv [23])

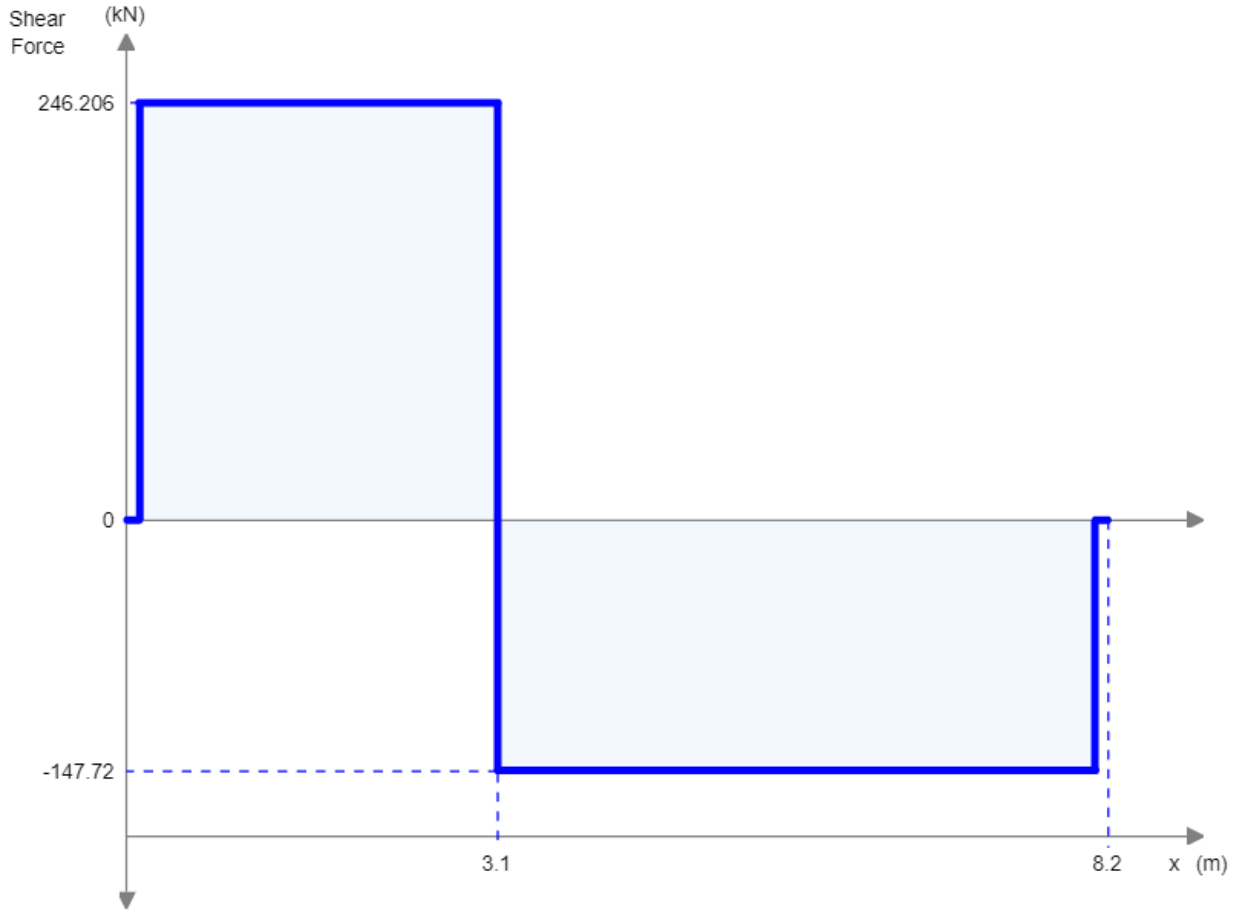

Appendix H: Bending moment diagram of specimen 1 imposed by load situation 1 with the ultimate load values based on the ultimate bending forces achieved in chapter 3 (scheme obtained with SkyCiv [23])

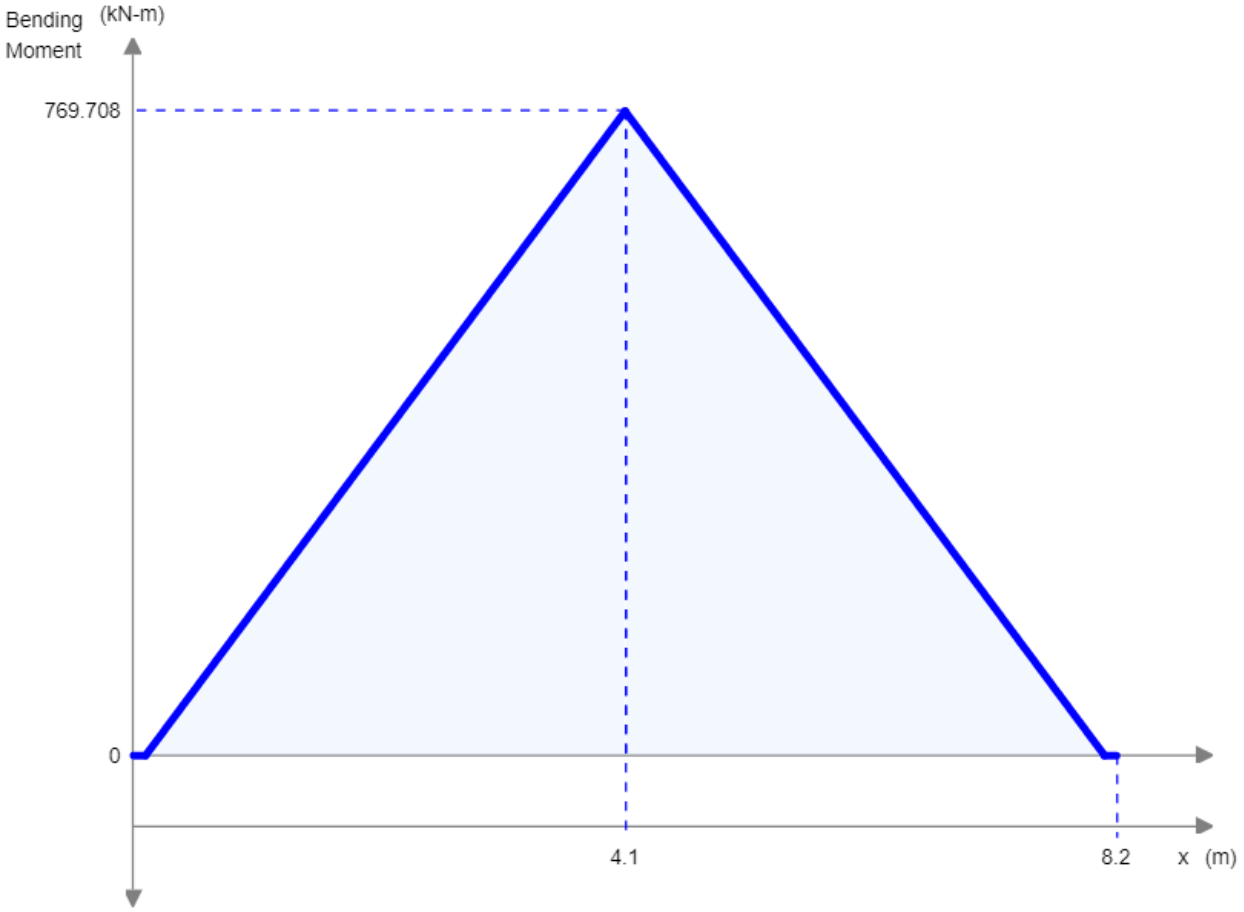

Appendix I: Bending moment diagram of specimen 3 imposed by load situation 3 with the ultimate load value based on the ultimate bending forces achieved in chapter 3 (scheme obtained with SkyCiv [23])

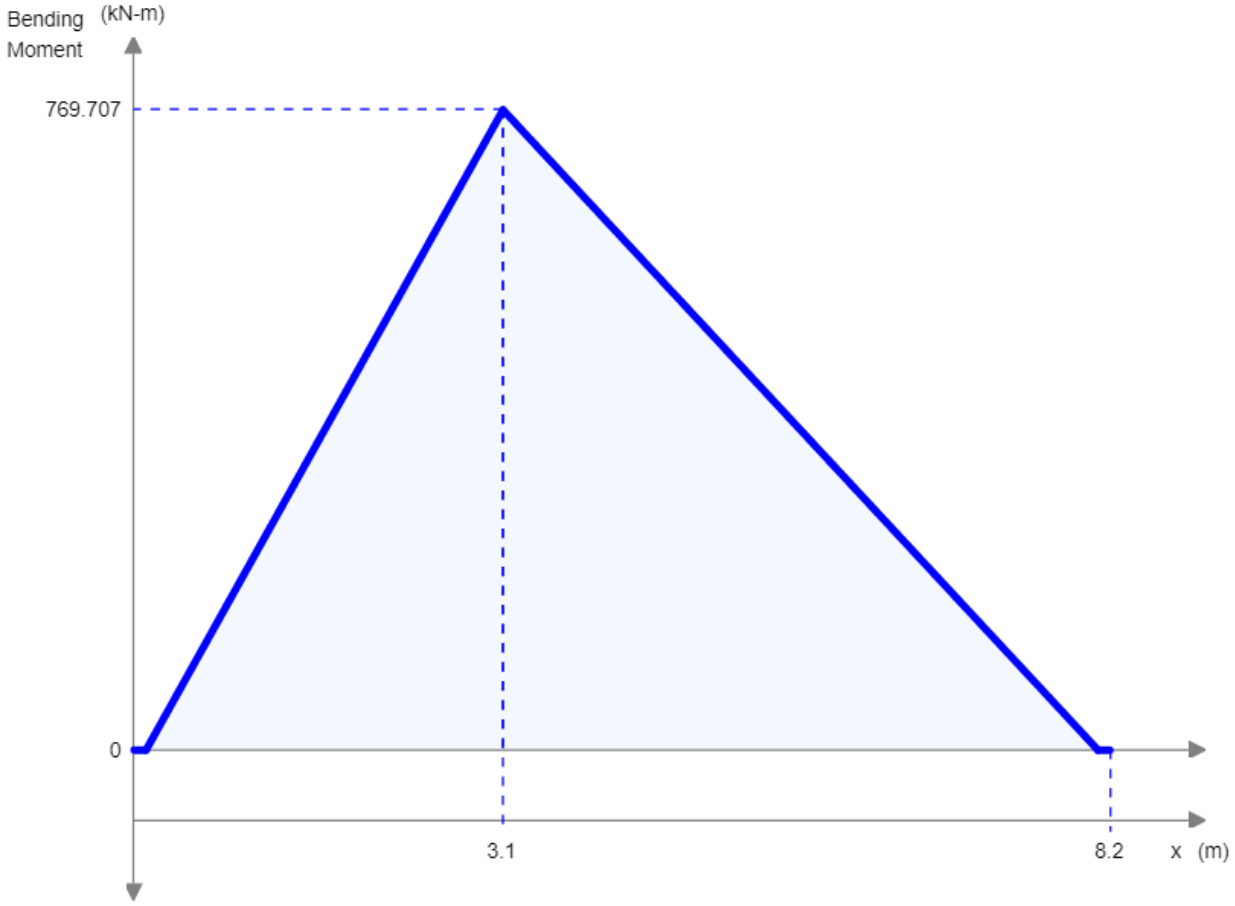

Auteursrechtelijke overeenkomst

Ik/wij verlenen het wereldwijde auteursrecht voor de ingediende eindverhandeling:
Load bearing capacity of compound box or I-girders with corrugated steel web

Richting: **master in de industriële wetenschappen: bouwkunde**
Jaar: **2018**

in alle mogelijke mediaformaten, - bestaande en in de toekomst te ontwikkelen - , aan de Universiteit Hasselt.

Niet tegenstaand deze toekenning van het auteursrecht aan de Universiteit Hasselt behoud ik als auteur het recht om de eindverhandeling, - in zijn geheel of gedeeltelijk -, vrij te reproduceren, (her)publiceren of distribueren zonder de toelating te moeten verkrijgen van de Universiteit Hasselt.

Ik bevestig dat de eindverhandeling mijn origineel werk is, en dat ik het recht heb om de rechten te verlenen die in deze overeenkomst worden beschreven. Ik verklaar tevens dat de eindverhandeling, naar mijn weten, het auteursrecht van anderen niet overtreedt.

Ik verklaar tevens dat ik voor het materiaal in de eindverhandeling dat beschermd wordt door het auteursrecht, de nodige toelatingen heb verkregen zodat ik deze ook aan de Universiteit Hasselt kan overdragen en dat dit duidelijk in de tekst en inhoud van de eindverhandeling werd genotificeerd.

Universiteit Hasselt zal mij als auteur(s) van de eindverhandeling identificeren en zal geen wijzigingen aanbrengen aan de eindverhandeling, uitgezonderd deze toegelaten door deze overeenkomst.

Voor akkoord,

Vandeweyer, Rob

Datum: **4/06/2018**